UNIVERSIDADE FEDERAL DE VIÇOSA

MATHEUS SANT'ANNA ANDRADE

EXPERIMENTAL EVALUATION OF THE RESIDUAL CONCRETE-REINFORCEMENT BOND AFTER EXPOSURE TO ELEVATED TEMPERATURES

VIÇOSA - MINAS GERAIS
2021

MATHEUS SANT'ANNA ANDRADE

EXPERIMENTAL EVALUATION OF THE RESIDUAL CONCRETE-REINFORCEMENT BOND AFTER EXPOSURE TO ELEVATED TEMPERATURES

Dissertation submitted to the Civil Engineering Graduate Program of the Universidade Federal de Viçosa in partial fulfillment of the requirements for the degree of *Magister Scientiae*.

Adviser: José Carlos Lopes Ribeiro

Co-advisers: Diôgo Silva de Oliveira
Leonardo Gonçalves Pedroti

VIÇOSA - MINAS GERAIS
2021

Ficha catalográfica elaborada pela Biblioteca Central da Universidade Federal de Viçosa - Campus Viçosa

T

A553e
2021

Andrade, Matheus Sant'Anna, 1994-

Avaliação experimental da aderência residual entre concreto e armadura após exposição à elevadas temperaturas / Matheus Sant'Anna Andrade. – Viçosa, MG, 2021.

1 dissertação eletrônica (127 f.): il. (algumas color.).

Texto em inglês .

Inclui apêndices.

Orientador: José Carlos Lopes Ribeiro.

Dissertação (mestrado) - Universidade Federal de Viçosa, Departamento de Engenharia Civil, 2021.

Inclui bibliografia.

DOI: https://doi.org/10.47328/ufvbbt.2022.070

Modo de acesso: World Wide Web.

1. Concreto armado. 2. Aderências. 3. Concreto armado - Efeito da temperatura. 4. Deformações e tensões - Métodos gráficos. I. Ribeiro, José Carlos Lopes, 1977-. II. Universidade Federal de Viçosa. Departamento de Engenharia Civil. Programa de Pós-Graduação em Engenharia Civil. III. Título.

CDD 22. ed. 624.18341

Bibliotecário(a) responsável: Alice Regina Pinto CRB6 2523

MATHEUS SANT'ANNA ANDRADE

EXPERIMENTAL EVALUATION OF THE RESIDUAL CONCRETE-REINFORCEMENT BOND AFTER EXPOSURE TO ELEVATED TEMPERATURES

Dissertation submitted to the Civil Engineering Graduate Program of the Universidade Federal de Viçosa in partial fulfillment of the requirements for the degree of *Magister Scientiae*.

APPROVED: October 05, 2021.

Assent:

Matheus Sant'Anna Andrade

Matheus Sant'Anna Andrade
Author

José Carlos Lopes Ribeiro
Adviser

ACKNOWLEDGMENTS

This work was developed during a period that will be forever remembered as an important part of human history; the Coronavirus pandemic has been a period in which we had to isolate ourselves and find ways to get together as one people. In a situation like this, we see how important it is to have people to help and support us. This is a space dedicated to acknowledging everyone who helped me during this incredibly challenging work.

To the Federal University of Viçosa, for giving me the opportunity and providing the infrastructure necessary to develop such challenging work.

To José Carlos Lopes Ribeiro, for the support and guidance throughout this work. Thank you for sharing your knowledge with me and for your contributions to my research.

To Diôgo Silva de Oliveira, for guiding me into this incredible work. Thank you for being more than a professor, and for listening to me when I felt lost and needed someone to talk to.

To Leonardo Golçaves Pedroti, for always being available to help and teach me whenever it was necessary. Thank you for all the great contributions to this work.

To the technical team of the Laboratory of Construction Materials, especially José Carlos and Wellington, for always being patient while teaching me. Thank you for all the help and assistance whenever necessary.

To the technical team of the UFV Microscopy and Microanalysis core facility, especially Carla, for doing everything she could to help me.

To all my colleagues who helped along the way with great suggestions and important contributions to this work. Special thanks to Ana Carolina, Beatriz, Gustavo Lima, Gustavo Nalon and Marina Altoé.

To my parents, Reinaldo e Conceição, and to my sister, Luciana, for all the emotional support and encouragement during this difficult time. I would not have been able to get this far without your love, help, and support.

To my brother, Hugo, who help me as much as he could and, literally came to the laboratory and worked by my side during one of the most challenging stages of this research.

To my roommate Marco Antônio Nakata, for always being there for me and giving me the strength to carry on. Your emotional support was essential so I could finish this work.

To all my other friends who encouraged me during this work, especially Giulia, for taking care of me and my well-being when I was completely focused on finishing this work and had let go of everything else.

Thanks also go to many others who helped during the development of this work. I would not have been able to complete this dissertation without the help of every one of you.

This work was carried out with the support of the Coordenação de Aperfeiçoamento de Pessoal do Nível Superior - Brazil (CAPES) - Funding Code 001.

ABSTRACT

ANDRADE, Matheus Sant'Anna, M.Sc., Universidade Federal de Viçosa, October, 2021. **Experimental evaluation of the residual concrete-reinforcement bond after exposure to elevated temperatures**. Adviser: José Carlos Lopes Ribeiro. Co-advisers: Diôgo Silva de Oliveira and Leonardo Gonçalves Pedroti.

The composite behavior of reinforced concrete structures is directly related to the bond between concrete and reinforcement. When a reinforced concrete structure is subjected to a fire event, the bond is damaged and the force-transfer mechanism is compromised, as well as the resistant capacity of the structure itself. This study consists of a review of post-fire concrete-reinforcement bond relationship and an experimental assessment of the influence of exposure to elevated temperatures on the bond between these materials. First, it was reviewed the state-of-the-art research on post-fire bond properties, as well as the parameters influencing bond relationship development after exposure to elevated temperatures. This work also presents an experimental assessment of the influence of degradation of concrete and reinforcing steel, induced by elevated temperatures, on the bond relationship between the materials and the influence of concrete cover to bar diameter ratio on concrete-reinforcement bond failure mechanism. The findings showed that bond degradation is directly related to the damage to the concrete and that the reinforcing steel is negligibly affected by temperatures under 600 ºC. It was also observed that exposure at 200 ºC had a positive effect both on the residual mechanical properties of concrete and residual bond strength. Exposure to higher temperatures progressively reduced the mechanical properties of concrete and the bond strength measured after the fire situation. Moreover, the bond failure mechanism was observed to shift from pull-out to splitting due to the concrete damage at elevated temperatures, although it could not be easily distinguished. It was also concluded that, even though the data available on the literature are extremely scattered, the bond strength prescribed by international standards for structures design is safe both at room temperature and after exposure to elevated temperatures.

Keywords: Reinforced concrete. Bond strength. Elevated temperatures. Bond-slip relationship. Bond failure mechanism.

RESUMO

ANDRADE, Matheus Sant'Anna, M.Sc., Universidade Federal de Viçosa, outubro de 2021. **Avaliação experimental da aderência entre concreto e armadura após exposição a elevadas temperaturas**. Orientador: José Carlos Lopes Ribeiro. Coorientadores: Diôgo Silva de Oliveira e Leonardo Gonçalves Pedroti.

O comportamento misto de estruturas de concreto armado está diretamente relacionado à aderência entre os materiais. Quando uma estrutura de concreto armado é submetida à situação de incêndio, a aderência entre os materiais é prejudicada e o mecanismo de transferência de forças é comprometido, assim como a capacidade resistente da estrutura em si. Este estudo compreende uma revisão bibliográfica sobre aderência pós-incêndio e a avaliação experimental do efeito da exposição à elevadas temperaturas na aderência entre os materiais. Inicialmente, foi feita uma revisão de literatura do estado-da-arte sobre aderência pós-incêndio e sobre os parâmetros que influenciam a relação aderência-deslizamento após exposição à elevadas temperaturas. Em seguida, fez-se a avaliação experimental da influência da degradação térmica do concreto e do aço na aderência entre os materiais e, também, do efeito da razão entre o cobrimento de concreto e o diâmetro da barra no mecanismo de ruptura da aderência aço-concreto. Os resultados mostraram que a deterioração da aderência está relacionada diretamente aos efeitos da temperatura sobre o concreto e que o aço pouco é afetado para temperaturas abaixo de 600 ºC. Verificou-se também o efeito positivo de exposição à 200 ºC, tanto nas propriedades mecânicas residuais do concreto quanto sobre a aderência residual. Conforme aumentou-se a temperatura de exposição acima desse nível, houve a redução progressiva tanto das propriedades mecânicas do concreto quanto da resistência de aderência. Além disso, apesar de o mecanismo de ruptura da aderência não ser facilmente identificado, observou-se a mudança de arrancamento para fendilhamento devido à fissuração térmica sofrida pelo concreto. Conclui-se também que, apesar de os dados disponíveis na literatura serem muito dispersos, a tensão de aderência obtida pelas prescrições normativas para o projeto de estruturas é segura tanto à temperatura ambiente quanto após exposição a elevadas temperaturas.

Palavras-chave: Concreto armado. Aderência. Elevadas temperaturas. Diagrama tensão-deslizamento. Mecanismos de ruptura da aderência.

TABLE OF CONTENTS

CHAPTER 1:

General Introduction

Abstract

Chapter 1 presents a general introduction to this work, which includes a basic presentation of the concepts further explored throughout this dissertation, the objectives of this research, the justification of the research theme and an explanation of the structure chosen for this work.

1.1. Introduction

When a reinforced concrete building is subjected to a fire incident, depending on how extensive the damage is, it could lead to a partial or total collapse of the structure. In the case of structures that did not collapse, a structural analysis is required to determine whether it is still structurally stable and capable to resist the loads to which it was designed.

In Brazil, the fire design of concrete structures is regulated by ABNT NBR 15200 [1]. This provision describes the deterioration laws for concrete and reinforcement mechanical properties at elevated temperatures; however, there is no information concerning the materials' residual mechanical properties, which are the mechanical properties of concrete and reinforcement after being exposed to elevated temperatures and cooled down to room temperature.

For the analysis of a structure in a post-fire situation, the residual mechanical properties become more critical than the same properties at high temperatures because the cooling process introduces new stresses into the materials, causing further deterioration and strength loss [2,3]. Therefore, the effects of exposing a concrete structure to elevated temperatures is not only influenced by the maximum temperature reached during a fire but also by how the fire is extinguished.

When a reinforced concrete structure is subjected to a fire event, both concrete and reinforcing steel are damaged by suffering physical changes and mechanical properties degradation. Due to its heterogeneous nature and to the wide variety of materials used for production, concrete may present different behavior trends when exposed to elevated temperatures [2–8]. On the other hand, reinforcing steel seems to be affected by elevated temperatures only above 600 ºC [9–16].

Reinforced concrete is a composite material capable of bearing both compressive and tensile stresses. This unique composite behavior is only possible due to the force-transfer mechanism between the materials; hence, to the bond between them. When a structure is affected by fire, not only the materials are damaged, but also the bond at their interface. In this situation, the force-transfer mechanisms are compromised, as well as the resistant capacity of the structure itself.

This study aimed to experimentally assess the influence of exposure to elevated temperatures on concrete-reinforcement bond development and on the bond failure mechanisms. First, a literature review was carried out on the state-of-the-art of research on post-fire bond properties and the parameters that influence bond development after exposure to elevated temperatures. Second, the influence of degradation, due to exposure to elevated temperatures, of concrete and reinforcing steel on the bond relationship between these materials was analyzed. Then, it was evaluated the influence of concrete cover to bar diameter ratio on concrete-reinforcement bond failure mechanism. Each of the aforementioned residual analyses was carried out after exposure to elevated temperatures (after fire situation) and compared to that of room temperature (before fire situation).

1.2. Objectives

The general objective of this work was to experimentally assess how elevated temperature exposure affects the concrete-reinforcement bond provided the minimum concrete cover allowed by the Brazilian Standards.

Therefore, the following specific objectives have been proposed:

- analysis of the influence of elevated temperatures exposure on the materials' residual mechanical properties and their interface;
- analysis of the influence of the maximum temperature on bond development and bond failure mechanism;
- analysis of the influence of both concrete and reinforcing steel residual mechanical properties on bond development and bond failure mechanism; and
- analysis of the influence of concrete cover to bar diameter ratio on bond development and bond failure mechanism after exposure to elevated temperatures.

1.3. Research significance

After exposure to a fire event, a reinforced concrete structure may be highly damaged. Much concern has been reported on the materials' deterioration and the overall strength loss. However, a key concept of reinforced concrete composite behavior, that is commonly overlooked, is the importance of the existence and integrity of the bond between the materials. The analysis of post-fire stability of a structure and its residual bearing capacity must include a force-transfer-mechanism point of view since this property allows reinforced concrete to work as a composite material.

Based on existing research data it is clear that, as the temperature increases, concrete and reinforcement show different mechanical responses. As a result, not only do both materials deteriorate but their interface is damaged as well. Therefore, the force-transfer mechanisms between the materials are compromised.

Surely, the effect of temperature exposure on bond properties is more complex than the effects on each material individually. Based on that, both the ultimate residual bond strength and the residual bond-slip relationship become critical when assessing the residual capacity of a fire-exposed structure. Hence, the post-fire bond development and bond failure mechanisms should be further studied in order to understand at what level bond damage can become critical and contribute to a structural collapse.

Thus, this work aims to collaborate with the knowledge about the structures behavior in a post-fire situation, aiming to support actions of structural recovery of buildings.

1.4. Dissertation structure

This dissertation has been structured in chapters. This chapter, the first one, contains a general introduction to the concepts that will be further explored throughout this dissertation, the objectives of this research, the research theme justification and an explanation of the structure chosen for this work.

Chapter 2 presents a comprehensive literature review on experimental analysis of concrete-reinforcement bond after exposure to elevated temperatures. This review includes the understanding of the bond mechanism at room temperature, how the materials and their interface are influenced by elevated temperature exposure and, finally, the state-of-the-art of research on residual bond properties.

Chapters 3 and 4 were conceived as articles, which means they are independent works that have abstract, introduction, materials and methods, results and discussion, conclusions, and bibliographic reference. Chapter 3 is a study on how elevated temperatures influence the physical and mechanical properties of the materials and how the changes in these properties may influence the bond behavior and the failure mechanism. Chapter 4 is a study on how bond parameters, as the concrete cover to bar diameter ratio, influences bond development at room temperature and how elevated temperature exposure may change the bond failure mechanism.

The final chapter is a general conclusion of the work presented in the previous chapters. Chapter 5 includes the final considerations and proposals for future research.

References

[1] ABNT - Associação Brasileira de Normas Técnicas. ABNT NBR 15200: Projeto de estruturas de concreto em situação de incêndio. 2011.

[2] Khoury GA. Compressive strength of concrete at high temperatures: A reassessment. Mag Concr Res 1992;44:291–309. https://doi.org/10.1680/macr.1992.44.161.291.

[3] Janotka I, Nürnbergerová T. Effect of temperature on structural quality of the cement paste and high-strength concrete with silica fume. Nucl Eng Des 2005;235:2019–32. https://doi.org/10.1016/j.nucengdes.2005.05.011.

[4] Arioz O. Effects of elevated temperatures on properties of concrete. Fire Saf J 2007;42:516–22. https://doi.org/10.1016/j.firesaf.2007.01.003.

[5] Hertz KD. Concrete strength for fire safety design. Mag Concr Res 2005;57:445–53. https://doi.org/10.1680/macr.2005.57.8.445.

[6] Khoury GA. Effect of fire on concrete and concrete structures. Prog Struct Eng Mater 2000;2:429–47. https://doi.org/10.1002/pse.51.

[7] Piasta J. Heat deformations of cement paste phases and the microstructure of cement paste. Matériaux Constr 1984;17:415–20. https://doi.org/10.1007/BF02473981.

[8] Chan YN, Peng GF, Anson M. Residual strength and pore structure of high-strength concrete and normal strength concrete after exposure to high temperatures. Cem Concr Compos 1999;21:23–7. https://doi.org/10.1016/S0958-9465(98)00034-1.

[9] Xiao J, Hou Y, Huang Z. Beam test on bond behavior between high-grade rebar and high-strength concrete after elevated temperatures. Fire Saf J 2014;69:23–35. https://doi.org/10.1016/j.firesaf.2014.07.001.

[10] Topçu IB, Karakurt C. Properties of reinforced concrete steel rebars exposed to high temperatures. Res Lett Mater Sci 2008;2008. https://doi.org/10.1155/2008/814137.

[11] Neves IC, Rodrigues JPC, Loureiro A de P. Mechanical properties of reinforcing and presstressing stells after heating. J Mater Civ Eng 1996;8:189–94.

[12] Elghazouli AY, Cashell KA, Izzuddin BA. Experimental evaluation of the mechanical properties of steel reinforcement at elevated temperature. Fire Saf J 2009;44:909–19. https://doi.org/10.1016/j.firesaf.2009.05.004.

[13] Tao Z, Wang XQ, Uy B. Stress-strain curves of structural and reinforcing steels after exposure to elevated temperatures. J Mater Civ Eng 2013;25:1306–16. https://doi.org/10.1061/(ASCE)MT.1943-5533.0000676.

[14] Ahmad MS. Effect of Sustained Elevated Temperature on Mechanical Behavior of Reinforcing Bar. Procedia Eng 2017;173:905–9. https://doi.org/10.1016/j.proeng.2016.12.139.

[15] Qian H, Yan D, Chen S, Chen G, Tian Y, Chen G. Effect of High Temperature Exposure and Strain Rate on Mechanical Properties of High-Strength Steel Rebars. J Mater Civ Eng 2019;31:04019261. https://doi.org/10.1061/(asce)mt.1943-5533.0002906.

[16] Qiang X, Bijlaard FSK, Kolstein H. Post-fire mechanical properties of high strength structural steels S460 and S690. Eng Struct 2012;35:1–10. https://doi.org/10.1016/j.engstruct.2011.11.005.

CHAPTER 2:

A review on experimental analysis of concrete-reinforcement bond after exposure to elevated temperatures

Abstract

The composite behavior of reinforced concrete structures is directly related to the bond between concrete and reinforcement. When a reinforced concrete structure is subjected to a fire event, the bond is damaged, the force-transfer mechanism is compromised, as well as the resistant capacity of the structure itself. Over the years, the local bond mechanism that governs the load transfer between the materials at room temperature has been extensively studied and it is well established how each materials' properties influence the bond development. Additionally, the effect of elevated temperature exposure on the materials' properties is also well known. Hence, this study reviewed both the conditions that influence bonding properties at room temperature and the effect of elevated temperature exposure on the materials separately. It was done in order to better understand how they influence each other when combined. The findings showed that elevated temperature exposure progressively reduced the bond strength as the temperature increases. Moreover, the bond failure mechanism can shift from pull-out to splitting due to the damage to the concrete at elevated temperatures, although bond failure mechanisms may not be easily distinguished. Further studies should be conducted to better understand the bond failure mechanism of reinforced concrete after elevated temperature exposure.

Keywords: Bond strength. Elevated temperatures. Concrete. Reinforcement. Bond-slip relationship. Bond failure mechanism.

2.1. Introduction

Reinforced concrete is a composite material that brings together the best of the individual materials' capabilities. As a result, it is a material capable of bearing both compressive and tensile stresses. However, the composite behavior of reinforced concrete structures is directly related to the force-transfer mechanism between the materials; hence, to the bond between them. When the bond is damaged, the force transfer is compromised, as well as the resistant capacity of the structure itself.

If a reinforced concrete structure is subjected to a fire event, both concrete and reinforcing steel are damaged by suffering physical changes and mechanical properties degradation. As the temperature is increased, concrete and reinforcement show different thermal expansion, and their interface is damaged as well; hence, the bond between the materials is compromised.

Surely, the effect of temperature on bond properties is more complex than the effects on each material individually. In this way, this study presents a review on both the conditions that influence bonding properties at room temperature and the effects observed after elevated temperature exposure on the materials separately. This comprehensive review aims to getter information to better understand how these phenomena influence each other when combined. Finally, it is made a review of the existing research on bond properties after exposure to elevated temperatures. The study of residual properties of reinforced concrete is necessary to support the analysis and interventions for the recovery of structures after a fire situation.

2.2. Concrete-reinforcement bond

2.2.1. Local bond mechanisms

Bond can be described as the interaction between the steel bar and the surrounding concrete that allows longitudinal forces to be transferred from one material to the other [1]. The local bond mechanism is composed of three components: chemical adhesion, friction, and, for ribbed bars, a mechanical interlock between the bar lugs and concrete, as shown in Fig. 1. For plain bars, bond is composed mainly of chemical adhesion and friction, although there is some mechanical interlocking due to the roughness of the bar surface [2–4].

For deformed bars, mechanical interlocking plays a major role, whereas chemical adhesion and friction are secondary. Initially, chemical adhesion combined with mechanical interaction prevents any differential slip between the concrete and the bar. After adhesion is destroyed, and slip occurs, the ribs of a bar restrain this movement by bearing against the concrete between the ribs. The compressive bearing forces on the ribs increase the value of the friction forces. As slip increases, friction on the cylindrical concrete surface between adjacent transverse ribs is reduced, leaving the forces at the contact faces between the ribs and the surrounding concrete as the principal mechanism of force transfer [3,4].

Fig. 1. Bond force-transfer mechanisms.

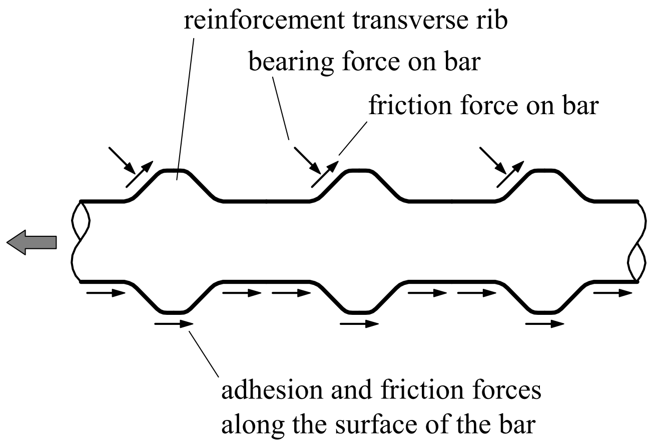

Source: Adapted from ACI 408R-03 (2003) [4].

Bond action generates inclined forces, which radiate outwards in the concrete. The inclined stress is often divided into a longitudinal component, denoted bond stress, and a radial component denoted splitting stress [2,5].

For small embedment length to bar diameter ratios, in which stress can be assumed to be uniformly distributed along the bar, stress resistance of maximum bond can be expressed by Eq. (1):

$$\tau = \frac{P_{max}}{\pi d l_d} \tag{1}$$

where P_{max} is the maximum pull-out load; d is the diameter of the reinforcement and l_d is the embedment length.

Over the years, the parameters influencing bond have been widely studied and previous works have confirmed that bond development is related to the mechanical properties of the concrete [6–9]; the concrete cover around the rebar [7–10]; the presence of confinement

[7,11,12]; bar type [11,13]; the bar diameter [6,10,14]; the embedment length [6,9]; and the geometry of ribs of the reinforcement bar [9,15,16].

2.2.2. Bond failure mechanisms

After adhesion is broken, and slip occurs, the ribs of a bar restrain this movement by bearing against the concrete between the ribs. The compressive stresses radiate from the ribs of the deformed reinforcing bar out into the surrounding concrete, and the radial components of bond forces are balanced by tensile ring stresses in the surrounding concrete. If the tensile stress becomes larger than the tensile strength of the concrete, it may give rise to the formation of a splitting crack along the bar, as shown in Fig. 2 [3–5,17–19].

Fig. 2. Formation of radial cracks.

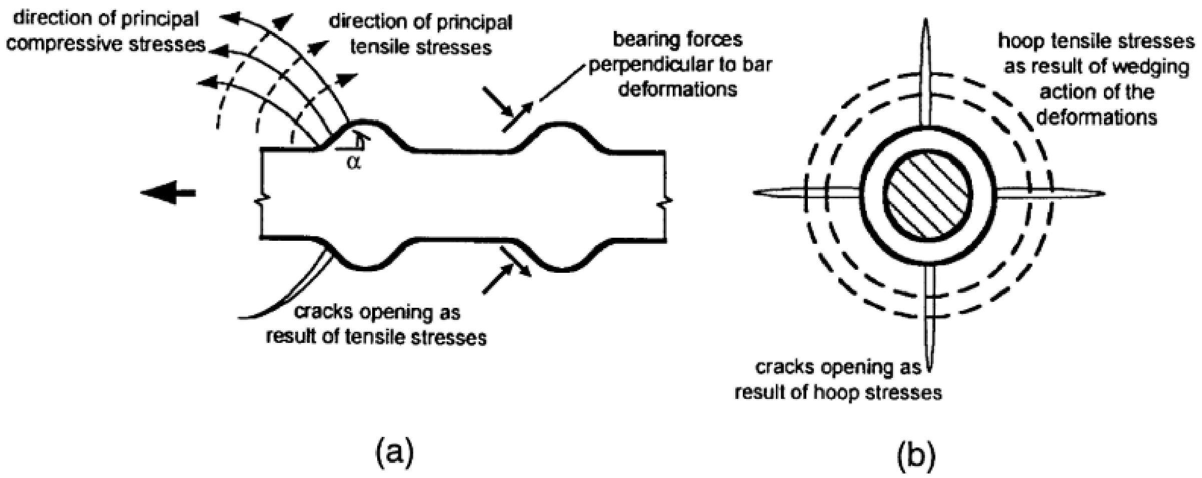

Source: ACI 408R-03 (2003) [4].

During the pull-out process, the concrete between the reinforcement ribs is gradually compressed into powder and compacted in front of the steel ribs, where a new slip surface is formed. It should be pointed out that it is not possible to produce extensive crushing and wedge action in front of every rib without having transverse and longitudinal cracking, caused by the forces produced by the ribs bearing on the concrete [1,3,5,19].

The force is transferred mainly by bearing against the reinforcement ribs, either exceeding the concrete tensile or shearing strength causing the failure by tensile splitting or pull-out (shearing of concrete), respectively. The shear cracking between the adjacent ribs is the upper limit of the bond strength [5,13,20].

To sum up, at room temperature, there are two main bond failure mechanisms, pull-out and splitting. Pull-out failure is due mostly to the shearing-off of the concrete between the rebar ribs and shows no visible splitting cracks. Splitting failure is due mostly to the longitudinal splitting of the concrete surrounding the rebar and bond capacity vanishes once the radial cracks get to the outer surface of the concrete. Generally, pull-out bond failure affects specimens well-confined or with large concrete covers; conversely, splitting failure occurs when there is no confinement or limited concrete cover [1,5,17,21].

However, actual anchorages and splices – which are usually long – exhibit more complex failure modes and there could occur a third bond failure mechanism, a pull-out failure induced by concrete splitting. This mechanism is identified when there are visible splitting cracks on the concrete cover but the bond fails by the shearing-off of the concrete between the reinforcement ribs [1].

2.2.3. Bond-slip relationship

According to the fib Model Code (2010) [21], the analytical bond stress-slip relationship for monotonic loading at room temperature can be represented by the curves shown in Fig. 3.

Fig. 3. Analytical bond stress-slip relationship for monotonic loading at room temperature

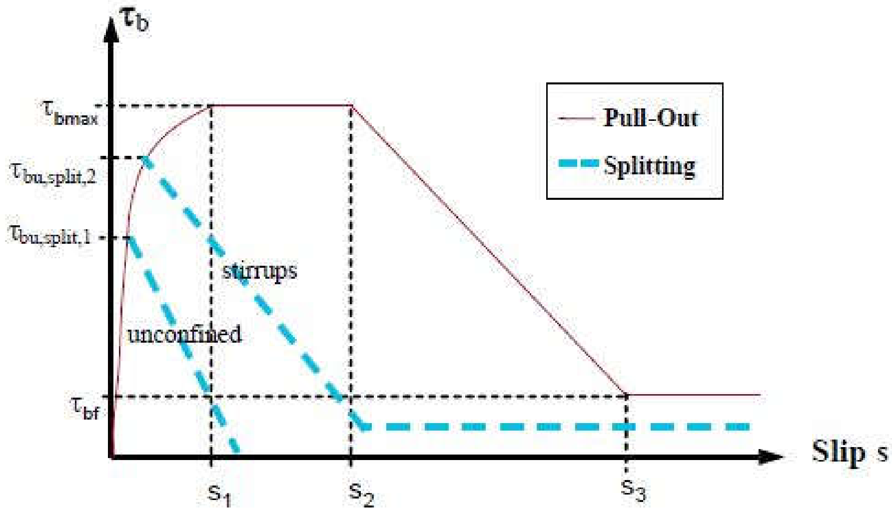

Source: fib Model Code (2010) [21].

In this model, maximum bond strength for pull-out failure is valid for well-confined concrete (concrete cover $\geq 5d$) and can be estimated as a function of the concrete compressive strength itself, as shown in Eq. (2). On the other hand, splitting failure is described as a much more complex mechanism that can be estimated as a function of various parameters, according to Eq. (3):

$$\tau_{bmax} = 2.5\sqrt{f_{cm}} \tag{2}$$

$$\tau_{bu,split} = 6.5\,\eta_2 \left(\frac{f_{cm}}{25}\right)^{0.25} \left(\frac{25}{\Phi}\right)^{0.25} \left[\left(\frac{c_{max}}{\Phi}\right)^{0.33} \left(\frac{c_{max}}{c_{min}}\right)^{0.10} + k_m k_{tr}\right] \leq \tau_{bmax} \tag{3}$$

where:

η_2 is a factor to consider whether the bar is anchored in good or bad conditions;

f_{cm} is the mean concrete compressive strength [MPa];

Φ is the bar diameter [mm];

c_{max}/c_{min} are the maximum and minimum concrete covers;

$k_m k_{tr}$ are factors to consider the existence of confinement by transverse reinforcement;

τ_{bmax} is the ultimate pull-out strength [MPa].

2.2.4. Bond testing

There are four main kinds of specimens used for bond testing, as shown in Fig. 4. The pull-out specimen is the most commonly used because of its simplicity; however, this is the least realistic of the four main test specimens, because as the bar is placed in tension, the concrete is placed in compression, which is not an actual representation of a real structure. This stress state differs markedly from most reinforced concrete members, in which both the bar and the surrounding concrete are in tension.

Fig. 4. Bond testing specimens: a) pull-out; b) beam-end specimen; c) beam anchorage specimen; and d) splice specimen.

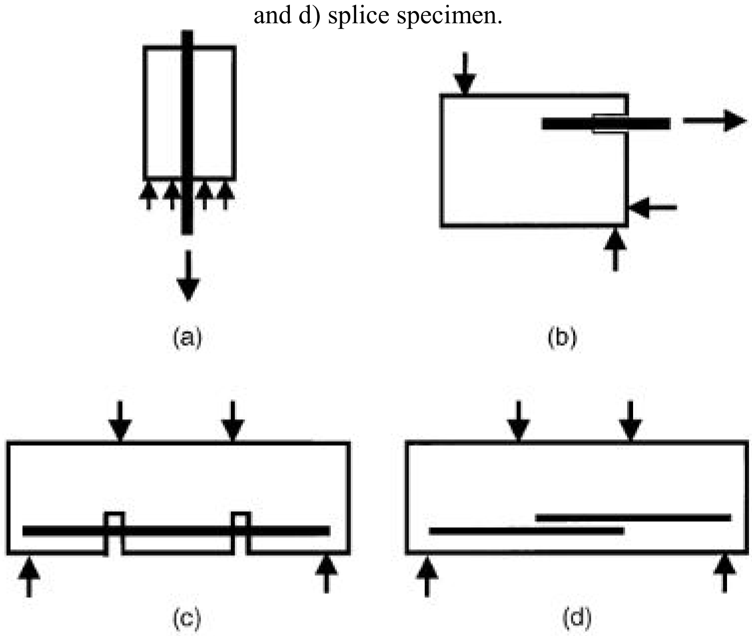

Source: ACI 408R-03 (2003) [4].

Beam-end specimens provide more realistic measures of bond strength in actual structures; the reinforcing steel and the surrounding concrete are simultaneously placed in tension. Beam anchorage and splice specimens represent larger-scale specimens designed to directly measure development and splice strengths in full-size members. The anchorage specimen simulates a member with a flexural crack and a known bonded length. The splice specimen, normally fabricated with the splice in a constant moment region, is easier to fabricate and produces similar bond strengths to those obtained with the anchorage specimen. [4]

2.3. Reinforced concrete after elevated temperature exposure

2.3.1. Concrete

The behavior of concrete, as a material, when exposed to elevated temperatures, is a complex process because it depends not only on its constitution (which is extremely adjustable) but also on experimental factors (e.g. target temperature, time of exposure, and heating rate). Generally, the higher the exposure temperature, the greater the reduction of concrete's residual mechanical properties (e.g. modulus of elasticity, compressive and tensile strengths) [22,23,32–38,24–31]. The heat exposure causes the deterioration of concrete due to physical and chemical changes on its microstructure, to the thermal incompatibility between the cement paste and the aggregates, and to the testing parameters adopted in the heating and cooling processes [22,23,39].

2.3.1.1. Physicochemical changes in the cement paste

The main concrete deterioration mechanism for temperatures up to 105 ºC is moisture loss. At this temperature range, concrete loses its free, physically adsorbed, and interlayer water [25,29,40–43]. When the temperature reaches the 100-200 ºC range, concrete starts to lose its chemically bound water as well due to the C-S-H dehydration [40,44]. At this temperature range, the partial C-S-H dehydration is associated with weight loss and concrete porosity increase [38,45,46] and the cement paste loses its stability due to physical and chemical reactions caused by water evaporation.

The pore pressure created by the evaporable moisture affects the rate of hydrothermal reactions and produces tensile stresses in the concrete. The temperature increase, combined with the rising vapor pressure, creates an autoclave effect in the inner concrete, enabling the thermal activation of un-hydrated cement grains. This phenomenon, which is especially verified in high-strength concrete, is responsible for the strength maintenance observed in some concretes for temperatures up to 300 ºC [29,47].

As temperature increases, the cement paste shrinks due to moisture loss, whereas the aggregates undergo a thermal-induced expansion. This thermal incompatibility produces high tensile stresses at the interfacial transition zone [26,39,44,48,49]. For temperatures above 300 ºC, the cement paste experiences the coarsening of its pore structure and a significant increase in microcracking [44]. As temperature increases, the microcracks around calcium-hydroxide (CH) crystals expand. When the temperature reaches 400 ºC, it is also possible to notice the formation of microcracks around the un-hydrated cement grains [39].

Chemical decomposition, moisture loss, and microcracking are responsible for major changes in the cement paste microstructure. The main physical effect observed is the increase in concrete porosity, which can be interpreted as the pore structure coarsening both in size and distribution [33,40,49–52]. This can be verified especially for temperatures above 400 ºC, due to the dehydration of the CH [25,33,42,44,49,51,53].

CH dehydration is associated with major concrete weight loss [38,46]; however, it does not result in immediate strength reduction at hot state. The critical issue of the CH decomposition does not present itself during heating, but afterward in the cooling process. The CH decomposition results in the presence of free limestone (CaO) in the concrete, which rehydrates in the cooling process due to moisture absorption. The CaO re-hydration results in concrete expansion, further cracking, and strength loss [44,49]. When the temperature exceeds 600 ºC, the C-S-H decomposition becomes the main mechanism influencing concrete cracking and strength loss [25,39,42,44,49,54]. This later stage of C-S-H decomposition starts around 560 ºC, but is only above 600 ºC that it becomes significant and, then, the dehydration rate increases drastically as temperature rises [54].

For temperatures in the range 580-900 ºC, concrete undergoes its third major weight loss, due to the decomposition of $CaCO_3$ [38,39,46,49].

2.3.1.2. High-strength concrete

Mostly, concrete's high strength is obtained by incorporating reactive products with ultrafine particles into the mixture. These particles have a pore-filler effect, resulting in a denser microstructure and lower porosity [26,47,48,50].

Although the denser microstructure is a major factor in enhancing the concrete's strength, it may also be destructive as it makes concrete more susceptible to spalling [23,26,28,35,48]. Due to its low permeability, high-strength concrete experiences the development of higher pore pressures during heating. Also, the peak pressure build-up is located closer to the heated surface [23].

Furthermore, the heating process creates a thermal gradient between the concrete surface and its inner part, inducing the development of compressive stresses near the surface (due to the restrained expansion) and tensile stresses in the inner part. As a result of the pore pressure build-up and the stresses created by the thermal gradient, cracks appear parallel to the concrete surface. The cracking can also be accompanied by a sudden energy release and violent failure of the heated surface region [23].

2.3.1.3. Aggregates

Since thermal incompatibility between aggregates and the cement paste plays a major role in microcracking, the concrete's residual strength is highly influenced by the aggregate type [25,40,44].

The properties of each aggregate type depend on its chemical composition. For instance, lightweight aggregates, as expand clay, which is formed by incineration or vulcan eruption, have low heat conductivity and high thermal stability. On the other hand, siliceous and calcareous aggregates are less stable when exposed to elevated temperatures [44,48].

Siliceous aggregates have higher expansion than calcareous aggregates and, as a result, cause more damage to concrete at high temperatures. Around 573 ºC the quartz crystal structure present in siliceous aggregates experiences an endothermic crystalline α–β phase transformation, which is accompanied by an instantaneous increase in volume. This transition is reversible, but the radial cracks around the quartz grains caused by the expansion can be traced after cooling [49,55,56].

The effects of heat exposure on concrete are summarized in Table 1.

Table 1.
Summary of the physicochemical changes on concrete due to elevated temperature exposure.

Temperature	Changes	Effect on concrete
Up to 100 ºC	Loss of free, physically adsorbed, and interlayer water	Porosity increase [25,29,38,40–43,45,46]
100 ºC - 200 ºC	C-S-H starts to dehydrate	
300 ºC	Autoclave effect in the inner region of concrete	Thermal activation of un-hydrated cement grains [29,47]
	Increase in ITZ microcracking and concrete porosity	Strength loss [44]
480 ºC - 550 ºC	CH dehydration	Weight loss [25,49,51,53] Extensive cracking and strength loss during the cooling process [44,49]
573 ºC	Quartz transformation	Aggregate expansion and concrete cracking [25,40,49,55,56]
600 ºC	Decomposition of calcareous aggregate	
600 ºC - 900 ºC	C-S-H complete decomposition	Weight and strength loss [25,38,39,42,44,46,49,54]
	CaCO3 decomposition	

Source: Author (2021).

2.3.1.4. Concrete residual mechanical properties

a) *Compressive strength*

Fig. 5 shows an overview of experimental results on the concrete residual compressive strength after exposure to elevated temperatures. Also, Fig. 5 presents regression curve obtained based on the available data among the references included. The regression curve shows an overall declining trend for the residual compressive strength, even though some results around 200 ºC show an increase of the residual compressive strength. The wide range of results is directly related to the concrete constitution, pore structure density, and experimental parameters.

Fig. 5. Overview of experimental results for residual compressive strength after high-temperature exposure.

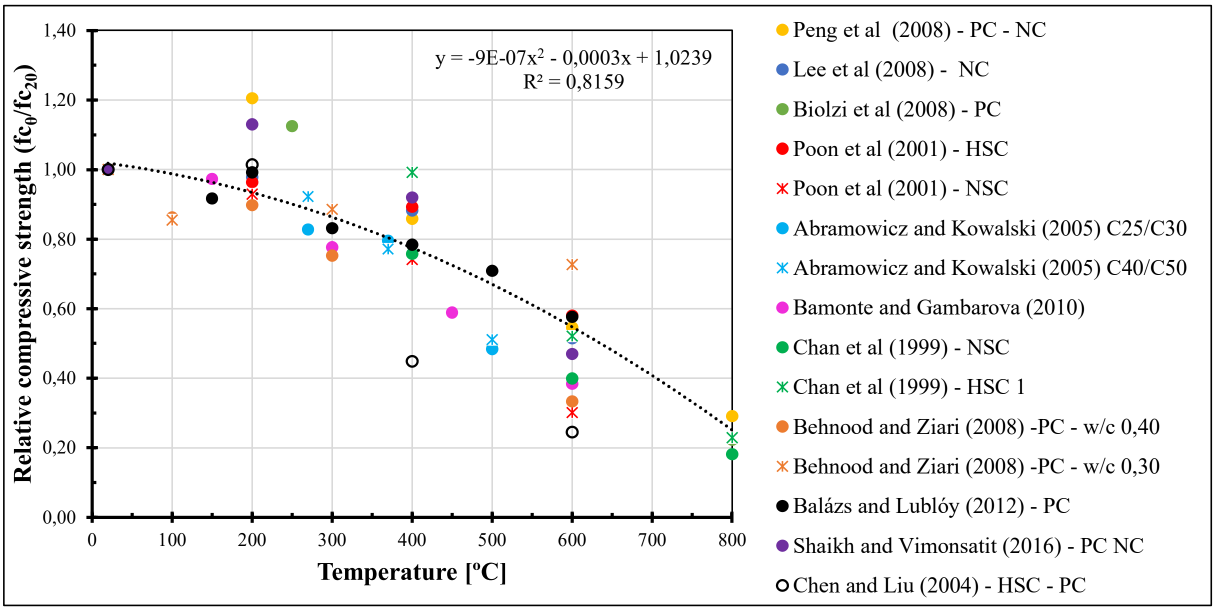

Source: Author (2021). Data extracted from [26,27,59,33–38,57,58].

Generally, only a small part of the initial strength is changed and most concrete mixtures maintain or even slightly increase their residual compressive strength up to 200 ºC [27,34,45,48]. After exposure to 400 ºC, the residual compressive strength is around 80%. For higher temperatures, concrete suffers a severe mechanical properties degradation due to the microcracking and the decomposition of the hydrated products [25,33,42,44,49,51,53,56,60].

b) Tensile strength

Fig. 6 shows an overview of experimental results on the concrete residual tensile splitting strength after exposure to elevated temperatures. As observed for the compressive strength, there is a high variation among the results obtained by each reference. Nonetheless, there is a clear deterioration trend as exposure temperature increases.

The concrete tensile strength reduction, both in bending and splitting, is sharper than the compressive strength [22,28,30,31,61]. This could be related to the key role played by the bond between the cement paste and the aggregates when analyzing the concrete tensile strength [29].

The interfacial transition zone (ITZ) microcracking reduces the valid area of concrete cross-section whereas the presence of tensile stresses increases the length of the cracks. Therefore, the effect of thermal cracking is more noticeable in the reduction of the tensile strength than the compressive strength [22,28]. Additionally, for both bending and splitting, the reduction of the concrete's residual tensile strength shows an almost linear tendency for temperatures above 200 ºC [48].

Fig. 6. Overview of experimental results for residual tensile splitting strength after high-temperature exposure.

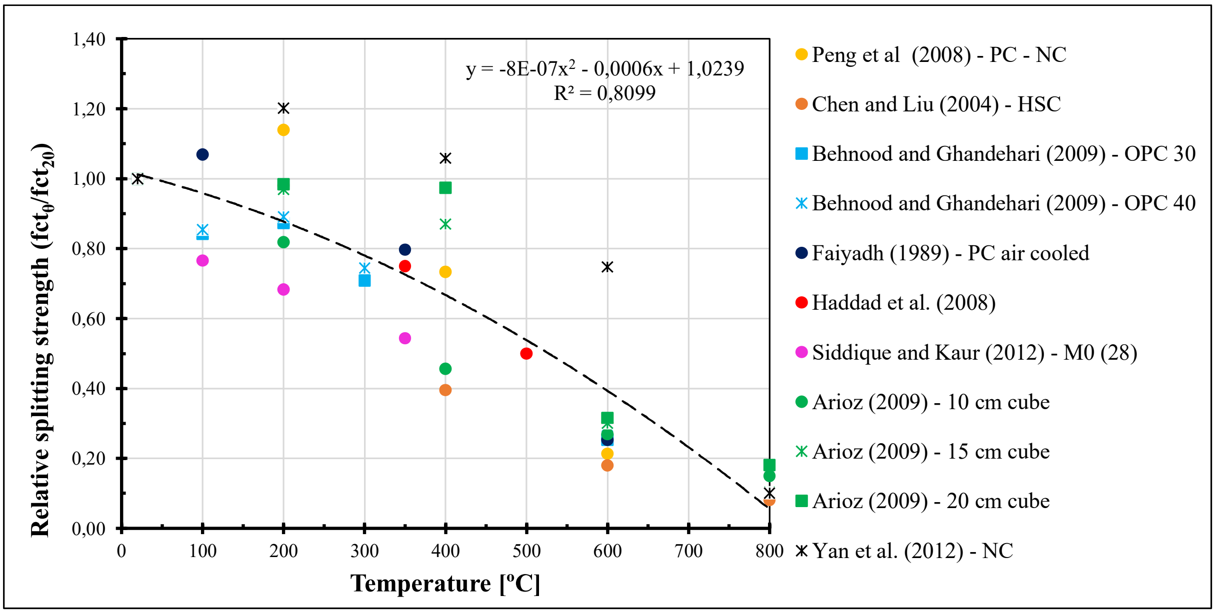

Source: Author (2021). Data extracted from [30,34,59,61–65].

c) Modulus of elasticity

The exposure to high temperatures seems to have a softening effect on the concrete, which means that the higher the temperature, the flatter the tension-strain curve. Hence, it leads to smaller peak tensions occurring to higher values of strains [45,48,56,60].

This behavior is similar to the concrete residual tensile strength, as both are more affected by elevated temperature exposure than the concrete compressive strength [23]. The modulus of elasticity reduction also shows an almost linear tendency [31,60,66], which could be related to the gradual moisture loss, the ITZ microcracking and the decomposition of the hydrated composites [67,68].

Fig. 7 shows an overview of experimental results on the concrete residual modulus of elasticity after exposure to elevated temperatures. In contrast to the compressive and tensile splitting strengths, commented before, the modulus of elasticity presents early signs of deterioration and is extremely reduced at temperatures above 300 ºC.

Fig. 7. Overview of experimental results for residual modulus of elasticity after high-temperature exposure.

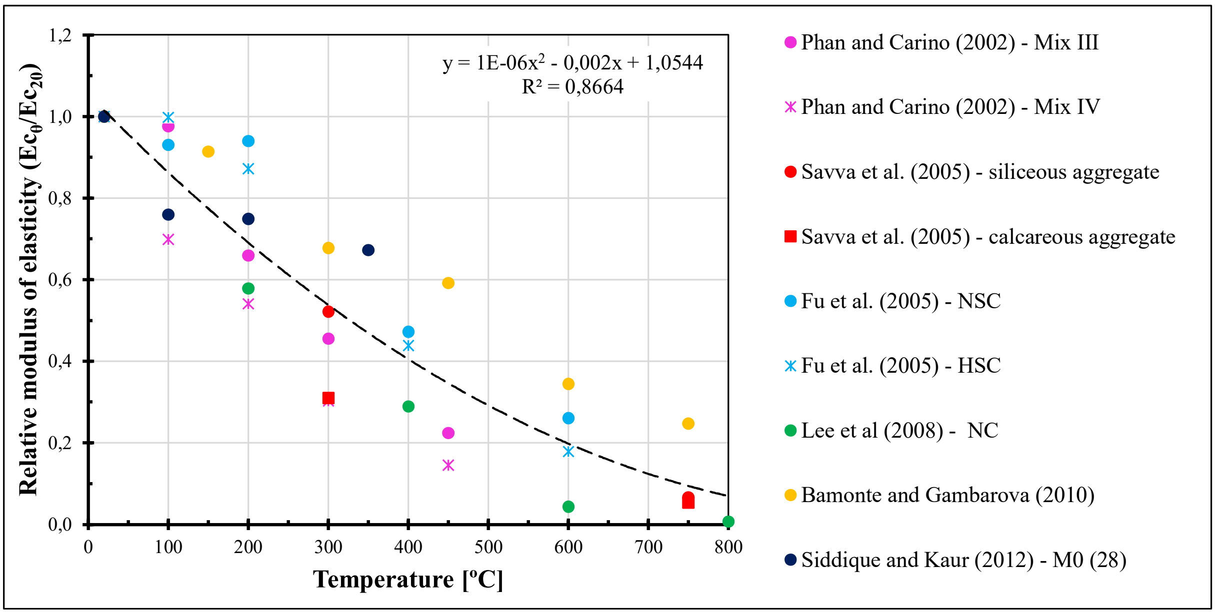

Source: Author (2021). Data extracted from [37,38,56,60,64,66].

2.3.1.5. Cooling method

The cooling process leads to further concrete damage, which causes an additional reduction of its mechanical properties. This late deterioration is due to concrete cracking induced by differential thermal deformations and the re-hydration of chemical compounds that have dehydrated in the heating process [40,45].

Furthermore, the damage can be related to the duration of the cooling process. Specimens quickly cooled (either by quenching water or immersion) present greater concrete deterioration when compared to air-cooled specimens, which could be explained by the extra concrete cracking produced by thermal shock [24,36,72,38,40,45,58,61,69–71].

2.3.2. Reinforcing steel bar

It has been reported by many researchers that heat exposure, up to 600 ºC, does not significantly affect the residual mechanical properties of both hot-rolled and cold-worked reinforcement bars [73–80], as shown in Fig. 8. As the exposure temperature increases above this temperature range, the steel's mechanical properties progressively deteriorate, the yield strength and ultimate strength decrease substantially due to pearlite in the rebar turned to austenite at around 727 ºC [73].

There is a decreasing trend of elastic modulus, yield strength and ultimate strength with an increase in temperature; also, the reduction in yield strength is higher in comparison to ultimate strength [73,78]. Moreover, it seems the grade of the rebar also influences its residual behavior, since researchers have observed that higher-grade rebars are more sensitive to heat exposure than ordinary steel bars [74,79,80].

It seems as reinforcing steel bars can regain their nominal yield strength after being exposed to temperatures below 600 °C, which is positive for the reuse of high strength steel structures after a fire [80].

Fig. 8. Stress-strain curves for HBR 600 steel at various temperatures.

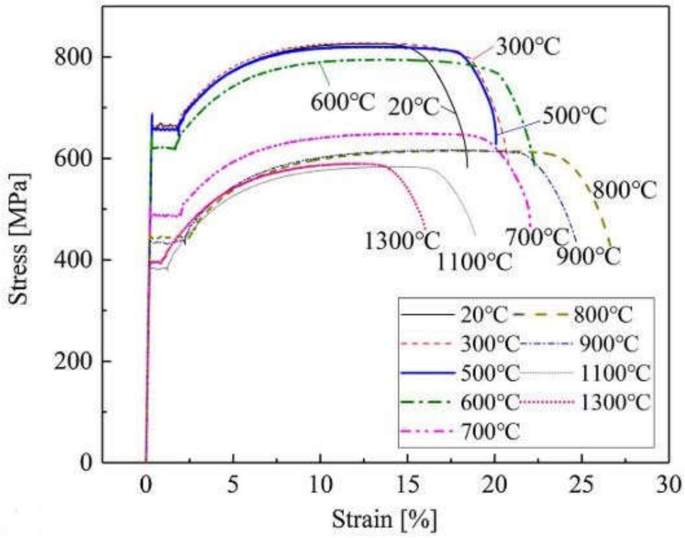

Source: Qian et al. (2019) [79]

2.3.3. Elevated temperature effects on concrete-reinforcement interface

The concrete and the reinforcing bar have different thermal expansion coefficients. So, when exposed to elevated temperatures, the rebar tends to expand more than the surrounding concrete. As a result of this differential thermal expansion, compressive stresses arise in the cement paste matrix acting perpendicular to the bar axis, as shown in Fig. 9. If the differential expansion stresses are higher than the splitting resistance of the concrete cover, then radial splitting cracks will be formed and the bond between the materials will be affected [17,81,82].

Fig. 9. Differential thermal expansion of concrete and steel rebar: (a) cross-section of the reinforced concrete cylinder at normal temperature; (b) expansion of the reinforcement bar and the concrete cover with the temperature increment; (c) radial pressure caused by differential thermal expansion.

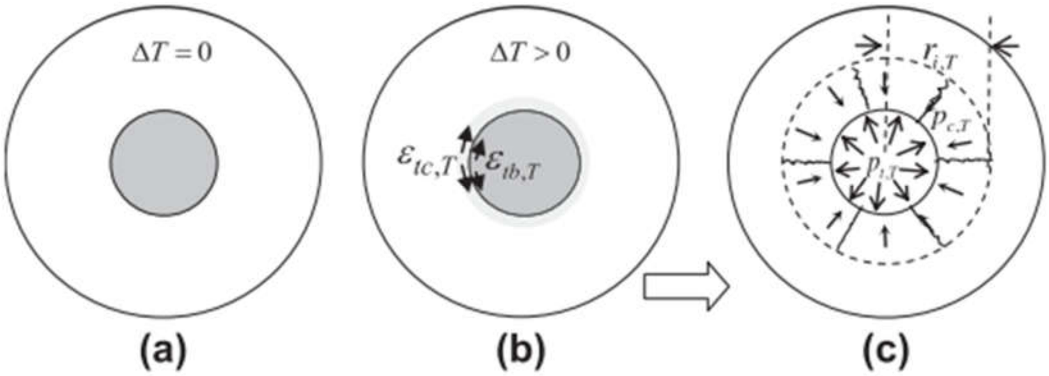

Source: Pothshiri and Panedpojaman (2012,2013) [81,82]

2.4. Bond behavior after elevated temperature exposure

After exposure to temperatures up to 600 ºC, a limited effect on the mechanical properties of reinforcing steel can be observed. Thus, changes in the bond-slip relationship and its characteristics upon exposure to fire may be attributed mainly to physical and chemical changes of the concrete [83].

Elevated temperature exposure affects bond behavior not only by thermal degradation of concrete but also by the interfacial cracking induced by the differential thermal expansion, which may limit the proportion of stress transfer from concrete to steel, triggering partial bond loss [17,83,84]. The high temperature induced interfacial cracking reduces the depth of uncracked concrete cover, hence reducing the confinement provided to the rebar. Furthermore, the later enforcement of the pull-out load enlarges the pre-existing heat-induced cracks, as shown in Fig. 10 [17,63,81,82,84].

Fig. 10. Modeling of the pressure resistance of the concrete cover under the pull-out load and the thermal effect: (a) residual concrete cover; (b) pressure resistance of the concrete cover.

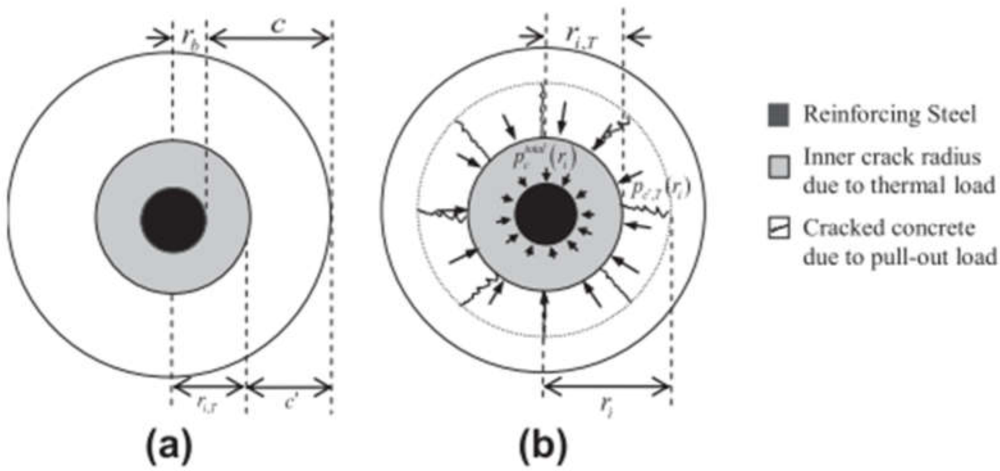

Source: Pothshiri and Panedpojaman (2012,2013) [81,82]

Zhao et al. [85] studied the effect of heat exposure on the concrete-reinforcement interface. They assessed the damage to chemical adhesion due to different thermal expansion between concrete and steel, and the coefficient of friction after elevated temperatures. The results show that the chemical adhesion decreases with a linear function of experienced temperatures within the range from 20 to 600 ºC. After 800 ºC, chemical adhesion is not measurable. The friction coefficient increases negligibly with elevated temperatures.

Over the years, some studies have been developed on concrete-reinforcement bond after exposure to elevated temperatures; however, as can be seen in Table 2, there is no standard test or specimen to assess bond properties both at room temperature and after heat exposure.

Table 2.
Summary of references that experimentally assessed the bond properties of reinforced concretes exposed to elevated temperatures.

Reference	Materials¹	Temperature	Specimen characteristics²	Embedment length³	Bond break	Test
Morley and Royles [86]	NSC, plain and deformed bar	20-750 ºC	Cylindrical (*h* = 30, *d* changeable)	*lb*/*d* = 2.0	Not mentioned	Pull-out
Morley and Royles [87]	NSC, plain and deformed bar	20-750 ºC	Cylindrical (*h* = 30, *d* = 12.6)	*lb*/*d* = 2.0	Not mentioned	Pull-out
Haddad and Shannis [83]	HSC, deformed bar	600, and 800 ºC	Cylindrical (*d* = 10, *h* = 15)	Full-length bond		Pull-out
Haddad et al. [63]	HSFRC (HS, BCS and PP fiber) Deformed and plain bars	350, 500, 600, and 700 ºC	Prismatic (10x10x40)	*lb*/*d* = 7.5	Both ends (plastic sleeves)	Double pull-out
Bingöl and Gül [88]	NSC, deformed bar	50 ºC interval up to 500 ºC, 600, and 700 ºC	Cylindrical (*d*=10, *h*=20)	6, 10 and 16 cm	Not mentioned	Pull-out
Yin et al. [89]	NSC, deformed bar	300, 500, and 700 ºC	Prismatic (15x15x16)	80 mm	Loaded-end (PVC tube)	Pull-out
Hassan [90]	NSFRC (Carbon Fibers) Ribber bar	150, 250, 350, 450, and 550 ºC	Cube (15x15x15)	*lb*/*d* = 3.0	Both ends (plastic tube)	Pull-out
Lublóy and György [91]	HSC, deformed bar	150, 300, 500, and 800 ºC	Cylindrical (*d* =12, *h* =10)	40 mm	Loaded-end (steel sleeves)	Pull-out
Arel and Yazici [92]	NSC, deformed bar	300, and 500 ºC	Cube (15x15x15)	*lb*/*d* = 5.0	Not mentioned	Pull-out
Xiao et al. [73]	HSC, deformed bar	200, 400, 500, and 600 ºC	Beam specimens (10x18x 68)	*lb*/*d* = 5.0 and 10.0	Both ends (PVC pipe)	Beam bond test
Yang et al. [93]	RAC, deformed and plain bars	300, 400, and 500 ºC	Cube (15x15x15)	*lb*/*d* = 5.0	Both ends (PVC pipe)	Pull-out
Ergün et al. [94]	NSC, deformed and plain bars	100, 200, 400, 600, and 800 ºC	Cylindrical (*d* = 15, *h* = 30)	250 mm	Not mentioned	Pull-out
Li et al. [95]	NSFRC (PVA fiber)	200, 400, 600, and 800 ºC	Cube (15x15x15)	40-100 mm	Both ends (PVC tube)	Pull-out
Hlavčka [96]	HSC, deformed bar	50, 150, 300, 500, 600, and 800 ºC	Cylindrical (*d* = 12, *h* = 10)	40 mm	Loaded-end (steel sleeves)	Pull-out
Bošnjak et al. [97]	NSC, deformed bar	ISO 834 fire curve	Prismatic (30x45x64)	*lb*/*d* = 5.0	Both ends (plastic tube)	Beam-em modified
Yang et al. [98]	NSC, deformed bar	300, 400, and 500 ºC	Cube (20x20x20)	*lb*/*d* = 2.0	Both ends (PVC sleeves)	Pull-out
Shamseldein et al. [99]	NSC Deformed and plain bars	800 ºC	Beam-end (20x30x60)	*lb*/*d* = 5.0	Both ends (plastic tube)	Beam-end
Varona et al. [100]	HSFRC (PP and steel fibers), deformed bar	450, 650, and 825 ºC	Cylindrical (*d* = 12,5, *h* = 12)	50 mm	Loaded-end (paper pipe.)	Pull-out

Reference	Materials[1]	Temperature	Specimen characteristics[2]	Embedment length[3]	Bond break	Test
Ghazaly et al. [101]	NSC, deformed bar	600, and 800 ºC	Beam-end (20x30x60)	*lb*/*d* = 5.0	Both ends (PVC pipe)	Beam-end
Zhang et al. [102]	HSC, deformed bar	200, 400, 600, and 800 ºC	Cube (20x20x20)	40 mm	Both ends (PVC tube)	Pull-out
Rashid et al. [103]	NSC, deformed bar	150, 250, 350, and 500 ºC	Cylindrical (*d* = 10, *h* = 20)	Full-length	Loaded-end groove.	Pull-out
Sharma et al. [104]	NSC, deformed bar	300, 500, and 700 ºC	Prismatic (16x16x30)	*lb*/*d* = 8.0	Both ends (glass tube)	Pull-out Eccentric pull-out
Deshpande et al. [105]	FRCC (Steel and PVA fibers), deformed bar	100, 200, 400, 600, and 800 ºC	Cylindrical (*d* = *h* =15,2)	*lb*/*d* = 3.0	Both ends (PVC pipe)	Pull-out
Ba et al. [106]	NSC, deformed bar	100, 200, 400, 600, and 700 ºC	Cube (15x15x15)	60 mm	Both ends (PVC sleeves)	Eccentric pull-out
Zou et al. [107]	NCA and RCA deformed bar	200, 400, and 600 ºC	Cube (15x15x15)	*lb*/*d* = 5.0	Loaded-end (glass tube)	Pull-out
Fakoor and Nematzadeh [108]	HSFRC (steel fiber) Deformed bars	200, 400, and 600 ºC	Cube (16x16x16)	*lb*/*d* = 5.0	Loaded-end (plastic sleeve)	Pull-out

[1] NSC is normal strength concrete, HSC is high strength concrete, NSFRC is normal strength fiber reinforced concrete, HSFRC is high strength fiber reinforced concrete, RAC is recycled aggregate concrete, RCA is recycled coarse aggregate, NCA is natural coarse aggregate, NWC is normal weight concrete and FRCC is fiber-reinforced cementitious composite.
[2] All the given dimensions are in cm (*h* is height, *d* is diameter, *a* x *b* x *c* are dimensions of the parallelepiped specimen)
[3] *lb* is bar embedded length and *d* is bar diameter.

Source: Author (2021).

2.4.1. Effect of elevated temperature exposure on bond strength and bar slip

Mostly, residual bond strength behavior with increasing temperatures is governed by concrete degradation (Fig. 11). Hence, for temperatures up to 200 ºC, maintenance or a slight decrease of bond strength has been observed. At 300 ºC, residual bond+ strength is around 80% of its value at room temperature. For temperatures above 400 ºC, a distinct fall in maximum residual bond strength is observed [63,73,99,101,109,110,83,86,88,89,92,94–96].

Fig. 11. Bond strength degradation after exposure to elevated temperatures as a function of concrete strength.

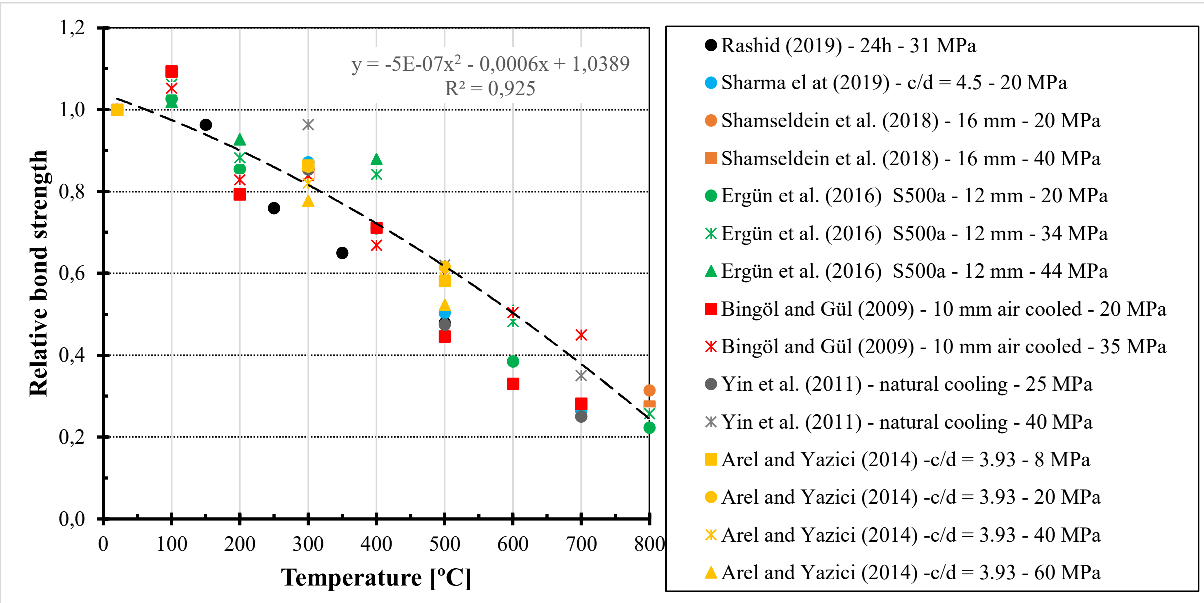

Source: Author (2021). Data extracted from [88,89,92,94,104,110].

Apparently, no additional bond-strength-deterioration trend can be identified compared to the residual compressive strength of concrete. Some researchers have identified that it follows a trend similar to the concrete residual compressive strength deterioration [86,104,108,109,111]; in contrast, there are also reports on the bond strength been more affected than the compressive strength [91,96,110]. Similar conflicting results have been reported for the bar slip at maximum bond strength. In some experiments, a higher slip was observed [63,73,83,86,99], whereas others exhibited a reduction of the slip at bond failure [89,101,110].

Although most references do not make a distinction between pull-out and splitting bond failure, this could be directly related to the bond failure mechanism. Bošnjak et al. [97] observed that heat exposure can lead to a change in the failure mode from pure bond failure to a combined bond/splitting failure and even to a splitting failure. Royles and Morley [86] and Sharma et al. [104] observed that the bond strength follows a similar trend as the compressive strength and presents higher slippage when the specimen fails by pull-out of the rebar. On the other hand, if a splitting failure takes place, the bond strength seems to follow a degradation trend closer to the concrete splitting tensile strength and the slip would be smaller.

Haddad and Shannis [83] observed that at relatively low to medium pullout loads, the cracks formed due to heating tended to close, allowing high slippage. Once the cracks were closed, resistance against slip increased, and so was pullout load needed to cause further slippage. Prior to failure, local crushing of concrete at the tips of rebars ribs accompanied with induced hoop stresses weakened resistance to slippage. This resulted in a significant slippage followed by a splitting sudden failure of concrete along the rebars.

Further studies should be carried out to evaluate the change in bond failure mechanism observed by Bošnjak et al. [97] and the degradation trend observed by Royles and Morley [86] and Sharma et al. [104]. Additionally, more tests should be conducted for providing data to build a better understanding of the effect of heat exposure on bond failure mechanism and bond-slip relationship.

2.4.2. Effect of elevated temperature exposure on the bond-slip curves

The shape of force-slip curves also changes after exposure to elevated temperatures. Once again, the temperatures above 400 ºC seem to be more harmful to the bond properties due to the advanced deterioration of concrete [86,87,109,111].

After elevated temperatures, the degradation of the bond strength can be verified also by the softening of the bond-slip relationship. The stiffness of the bond strength-slip curve reduces as the exposure temperature is increased. The slope of ascending portion of the bond-slip curves gradually declined with increasing temperature and the descending portion of the curves tended to flatten [81,93,99,104,107,109].

Moreover, the reduction of the bond stiffness does not seem to be affected by the bond failure mechanism. Sharma et al. [104] observed that irrespective of the failure mode or concrete cover, the bond stiffness after exposure to relatively high temperatures (500 °C and 700 °C) was found to be quite low and of a similar order for all the specimens.

Based on the information observed by previous researchers, it was created a schematic diagram that illustrates the effect of elevated temperatures on the bond-slip curve, as shown in Fig. 12. In general, above 400 °C, it is observed that the initial stiffness decreases, the value of maximum adhesion decreases and the maximum stress level tends to present greater displacements.

Fig. 12. Schematic representation of the effect of elevated temperature exposure on the bond-slip curves.

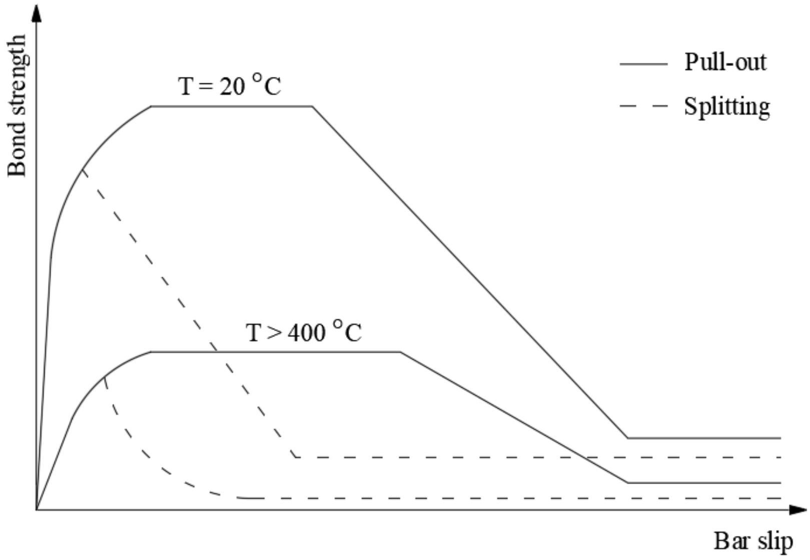

Source: The author (2021)

2.4.3. Parametric analysis

Table 3 presents a summary of the parameters analyzed by researchers over the years concerning concrete-reinforcement bond properties after heat exposure. The effect of elevated temperatures in each of these parameters will be analyzed in the section.

Table 3.
Summary of parameters analyzed experimentally by the references on bond properties of reinforced concretes after exposed to elevated temperatures.

Year	Reference	Concrete properties	Rebar properties	Embedment length	Concrete cover	Confinement	Cooling method	Fiber	Corrosion	Empirical Model	Numerical Model
1983	Royles and Morley [86,87]		✓		✓						
2004	Haddad [83]	✓			✓					✓	
2008	Haddad et al. [63]	✓						✓		✓	
2009	Bingöl and Gül [88]	✓		✓			✓				
2011	Yin et al. [89]	✓					✓				
2012	Hassan [90]							✓			
2014	Lublóy and György [91]	✓						✓		✓	
2014	Arel and Yazici [92]	✓			✓					✓	
2014	Xiao et al.[73]	✓	✓	✓		✓			✓	✓	
2016	Yang et al. [93]	✓				✓				✓	
2016	Ergün et al. [94]	✓	✓							✓	
2016	Khalaf et al. [112]									✓	
2016	Sharma et al. [84]				✓						✓
2017	Li et al. [95]		✓	✓			✓	✓			
2017	Hlavčka [96]	✓						✓		✓	✓
2018	Yang et al. [98]	✓							✓	✓	
2018	Bošnjak et al. [97]				✓						✓
2018	Shamseldein et al. [99]	✓	✓			✓					
2018	Raouffard and Nishiyama [111]	✓								✓	
2018	Varona et al. [100]	✓						✓		✓	
2018	Ghazaly et al. [101]	✓		✓	✓					✓	
2019	Zhang et al. [102]								✓		
2019	Rashid et al. [103]	✓									
2019	Sharma et al. [104]				✓	✓				✓	
2020	Deshpande et al. [105]							✓			
2020	Ba et al. [106]				✓	✓			✓		
2020	Zou et al. [107]	✓								✓	
2021	Fakoor and Nematzadeh [113]		✓		✓			✓		✓	

Source: Author (2021).

2.4.3.1. *Bar diameter and embedment length*

The experimental results of residual bond strength after exposure to elevated temperatures as a function of the embedment length to bar diameter ratio are shown in Fig. 13.

Fig. 13. Bond strength degradation after exposure to elevated temperatures as a function of *lb*/*d* ratio.

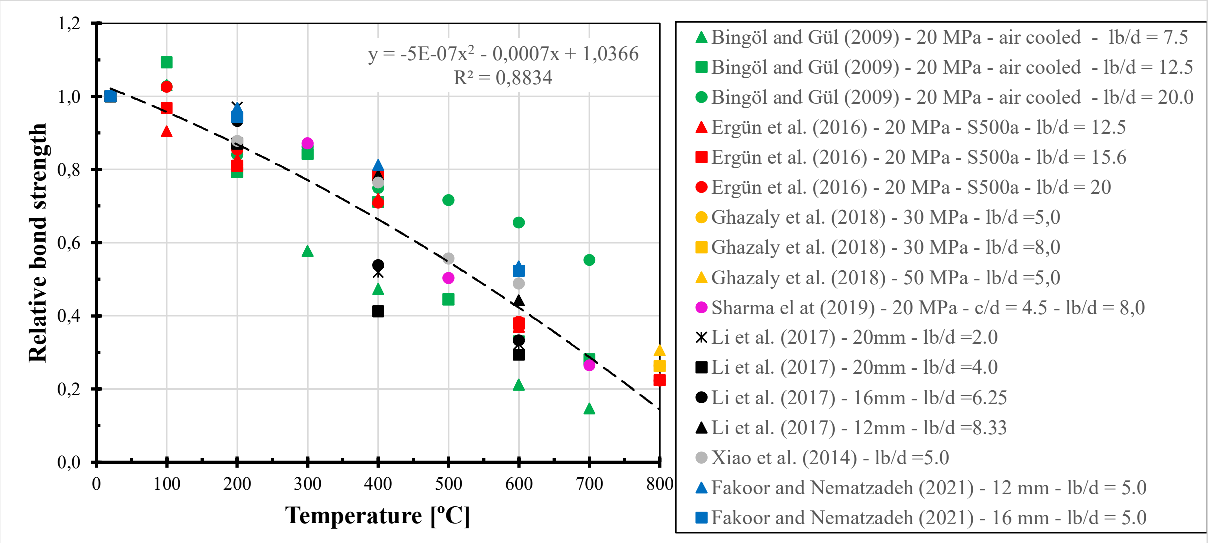

Source: Author (2021). Data extracted from [73,88,94,95,104,113,114].

Bingöl and Gül [88] tested 8.0 mm rebars embedded into concrete blocks with three embedment lengths: 6, 10, and 16 cm. It was observed that an increase in the embedment length – hence, an increase in embedment length to bar diameter ratio – caused an increase in residual bond strength.

Ergün et al. [94] studied the post-heating bond strengths of 12, 16, and 20 mm rebars with 250 mm embedment length. As the diameter of the bar increased – and the embedment length to bar diameter ratio decreased – the residual bond strength decreased. According to the authors, this would be explained by the fact that increasing the bar diameter, reduces the ratio of perimeter to area; hence, the bond strength is reduced as well.

Li et al. [95] studied the bond strength of steel bars embedded in high-performance fiber-reinforced cementitious composite before and after exposure to elevated temperatures. The authors analyzed three bar diameters and 40, 60, 80, and 100 mm embedment length. The results show that increasing the embedment length from 40 to 100 mm reduced the bond strength by up to 41% at room temperature, 46% at 400 ºC, and 55% at 800 ºC.

Ghazaly et al. [101] evaluated the bond strength for heat-damaged and repaired beam-end specimens. The authors observed a slight decrease in bond strength with the increase of the bonded length from 5d to 8d.

Shamseldein et al. [99] studied the restoration of heat-damaged reinforced concrete members. They observed that for the same embedment length to bar diameter ratio, the original, residual, and restored bond strengths decreased with the increase of the bar diameter from 16 to 22 mm.

Undoubtedly, the data analyzed do not show a clear tendency; hence, further studies should be conducted to clarify the relationship between the bar diameter and the embedment length in bond strength degradation after exposure to elevated temperatures.

2.4.3.2. Concrete cover and bar diameter

Increasing the bar diameter seems to have a negative effect on the bond strength [94,95,99]. Nevertheless, this parameter should not be singly analyzed, since its influence is highly connected to that of the concrete cover depth and embedment length. As listed in Table 3, some references have chosen to study the influence of bar diameter, whereas others have chosen to analyze the effect of concrete cover; however, since there are no standards for the shape or size of the specimens used in those studies, to compare the results based on absolute values of concrete cover does not seem ideal. Hence, this section was conceived around the relative variable that combines both factors into one single parameter, the concrete cover to bar diameter ratio (c/d).

It is important to point out that all the effects of concrete cover investigated in this section were analyzed from a residual-bond-strength perspective, which means that the absolute values of bond strength were not considered, since it depends on each specimen configuration. The experimental results of residual bond strength after exposure to elevated temperatures, as a function of the concrete cover to bar diameter ratio, are shown in Fig. 14.

The c/d ratio is directly related to the bond failure mechanism, as the confinement provided by the concrete cover may define the extent of the pull-out splitting cracks. As the exposure temperature increases and the c/d ratio declines, the failure of the specimen tends toward the splitting failure mode [106,108].

Reinforced concrete with lower concrete cover values is more sensitive to bond strength degradation at elevated temperatures, particularly when concrete with lower compressive strength is used. This could be explained by the fact that a thicker concrete cover is able to act better as a thermal barrier and causes fewer thermal cracks [82]. Generally, the thicker the concrete cover, the higher the bond strength and the ultimate slip at failure [81,82,86,87,92,101,104].

Specimens with larger c/d usually fail by pull-out of the bar and, the reduction of bond strength with increasing temperatures is comparable to the concrete compressive strength reduction. On the other hand, specimens with smaller c/d generally fail by splitting of the concrete cover and are comparable to the pattern of the tensile strength reduction. Furthermore, there is a substantial reduction in absolute peak bond strength when bond failure mode changes from bar pull-out to splitting [86,104,108].

For exposure temperatures below 500 ºC, the concrete cover has a major effect on bond strength. However, for temperatures above 500 ºC, the concrete cover thickness has a limited effect on the bond strength. This can be explained by the fact that, after exposure to this range of temperature, both the strength and the stiffness of concrete are drastically lowered, and therefore, the concrete cover cannot provide a similar level of confinement to the rebar as present in the case of ambient temperatures [104,106].

Fig. 14. Bond strength degradation after exposure to elevated temperatures as a function of the c/d ratio.

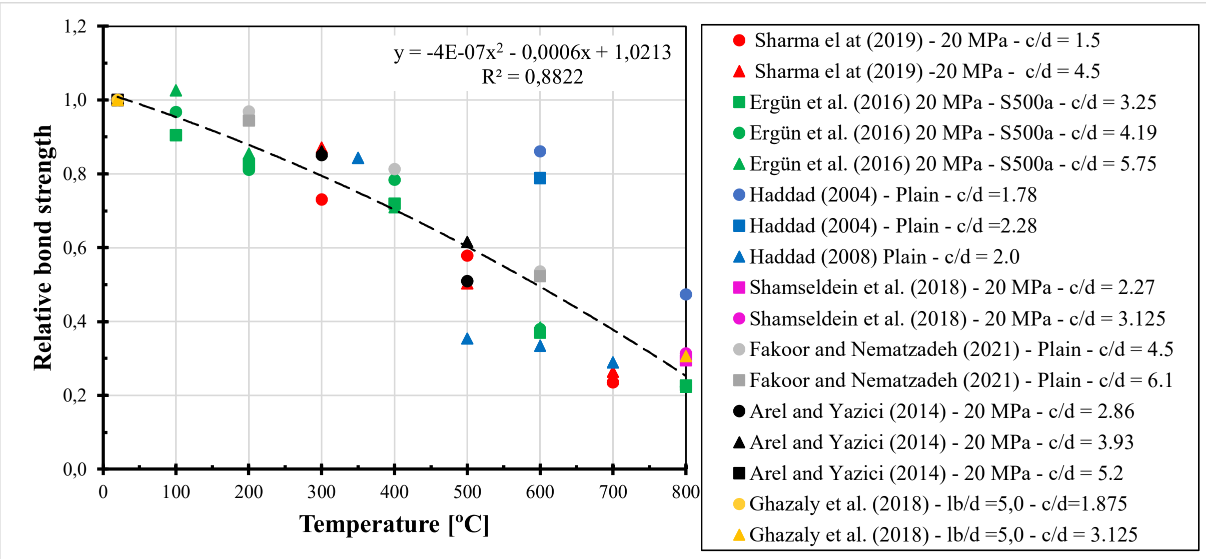

Source: Author (2021). Data extracted from [83,92,94,99,104,113,114].

2.4.3.3. *Confinement*

Generally, higher confinement leads to higher residual bond strengths and bar slips. The results observed over the years suggest that the confinement provided by stirrups prevent early concrete cracking and contributes to avoiding or delaying splitting bond failure.

Yang et al. [93] analyzed the bond performance between deformed bars and recycled aggregate concrete (RAC) after exposure to elevated temperatures. The authors observed that specimens with stirrups exhibit higher values of bond strength and peak slip than those of specimens without stirrups. However, as the temperature elevates, the deviations of the bond strength and the peak slip between the specimens with stirrups and the specimens without stirrups continually grow small.

Sharma et al. [104] tested the influence of concrete cover on residual bond strength. They observed that the presence of a stirrup in the mid-length of the bonded zone could not limit the splitting crack width as compared to the case without stirrup. However, a stronger increase in the splitting crack width was observed in the post-peak region for the specimen without the stirrup in the bonded zone. Hence, the presence of stirrups would collaborate to a ductile behavior of bond failure by limiting the crack opening and, as a result, the degradation in bond strength would be relatively gradual.

Shamseldein et al. [99] studied the assessment and restoration of the bond of heat-damaged reinforced concrete elements. They tested beam-end specimens and positioned the pull-out rebar inside and outside the stirrups. The results showed that ultimate bond strength slightly increased while the bar slip significantly increased for the bar located inside the transverse reinforcement.

2.4.3.4. Cooling method

Since elevated temperatures induced concrete degradation is the key reason for bond strength degradation after elevated temperatures exposure, it is clear that the cooling method used in pull-out specimens would affect bond strength similarly.

Bingöl and Gül [88] observed that the cooling process does not affect bond strength for small embedment lengths. However, specimens with greater embedment lengths seem to be affected by the thermal shock caused by rapid cooling.

Yin et al. [89] tested the residual bond strength of two concrete mixes after exposure to elevated temperatures and being cooled naturally or in water. They observed that the cooling method has a great influence on the bonding strength and that on water-cooled specimens bond strength reduces much more than natural-cooled specimens.

Li et al. [95] observed that water cooling further reduced bond strength. This is likely because water-cooling caused a sudden change of temperature gradient, resulting in more thermal cracks and thus reduced bond strength.

2.4.4. Residual bond of fiber-reinforced concrete

Generally, fibers are used in concrete because of their contribution to controlling crack formation and propagation [63,115,116]. Moreover, for elevated temperature exposed concretes, fibers may limit spalling and improve residual mechanical properties.

The incorporation of polypropylene (PP) fibers results in the reduction of spalling effects after elevated temperature exposure. The PP fibers melt around 170 ºC and, the melted fiber beds create a porous network that enables the water to be vaporized and expelled at a lower temperature. Therefore, the use of fibers leads to a large decrease in the extent of the pressure fields that build up in the concrete during heating, hence reducing internal pressure damage and spalling effects [57,95,116–118]. At the same time, the significant increase in void proportion may also lead to strength reduction and material softening after exposure to elevated temperature [50,108,117,119].

On the other hand, steel fibers do not melt, and they act as a bridging component, preventing the formation and propagation of cracks. Hence, the incorporation of steel fiber leads to an improvement in mechanical properties and a better resistance to high temperature effects [50,57,108,119–121].

Steel fiber addition to normal and high strength concretes is capable of improving not only the concrete's mechanical properties but also the post-heating residual bond strength and the stiffness of the bonding law [63,121]. Furthermore, due to its crack-limiting properties, steel fibers seem to be able to control the splitting failure of the concrete cover [100].

Although the effect of fiber addition on concrete's residual mechanical properties has been extensively studied, data on its effect on bond behavior is still limited. Some of the results observed in available works are summarized in Fig. 15. Generally, fiber addition contributes positively to the bond properties after exposure to elevated temperature when compared to plain concrete; however, it could also be destructive depending on factors as the type of fiber and fiber content [63,96,105,108,118].

Fig. 15. Bond strength degradation of fiber reinforced concrete after exposure to elevated temperatures.

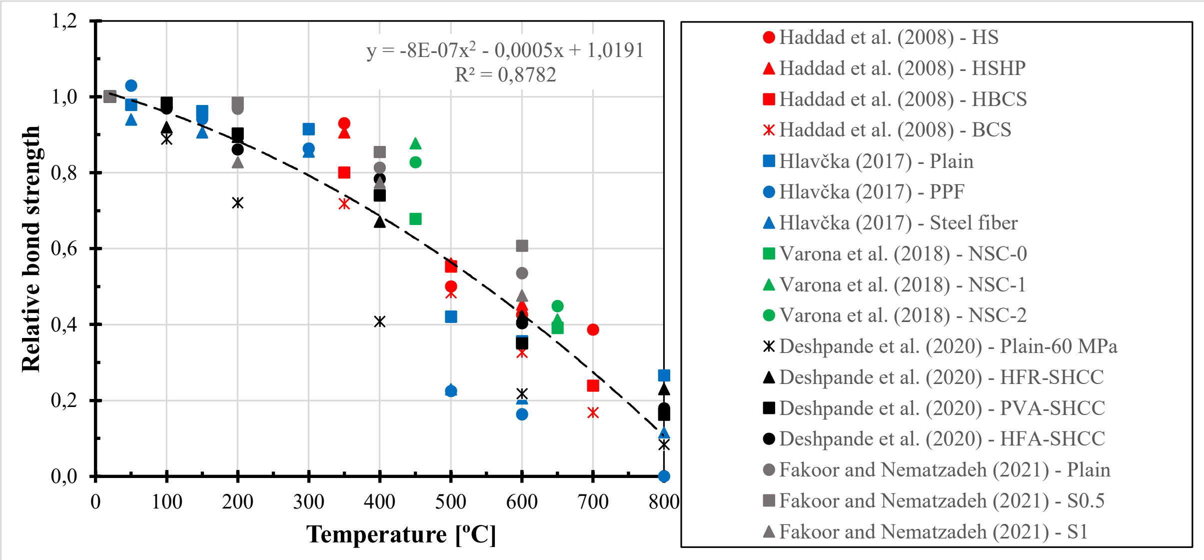

Source: Author (2021). Data extracted from [63,96,100,105,113]

2.4.5. Residual bond of corroded reinforcement

For deformed bars at ambient temperature, the influence of corrosion in bond strength is directly related to the existence of confinement provided by stirrups. Generally, without confinement, the corrosion products tend to expand which, for low levels of corrosion, is beneficial for both concrete strength and bond strength [122–125]. This effect may be amplified by temperatures up to 200 ºC with relatively low corrosion loss [98].

However, as the level of corrosion increases, the expansion of the corrosion products induces concrete cracking, and the integrity of the concrete cover is destroyed, which lowers the confinement and accelerates the deterioration of bond even at ambient temperature [122–125]. The rate and severity of bond performance degradation after temperatures exposure for corroded specimens with corrosion-induced cracks generally increases with temperature, which means that highly corroded specimens are more sensitive to temperature exposure than uncorroded specimens [102].

When the rebar is severely corroded, the deformed ribs are damaged and the mechanical interlocking is lessened, hence the bond failure mechanism is more prone to pull-out both at room temperature and after heat exposure [106,125].

On the other hand, when there is proper confinement, corrosion-induced concrete cracking is limited or inexistent, and the bond strength is not substantially affected at ambient temperature [122,123]. In this case, high-temperature exposure reduces both the concrete strength and the cohesion between concrete and steel bar as micro-cracks propagate in the concrete matrix. Thus, the bond failure mechanism is dependent on the ultimate temperature reached, under 600 ºC specimens are prone to pull-out failure and, for 700 ºC or higher, specimens tend to exhibit splitting failure [106].

For smooth bars, a similar behavior can be observed. For low levels of corrosion, there is a beneficial effect on bond strength. However, as soon as the corrosion-induced cracks appear, bond strength decreases rapidly. Nevertheless, there is an important difference in bond mechanism when compared to deformed bars. As bond to plain bars is made up only of chemical adhesion and friction, the expansion of the corrosion products and the increase in friction may have a greater impact than that of deformed bars [122].

The experimental results of residual bond strength after exposure to elevated temperatures as a function of the corrosion level is shown in Fig. 16.

Fig. 16. Bond strength degradation after exposure to elevated temperatures as a function of the corrosion level (CL).

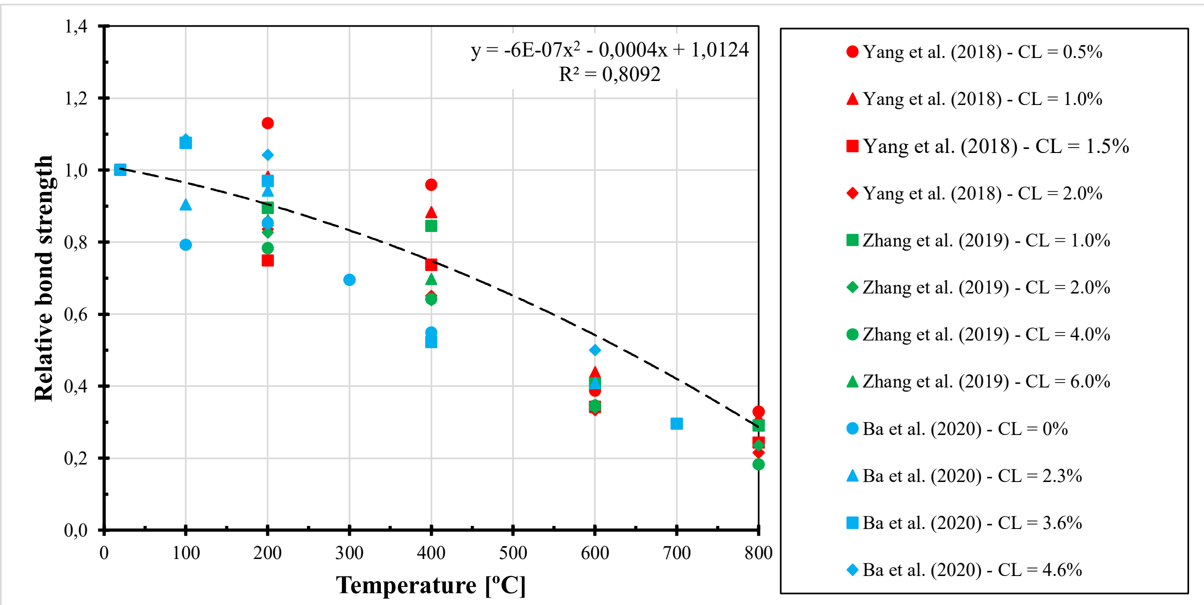

Source: Author (2021). Data extracted from [98,102,106]

2.5. Conclusions

This work conducted a review on bond mechanism at room temperature, the elevated temperature exposure effects on concrete and reinforcement, and, finally, the bond properties after exposure to elevated temperatures. According to the studies analyzed in this paper, the following conclusions are drawn:

- The high temperature induced physical-chemical changes in concrete's microstructure are the critical issue affecting the concrete-reinforcement bond degradation after exposure to elevated temperatures. The steel suffers negligible damage for temperatures up to 600 ºC.
- The ultimate bond strength and the associated bar slip are highly affected by elevated temperatures. As exposure temperature increases, the ultimate bond strength reduces. For temperatures above 400 ºC, bond strength is considerably damaged.
- As temperature increases, the bond stiffness reduces. The slope of ascending portion of the bond-slip curves gradually declined with increasing temperature and the descending portion of the curves tended to flatten.
- The concrete cover to bar diameter ratio becomes especially important in post-heating situations because the elevated temperature induced cracks make concrete susceptible to a splitting bond failure.
- The cooling process is also a critical stage for post-heating situations because the use of quenching water accelerates the free limestone rehydration process, which results in further damage both to the concrete's compressive strength and to the bond.
- Incorporation of fibers in pullout specimens enhanced post-heating residual bond strength between reinforcing steel and concrete. Furthermore, the fibers contributed to increasing bond ductility and the stiffness of the bonding law.
- For low levels of corrosion and temperatures up to 200 ºC, the expansion of corrosion products has a beneficial effect on bond properties. However, as corrosion level increases, the concrete cover cracks and the specimen becomes more vulnerable to high temperature damage.
- Further studies should be conducted to better understand the bond failure mechanism of reinforced concrete after elevated temperature exposure.

References

[1] Tepfers R, Achillides Z, Azizinamini A, Balázs G, Bigaj-van-Vliet A, Cabrera J, et al. fib Bulletin 10. Bond of reinforcement in concrete. vol. 7. fib. The International Federation for Structural Concrete; 2000. https://doi.org/10.35789/fib.BULL.0010.

[2] Sulaiman MF, Ma CK, Apandi NM, Chin S, Awang AZ, Mansur SA, et al. A Review on Bond and Anchorage of Confined High-strength Concrete. Structures 2017;11:97–109. https://doi.org/10.1016/j.istruc.2017.04.004.

[3] Lutz BLA, Gergely P. Mechanics of Bond and Slip of Deformed Bars in Concrete. ACI J Proc 1967;64:711–21. https://doi.org/10.14359/7600.

[4] ACI Committee 408. ACI 408R-03 Bond and Development of Straight Reinforcing Bars in Tension. Am Concr Inst 2003:1–49.

[5] Lundgren K. Bond between ribbed bars and concrete. Part 1: Modified model. Mag Concr Res 2005;57:371–82. https://doi.org/10.1680/macr.2005.57.7.371.

[6] Diab AM, Elyamany HE, Hussein MA, Al Ashy HM. Bond behavior and assessment of design ultimate bond stress of normal and high strength concrete. Alexandria Eng J 2014;53:355–71. https://doi.org/10.1016/j.aej.2014.03.012.

[7] Desnerck P, Lees JM, Morley CT. Bond behaviour of reinforcing bars in cracked concrete. Constr Build Mater 2015;94:126–36. https://doi.org/10.1016/j.conbuildmat.2015.06.043.

[8] Arel HŞ, Yazici Ş. Concrete-reinforcement bond in different concrete classes. Constr Build Mater 2012;36:78–83. https://doi.org/10.1016/j.conbuildmat.2012.04.074.

[9] Tastani SP, Pantazopoulou SJ. Direct tension pullout bond test: Experimental results. J Struct Eng 2010;136:731–43. https://doi.org/10.1061/(ASCE)ST.1943-541X.0000159.

[10] Hadi MNS. Bond of High Strength Concrete with High Strength Reinforcing Steel~!2008-07-24~!2008-10-28~!2008-11-26~! Open Civ Eng J 2008;2:143–7. https://doi.org/10.2174/1874149500802010143.

[11] Torre-Casanova A, Jason L, Davenne L, Pinelli X. Confinement effects on the steel-concrete bond strength and pull-out failure. Eng Fract Mech 2013;97:92–104. https://doi.org/10.1016/j.engfracmech.2012.10.013.

[12] Hamad BS, Machaka MF. Effect of transverse reinforcement on bond strength of reinforcing bars in silica fume concrete. Mater Struct Constr 1999;32:468–76. https://doi.org/10.1007/bf02482719.

[13] Ahmad S, Pilakoutas K, Rafi MM, Uz Zaman Khan Q, Neocleous K. Experimental investigation of bond characteristics of deformed and plain bars in low strength concrete. Sci Iran 2018;25:2954–66. https://doi.org/10.24200/sci.2017.4570.

[14] Harajli M, Hamad B, Karam K. Bond-slip response of reinforcing bars embedded in plain and fiber concrete. J Mater Civ Eng 2002;14:503–11. https://doi.org/10.1061/(ASCE)0899-1561(2002)14:6(503).

[15] Barbosa MTG, de Souza Sánchez Filho E, de Oliveira TM, dos Santos WJ. Analysis of the relative rib area of reinforcing bars pull out tests. Mater Res 2008;11:453–7. https://doi.org/10.1590/S1516-14392008000400013.

[16] Darwin D, Zuo J, Tholen ML, Idun EK. Development length criteria for conventional and high relative rib area reinforcing bars. ACI Struct J 1996;93:347–59. https://doi.org/10.14359/9694.

[17] Hertz K. The anchorage capacity of reinforcing bars at normal and high temperatures n.d.

[18] Tepfers R. A Theory of Bond Applied to Overlapped Tensile Reinforcement Splices for Deformed Bars. PhD Thesis, Chalmers Univ Technol 1973:1–330.

[19] Goto Y, Otsuka K. Internal Cracks Formed in Concrete Around Deformed Tension Bars. 1978:160–2.

[20] Zhao W, Zhu B. Basic parameters test and 3D modeling of bond between high-strength concrete and ribbed steel bar after elevated temperatures. Struct Concr 2017;18:653–67. https://doi.org/10.1002/suco.201600005.

[21] fib. fib Model Code 2010 - Final draft - Volume 1. vol. 7. Weinheim, Germany: Wiley-VCH Verlag GmbH & Co. KGaA; 2013.

[22] Chan YN, Peng GF, Anson M. Residual strength and pore structure of high-strength concrete and normal strength concrete after exposure to high temperatures. Cem Concr Compos 1999;21:23–7. https://doi.org/10.1016/S0958-9465(98)00034-1.

[23] Khoury GA. Effect of fire on concrete and concrete structures. Prog Struct Eng Mater 2000;2:429–47. https://doi.org/10.1002/pse.51.

[24] Chan SYN, Luo X, Sun W. Effect of high temperature and cooling regimes on the compressive strength and pore properties of high performance concrete. Constr Build Mater 2000;14:261–6. https://doi.org/10.1016/S0950-0618(00)00031-3.

[25] Arioz O. Effects of elevated temperatures on properties of concrete. Fire Saf J 2007;42:516–22. https://doi.org/10.1016/j.firesaf.2007.01.003.

[26] Behnood A, Ziari H. Effects of silica fume addition and water to cement ratio on the properties of high-strength concrete after exposure to high temperatures. Cem Concr Compos 2008;30:106–12. https://doi.org/10.1016/j.cemconcomp.2007.06.003.

[27] Biolzi L, Cattaneo S, Rosati G. Evaluating residual properties of thermally damaged concrete. Cem Concr Compos 2008;30:907–16. https://doi.org/10.1016/j.cemconcomp.2008.09.005.

[28] Li M, Qian CX, Sun W. Mechanical properties of high-strength concrete after fire. Cem Concr Res 2004;34:1001–5. https://doi.org/10.1016/j.cemconres.2003.11.007.

[29] Cülfik MS, Özturan T. Mechanical properties of normal and high strength concretes subjected to high temperatures and using image analysis to detect bond deteriorations. Constr Build Mater 2010;24:1486–93. https://doi.org/10.1016/j.conbuildmat.2010.01.020.

[30] Arioz O. Retained properties of concrete exposed to high temperatures: Size effect. Fire Mater 2009:211–22. https://doi.org/10.1002/fam.996.

[31] Xiao J, König G. Study on concrete at high temperature in China - An overview. Fire Saf J 2004;39:89–103. https://doi.org/10.1016/S0379-7112(03)00093-6.

[32] Ergün A, Kürklü G, Serhat Başpnar M, Mansour MY. The effect of cement dosage on mechanical properties of concrete exposed to high temperatures. Fire Saf J 2013;55:160–7. https://doi.org/10.1016/j.firesaf.2012.10.016.

[33] Janotka I, Bágel L. Pore structures, permeabilities, and compressive strengths of concrete at temperatures up to 800°C. ACI Mater J 2002;99:196–200. https://doi.org/10.14359/11713.

[34] Peng G-F, Bian S-H, Guo Z-Q, Zhao J, Peng X-L, Jiang Y-C. Effect of thermal shock due to rapid cooling on residual mechanical properties of fiber concrete exposed to high temperatures. Constr Build Mater 2008;22:948–55. https://doi.org/10.1016/j.conbuildmat.2006.12.002.

[35] Poon CS, Azhar S, Anson M, Wong YL. Comparison of the strength and durability performance of normal- and high-strength pozzolanic concretes at elevated temperatures. Cem Concr Res 2001;31:1291–300. https://doi.org/10.1016/S0008-8846(01)00580-4.

[36] Abramowicz M, Kowalski R. The influence of short time water cooling on the mechanical properties of concrete heated up to high temperature. J Civ Eng Manag 2005;11:85–90. https://doi.org/10.1080/13923730.2005.9636336.

[37] Bamonte P, Gambarova PG. Thermal and mechanical properties at high temperature of a very high-strength durable concrete. J Mater Civ Eng 2010;22:545–55. https://doi.org/10.1061/(ASCE)MT.1943-5533.0000058.

[38] Lee J, Xi Y, Willam K. Properties of concrete after high-temperature heating and cooling. ACI Mater J 2008;105:334–41. https://doi.org/10.14359/19894.

[39] Piasta J. Heat deformations of cement paste phases and the microstructure of cement paste. Matériaux Constr 1984;17:415–20. https://doi.org/10.1007/BF02473981.

[40] Khoury GA. Compressive strength of concrete at high temperatures: A reassessment. Mag Concr Res 1992;44:291–309. https://doi.org/10.1680/macr.1992.44.161.291.

[41] Georgali B, Tsakiridis PE. Microstructure of fire-damaged concrete. A case study. Cem Concr Compos 2005;27:255–9. https://doi.org/10.1016/j.cemconcomp.2004.02.022.

[42] Kim KY, Yun TS, Park KP. Evaluation of pore structures and cracking in cement paste exposed to elevated temperatures by X-ray computed tomography. Cem Concr Res 2013;50:34–40. https://doi.org/10.1016/j.cemconres.2013.03.020.

[43] Feldman RF, Ramachandran VS. Differentiation of interlayer and adsorbed water in hydrated portland cement by thermal analysis. Cem Concr Res 1971;1:607–20. https://doi.org/10.1016/0008-8846(71)90016-0.

[44] Hertz KD. Concrete strength for fire safety design. Mag Concr Res 2005;57:445–53. https://doi.org/10.1680/macr.2005.57.8.445.

[45] Janotka I, Nürnbergerová T. Effect of temperature on structural quality of the cement paste and high-strength concrete with silica fume. Nucl Eng Des 2005;235:2019–32. https://doi.org/10.1016/j.nucengdes.2005.05.011.

[46] Mendes A, Sanjayan JG, Collins F. Long-term progressive deterioration following fire exposure of OPC versus slag blended cement pastes. Mater Struct Constr 2009;42:95–101. https://doi.org/10.1617/s11527-008-9369-7.

[47] Saad M, Abo-El-ENein SA, Hanna GB, Kotkata MF. Effect of temperature on physical and mechanical properties of concrete containing silica fume. Cem Concr Res 1996;26:669–75.

[48] Ma Q, Guo R, Zhao Z, Lin Z, He K. Mechanical properties of concrete at high temperature-A review. Constr Build Mater 2015;93:371–83. https://doi.org/10.1016/j.conbuildmat.2015.05.131.

[49] Lin W, Lin TD. Microstructures of Fire-Damaged Concrete 1997:199–205.

[50] Chan YN, Luo X, Sun W. Compressive strength and pore structure of high-performance concrete after exposure to high temperature up to 800 °C. Cem Concr Res 2000;30:247–51.

https://doi.org/10.1016/S0008-8846(99)00240-9.
[51] Mendes A, Sanjayan J, Collins F. Phase transformations and mechanical strength of OPC/Slag pastes submitted to high temperatures. Mater Struct Constr 2008;41:345–50. https://doi.org/10.1617/s11527-007-9247-8.
[52] Rostásy FS, Weiß R, Wiedemann G. Changes of pore structure of cement mortars due to temperature. Cem Concr Res 1980;10:157–64. https://doi.org/10.1016/0008-8846(80)90072-1.
[53] Lea FC, Stradling RE. The resistance to fire of concrete and reinforced concrete. J Soc Chem Ind 1922;41:395R-396R.
[54] Peng GF, Huang ZS. Change in microstructure of hardened cement paste subjected to elevated temperatures. Constr Build Mater 2008;22:593–9. https://doi.org/10.1016/j.conbuildmat.2006.11.002.
[55] Annerel E, Taerwe L. Revealing the temperature history in concrete after fire exposure by microscopic analysis. Cem Concr Res 2009;39:1239–49. https://doi.org/10.1016/j.cemconres.2009.08.017.
[56] Savva A, Manita P, Sideris KK. Influence of elevated temperatures on the mechanical properties of blended cement concretes prepared with limestone and siliceous aggregates. Cem Concr Compos 2005;27:239–48. https://doi.org/10.1016/j.cemconcomp.2004.02.013.
[57] Balázs GL, Lublóy É. Post-heating strength of fiber-reinforced concretes. Fire Saf J 2012;49:100–6. https://doi.org/10.1016/j.firesaf.2012.01.002.
[58] Shaikh FUA, Vimonsatit V. Effect of cooling methods on residual compressive strength and cracking behavior of fly ash concretes exposed at elevated temperatures. Fire Mater 2016;40:335–50. https://doi.org/10.1002/fam.2276.
[59] Chen B, Liu J. Residual strength of hybrid-fiber-reinforced high-strength concrete after exposure to high temperatures. Cem Concr Res 2004;34:1065–9. https://doi.org/10.1016/j.cemconres.2003.11.010.
[60] Fu YF, Wong YL, Poon CS, Tang CA. Stress-strain behaviour of high-strength concrete at elevated temperatures. Mag Concr Res 2005;57:535–44. https://doi.org/10.1680/macr.2005.57.9.535.
[61] Faiyadh F. Effect of elevated temperature on splitting tensile strength of fibre concrete. Cem Concr Compos 1989;11:175–8. https://doi.org/10.1016/0958-9465(89)90007-3.
[62] Behnood A, Ghandehari M. Comparison of compressive and splitting tensile strength of high-strength concrete with and without polypropylene fibers heated to high temperatures. Fire Saf J 2009;44:1015–22. https://doi.org/10.1016/j.firesaf.2009.07.001.
[63] Haddad RH, Al-Saleh RJ, Al-Akhras NM. Effect of elevated temperature on bond between steel reinforcement and fiber reinforced concrete. Fire Saf J 2008;43:334–43. https://doi.org/10.1016/j.firesaf.2007.11.002.
[64] Siddique R, Kaur D. Properties of concrete containing ground granulated blast furnace slag (GGBFS) at elevated temperatures. J Adv Res 2012;3:45–51. https://doi.org/10.1016/j.jare.2011.03.004.
[65] Yan L, Xing Y, Li J. High-temperature mechanical properties and microscopic analysis of hybrid-fibre-reinforced high-performance concrete. Mag Concr Res 2013;65:139–47. https://doi.org/10.1680/macr.12.00034.
[66] Phan LT, Carino NJ. Effects of test conditions and mixture proportions on behavior of high-strength concrete exposed to high temperatures. ACI Mater J 2002;99:54–66. https://doi.org/10.14359/11317.
[67] Dias WPS, Khoury GA, Sullivan PJE. Mechanical propertie of hardened cement paste exposed to temperatures up to 700 C (1292 F). ACI Mater J 1990;87:160–6. https://doi.org/10.14359/2137.
[68] Khaliq W, Kodur V. Thermal and mechanical properties of fiber reinforced high performance self-consolidating concrete at elevated temperatures. Cem Concr Res 2011;41:1112–22. https://doi.org/10.1016/j.cemconres.2011.06.012.
[69] Peng GF, Bian SH, Guo ZQ, Zhao J, Peng XL, Jiang YC. Effect of thermal shock due to rapid cooling on residual mechanical properties of fiber concrete exposed to high temperatures. Constr Build Mater 2008;22:948–55. https://doi.org/10.1016/j.conbuildmat.2006.12.002.
[70] Mendes A, Sanjayan JG, Collins F. Effects of slag and cooling method on the progressive deterioration of concrete after exposure to elevated temperatures as in a fire event. Mater Struct Constr 2011;44:709–18. https://doi.org/10.1617/s11527-010-9660-2.
[71] Husem M. The effects of high temperature on compressive and flexural strengths of ordinary and high-performance concrete. Fire Saf J 2006;41:155–63. https://doi.org/10.1016/j.firesaf.2005.12.002.
[72] Bingöl AF, Gül R. Effect of elevated temperatures and cooling regimes on normal strength concrete. Fire Mater 2009:79–88. https://doi.org/10.1002/fam.987.
[73] Xiao J, Hou Y, Huang Z. Beam test on bond behavior between high-grade rebar and high-strength concrete after elevated temperatures. Fire Saf J 2014;69:23–35. https://doi.org/10.1016/j.firesaf.2014.07.001.
[74] Topçu IB, Karakurt C. Properties of reinforced concrete steel rebars exposed to high temperatures. Res Lett Mater Sci 2008;2008. https://doi.org/10.1155/2008/814137.
[75] Neves IC, Rodrigues JPC, Loureiro A de P. Mechanical properties of reinforcing and presstressing stells after heating. J Mater Civ Eng 1996;8:189–94.

[76] Elghazouli AY, Cashell KA, Izzuddin BA. Experimental evaluation of the mechanical properties of steel reinforcement at elevated temperature. Fire Saf J 2009;44:909–19. https://doi.org/10.1016/j.firesaf.2009.05.004.

[77] Tao Z, Wang XQ, Uy B. Stress-strain curves of structural and reinforcing steels after exposure to elevated temperatures. J Mater Civ Eng 2013;25:1306–16. https://doi.org/10.1061/(ASCE)MT.1943-5533.0000676.

[78] Ahmad MS. Effect of Sustained Elevated Temperature on Mechanical Behavior of Reinforcing Bar. Procedia Eng 2017;173:905–9. https://doi.org/10.1016/j.proeng.2016.12.139.

[79] Qian H, Yan D, Chen S, Chen G, Tian Y, Chen G. Effect of High Temperature Exposure and Strain Rate on Mechanical Properties of High-Strength Steel Rebars. J Mater Civ Eng 2019;31:04019261. https://doi.org/10.1061/(asce)mt.1943-5533.0002906.

[80] Qiang X, Bijlaard FSK, Kolstein H. Post-fire mechanical properties of high strength structural steels S460 and S690. Eng Struct 2012;35:1–10. https://doi.org/10.1016/j.engstruct.2011.11.005.

[81] Pothisiri T, Panedpojaman P. Modeling of mechanical bond-slip for steel-reinforced concrete under thermal loads. Eng Struct 2013;48:497–507. https://doi.org/10.1016/j.engstruct.2012.10.015.

[82] Pothisiri T, Panedpojaman P. Modeling of bonding between steel rebar and concrete at elevated temperatures. Constr Build Mater 2012;27:130–40. https://doi.org/10.1016/j.conbuildmat.2011.08.014.

[83] Haddad RH, Shannis LG. Post-fire behavior of bond between high strength pozzolanic concrete and reinforcing steel. Constr Build Mater 2004;18:425–35. https://doi.org/10.1016/j.conbuildmat.2004.03.006.

[84] Sharma A, Bošnjak J, Ožbolt J, Hofmann J. Numerical modeling of reinforcement pull-out and cover splitting in fire-exposed beam-end specimens. Eng Struct 2016;111:217–32. https://doi.org/10.1016/j.engstruct.2015.12.017.

[85] Zhao W, Zhu B. Basic parameters test and 3D modeling of bond between high-strength concrete and ribbed steel bar after elevated temperatures. Struct Concr 2017;18:653–67. https://doi.org/10.1002/suco.201600005.

[86] Royles R, Morley PD. Response of the bond in reinforced concrete to high temperatures. Mag Concr Res 1983;35:157–63. https://doi.org/10.1680/macr.1983.35.124.157.

[87] Royles R, Morley PD. Further responses of the bond in reinforced concrete to high temperatures. Mag Concr Res 1983;35:157–63. https://doi.org/10.1680/macr.1983.35.124.157.

[88] Bingöl AF, Gül R. Residual bond strength between steel bars and concrete after elevated temperatures. Fire Saf J 2009;44:854–9. https://doi.org/10.1016/j.firesaf.2009.04.001.

[89] Yin K, Han Y, Liu Y. Experimental research on bond strength between rebar and concrete after high temperature. Appl Mech Mater 2011;71–78:1057–61. https://doi.org/10.4028/www.scientific.net/AMM.71-78.1057.

[90] A. Hassan S. Effect of Elevated Temperatures on Bond Strength of Steel Reinforcement and Concrete Enhanced with Discrete Carbon Fibers. J Eng Dev 2012;16:1813–7822.

[91] Lublóy É, György BL. Temperature Effects on Bond Between Concrete and Reinforcing Steel. Zb Rad Građevinskog Fak 2014;30:27–35. https://doi.org/10.14415/zbornikgfs26.03.

[92] Arel HŞ, Yazici Ş. Effect of different parameters on concrete-Bar bond under high temperature. ACI Mater J 2014;111:633–40. https://doi.org/10.14359/51686992.

[93] Yang H, Lan W, Qin Y, Wang J. Evaluation of bond performance between deformed bars and recycled aggregate concrete after high temperatures exposure. Constr Build Mater 2016;112:885–91. https://doi.org/10.1016/j.conbuildmat.2016.02.220.

[94] Ergün A, Kürklü G, Başpinar MS. The effects of material properties on bond strength between reinforcing bar and concrete exposed to high temperature. Constr Build Mater 2016;112:691–8. https://doi.org/10.1016/j.conbuildmat.2016.02.213.

[95] Li X, Bao Y, Xue N, Chen G. Bond strength of steel bars embedded in high-performance fiber-reinforced cementitious composite before and after exposure to elevated temperatures. Fire Saf J 2017;92:98–106. https://doi.org/10.1016/j.firesaf.2017.06.006.

[96] Hlavička ÉLV. Bond after fire. Constr Build Mater 2017;132:210–8. https://doi.org/10.1016/j.conbuildmat.2016.11.131.

[97] Bošnjak J, Sharma A, Öttl C. Modified beam-end test setup to study the bond behavior of reinforcement in concrete after fire. Mater Struct Constr 2018;51. https://doi.org/10.1617/s11527-018-1138-7.

[98] Yang O, Zhang B, Yan G, Chen J. Bond Performance between Slightly Corroded Steel Bar and Concrete after Exposure to High Temperature. J Struct Eng (United States) 2018;144:1–10. https://doi.org/10.1061/(ASCE)ST.1943-541X.0002217.

[99] Shamseldein A, Elshafie H, Rashad A, Kohail M. Assessment and restoration of bond strength of heat-damaged reinforced concrete elements. Constr Build Mater 2018;169:425–35. https://doi.org/10.1016/j.conbuildmat.2018.03.008.

[100] Varona FB, Baeza FJ, Bru D, Ivorra S. Evolution of the bond strength between reinforcing steel and fibre reinforced concrete after high temperature exposure. Constr Build Mater 2018;176:359–70. https://doi.org/10.1016/j.conbuildmat.2018.05.065.

[101] Ghazaly N, Rashad A, Kohail M, Nawawy O. Evaluation of bond strength between steel rebars and concrete for heat-damaged and repaired beam-end specimens. Eng Struct 2018;175:661–8. https://doi.org/10.1016/j.engstruct.2018.08.056.

[102] Zhang B, Zhu H, Chen J, Yang O. Evaluation of bond performance of corroded steel bars in concrete after high temperature exposure. Eng Struct 2019;198:109479. https://doi.org/10.1016/j.engstruct.2019.109479.

[103] Hameed R, Turatsinze A, Duprat F, Sellier A. Bond stress-slip behaviour of steel reinforcing bar embedded in hybrid fiber-reinforced concrete. KSCE J Civ Eng 2013;17:1700–7. https://doi.org/10.1007/s12205-013-1240-x.

[104] Sharma A, Bošnjak J, Bessert S. Experimental investigations on residual bond performance in concrete subjected to elevated temperature. Eng Struct 2019;187:384–95. https://doi.org/10.1016/j.engstruct.2019.02.061.

[105] Deshpande AA, Kumar D, Ranade R. Temperature effects on the bond behavior between deformed steel reinforcing bars and hybrid fiber-reinforced strain-hardening cementitious composite. Constr Build Mater 2020;233:117337. https://doi.org/10.1016/j.conbuildmat.2019.117337.

[106] Ba G, Weng X, Liu C, Miao J. Bond strength of corroded reinforcements in concrete after high-temperature exposure. Constr Build Mater 2020. https://doi.org/10.1016/j.conbuildmat.2020.121400.

[107] Zou W, Liang J, Liu D, Zhang G. Bond Behavior between Steel Rebar and RCA Concrete after Exposure to Elevated Temperatures. Adv Mater Sci Eng 2020;2020. https://doi.org/10.1155/2020/5230295.

[108] Fakoor M, Nematzadeh M. A new post-peak behavior assessment approach for effect of steel fibers on bond stress-slip relationship of concrete and steel bar after exposure to high temperatures. Constr Build Mater 2021;278:122340. https://doi.org/10.1016/j.conbuildmat.2021.122340.

[109] Diederichs U, Schneider U. Bond strength at high temperatures. Mag Concr Res 1981;33:75–84. https://doi.org/10.1680/macr.1981.33.115.75.

[110] Rashid MH, Molla MM, Taki IM. Effect of Elevated Temperature on Bond Strength of Concrete. Mater Sci Forum 2019;972:26–33. https://doi.org/10.4028/www.scientific.net/msf.972.26.

[111] Raouffard MM, Nishiyama M. Idealization of bond stress-slip relationship at elevated temperatures based on pullout tests. ACI Struct J 2018;115:391–400. https://doi.org/10.14359/51701120.

[112] Khalaf J, Huang Z, Fan M. Analysis of bond-slip between concrete and steel bar in fire. Comput Struct 2016;162:1–15. https://doi.org/10.1016/j.compstruc.2015.09.011.

[113] Fakoor M, Nematzadeh M. A new post-peak behavior assessment approach for effect of steel fibers on bond stress-slip relationship of concrete and steel bar after exposure to high temperatures. Constr Build Mater 2021;278. https://doi.org/10.1016/j.conbuildmat.2021.122340.

[114] Ghazaly N, Rashad A, Kohail M, Nawawy O. Evaluation of bond strength between steel rebars and concrete for heat-damaged and repaired beam-end specimens. Eng Struct 2018;175:661–8. https://doi.org/10.1016/j.engstruct.2018.08.056.

[115] Aslani F, Samali B. High Strength Polypropylene Fibre Reinforcement Concrete at High Temperature. Fire Technol 2014;50:1229–47. https://doi.org/10.1007/s10694-013-0332-y.

[116] Kalifa P, Chéné G, Gallé C. High-temperature behaviour of HPC with polypropylene fibres - From spalling to microstructure. Cem Concr Res 2001;31:1487–99. https://doi.org/10.1016/S0008-8846(01)00596-8.

[117] Ríos JD, Cifuentes H, Leiva C, García C, Alba MD. Behavior of High-Strength Polypropylene Fiber-Reinforced Self-Compacting Concrete Exposed to High Temperatures. J Mater Civ Eng 2018;30:04018271. https://doi.org/10.1061/(asce)mt.1943-5533.0002491.

[118] Varona FB, Baeza FJ, Bru D, Ivorra S. Influence of high temperature on the mechanical properties of hybrid fibre reinforced normal and high strength concrete. Constr Build Mater 2018;159:73–82. https://doi.org/10.1016/j.conbuildmat.2017.10.129.

[119] Poon CS, Shui ZH, Lam L. Compressive behavior of fiber reinforced high-performance concrete subjected to elevated temperatures. Cem Concr Res 2004;34:2215–22. https://doi.org/10.1016/j.cemconres.2004.02.011.

[120] Lau A, Anson M. Effect of high temperatures on high performance steel fibre reinforced concrete. Cem Concr Res 2006;36:1698–707. https://doi.org/10.1016/j.cemconres.2006.03.024.

[121] Varona FB, Baeza FJ, Ivorra S, Bru D. Análisis experimental de la pérdida de adherencia hormigón-acero en hormigones sometidos a altas temperaturas. Dyna 2015;90:78–86. https://doi.org/10.6036/7184.

[122] Fang C, Lundgren K, Chen L, Zhu C. Corrosion influence on bond in reinforced concrete. Cem Concr Res 2004;34:2159–67. https://doi.org/10.1016/j.cemconres.2004.04.006.

[123] Tondolo F. Bond behaviour with reinforcement corrosion. Constr Build Mater 2015;93:926–32. https://doi.org/10.1016/j.conbuildmat.2015.05.067.

[124] Coccia S, Imperatore S, Rinaldi Z. Influence of corrosion on the bond strength of steel rebars in concrete. Mater Struct Constr 2016;49:537–51. https://doi.org/10.1617/s11527-014-0518-x.

[125] Ma Y, Guo Z, Wang L, Zhang J. Experimental investigation of corrosion effect on bond behavior between reinforcing bar and concrete. Constr Build Mater 2017;152:240–9. https://doi.org/10.1016/j.conbuildmat.2017.06.169.

CHAPTER 3:

Experimental evaluation of heat-induced degradation on concrete-reinforcement bond after exposure to elevated temperatures

Abstract

This work presents an experimental assessment of the influence of heat-induced degradation of concrete and reinforcing steel on the bond relationship between these materials. Two concrete mixes were analyzed, with 30 and 50 MPa compressive strength, and three bar diameters. Bond tests were performed using pull-out specimens. In the case of tests after exposure to elevated temperatures, the specimens were first heated in a furnace and kept until they reached thermal equilibrium. Second, they were cooled to room temperature and after then were tested. The reinforcing bars did not show evidence of being affected by heat exposure for temperatures up to 400 ºC, but the CA60 grade rebar showed extensive deterioration at 600 ºC. The physicochemical changes in concrete's microstructure after exposure to elevated temperatures were verified through SEM and XRD. It was observed that both concretes mechanical properties were positively affected by heat exposure up to 200 ºC, with exception of Young's Modulus. This is reflected in the bond strength, which increased up to 73% for C30 concrete at this temperature level. Higher temperature exposures progressively deteriorated the concretes mechanical properties and the bond between the materials. Besides the materials' deterioration, their differential thermal expansion induced interfacial cracking, which showed to be an important factor of bond degradation after heat exposure.

Keywords: Bond strength. Elevated temperatures. Pull-out test. Materials Properties. Bond-slip relationship. Bond failure mechanism.

3.1. Introduction

Reinforced concrete is a composite material that brings together the best of the individual materials' capabilities. As a result, there is a material capable of bearing both compressive and tensile stresses. However, the composite behavior of reinforced concrete structures is directly related to the force-transfer mechanism between the materials; hence, to the bond between them. When the bond is damaged, the force transfer is compromised and so is the workability of the structure itself.

At room temperature, there are two main bond failure mechanisms for short specimens (l_b/d <10), pull-out and splitting. Pull-out failure is due mostly to the shearing-off of the concrete between the rebar transversal ribs and shows no visible splitting cracks. Splitting failure is due mostly to the longitudinal splitting of the concrete surrounding the rebar and bond capacity vanishes once the radial cracks get to the outer surface of the specimen. Generally, pull-out bond failure affects specimens well-confined or with large concrete covers; conversely, splitting failure occurs when there is no confinement or limited concrete cover [1]. The bond-slip relationship for each bond failure mechanism is shown in Fig. 1.

Fig. 1. Bond-slip relationship and bond failure mechanisms at room temperature.

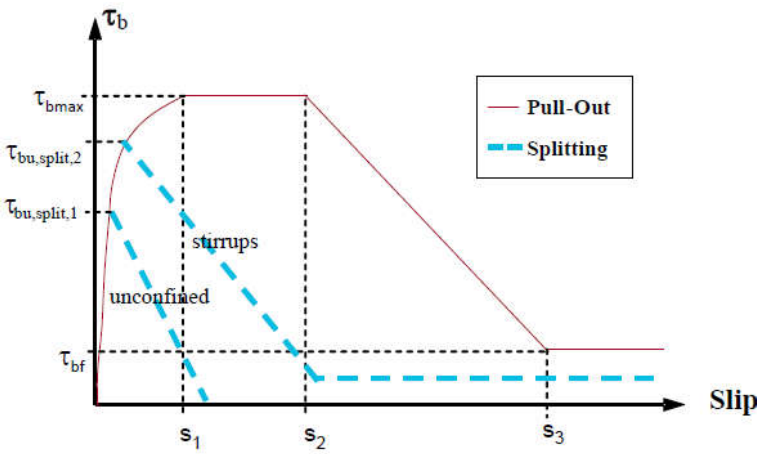

Source: FIB Model Code (2013) [2]

During its lifespan, a reinforced concrete structure may be subjected to a fire situation. At elevated temperatures, concrete undergoes a series of physical and chemical changes due to water evaporation. For elevated temperatures up to 105 ºC, concrete loses its free, physically adsorbed, and interlayer water [3–8]. As temperature increases, the cement paste shrinks due to moisture loss, whereas the aggregates undergo a thermal-induced expansion. This thermal incompatibility produces high tensile stresses at the interfacial transition zone [9–13]. For temperatures above

300 ºC, the cement paste experiences the coarsening of its pore structure and a significant increase in microcracking around calcium-hydroxide (CH) crystals [10].

When the temperature is further increased, the microstructure of concrete suffers major changes due to chemical decomposition, moisture loss, and microcracking. The main physical effect observed is the increase in concrete porosity, which can be interpreted as the pore structure coarsening in both size and distribution [8,9,14–17]. This can be verified especially for temperatures above 400 ºC, due to the dehydration of the CH [6,7,9,10,14,16,18].

When the temperature exceeds 600 ºC, the hydrated calcium silicates (C-S-H) decomposition becomes the main mechanism influencing concrete cracking and strength loss [6,7,9–11,19]. For temperatures in the range of 580-900 ºC, concrete undergoes its third major weight loss, due to the decomposition of $CaCO_3$ [9,11,20,21].

Concrete's mechanical properties response to heat exposure has been studied by many researchers over the years. It has been established that, depending on its constitution, concrete may present insignificant compressive strength loss, or even a slight increase for elevated temperatures up to 300 ºC. [13,22–24]. However, for temperatures above 400 ºC, concrete is highly damaged and a drastic reduction of the compressive strength is observed [6,7,9,10,14,16,18].

On the other hand, the reinforcing steel residual mechanical properties do not seem to be affected by temperature exposure up to 600 ºC, either for hot-rolled and cold-worked reinforcement bars [25–32]. As the exposure temperature increases above this temperature range, steel progressively deteriorates, and its yield strength and ultimate strength decrease substantially due to pearlite transformation to austenite at around 727 ºC [25].

Based on the existing data, it is clear that concrete and reinforcement have different responses to heat exposure; surely, this differential behavior affects their interface and the bond between the materials. The present study experimentally investigates the influence of the materials' mechanical properties on concrete-reinforcement bond after exposure to elevated temperatures. Two different concrete mixes are tested to assess how the concrete deterioration process takes place as the temperature increases. Moreover, the reinforcing steel bar response to elevated temperatures is also analyzed. Finally, pull-out tests are performed and the effect of heat exposure on bond-slip relationship and bond failure mechanisms are analyzed.

3.2. Experimental procedure

3.2.1. Design of experiments (DOE)

This work proposed to study the effect of exposure to elevated temperatures on residual properties of concrete and reinforcing steel and to evaluate its influence on the bond between these materials. For each material, a series of physical and mechanical properties were analyzed. The residual properties analyzed for the reinforcing steel were its yield and ultimate strength and the Young's Modulus.

Since concrete is a heterogeneous material, a more comprehensive analysis was carried out. The concrete's mechanical properties analyzed in this work are the compressive strength, splitting strength, shear strength, and Young's Modulus. In addition, complementary scanning electron microscopy (SEM) and X-Ray diffraction (XRD) analyses were carried out to enlighten the physical and chemical changes that concrete undergoes as exposure temperature increases.

The analysis of the effect of exposure to elevated temperatures on bond strength was designed as a factorial experiment with two factors: the concrete mix and the exposure temperature. Despite the analysis of heat-induced deterioration on three different bar diameters, only one bar was used for the pull-out tests, the 12.5 mm diameter bar. This parameter was kept constant because the concrete cover to bar diameter ratio also influences the bond behavior, and the goal of this work was to analyze exclusively the effect of the heat-induced deterioration of the materials on bond behavior.

Each of the aforementioned residual properties was measured after exposure to elevated temperature and compared to that of room temperature. The target temperatures examined in this work are 200 ºC, 400 ºC, and 600 ºC. All the parameters analyzed and the tests performed in this work are summarized in Table 1.

Table 1.
Tests performed in this experimental program.

Component	Properties	Tests
Concrete	30 MPa 50 MPa	Compressive strength Splitting strength Shear strength Young's Modulus XRD, SEM
Reinforcing bars	5.0 mm 8.0 mm 12.5 mm	Yielding strength Ultimate strength Young's Modulus

3.2.2. *Test program and materials*

The experimental program consisted of testing the residual mechanical properties of two concrete mixes with initial compressive strengths of 30 and 50 MPa, which proportions are detailed in Table 2. The concrete mixes were prepared with Portland cement CP II-E-32, which is a slag-modified Portland cement that complies with the type I (SM) cement of ASTM C595 [33]. The aggregates used in this work were river natural sand and granite gravel. The physical and mechanical properties of the materials used in the concrete mixes are given in Table 3 and Table 4.

Table 2.
Concrete mixes used for the tests.

Component	**Quantity (kg/m³)**	
	Mix 1 – C30	Mix 2 – C50
Cement	330	690
River quartz sand	841	432
Granite gravel	1051	1051
Water	190	228

Source: Author (2021).

Table 3.
Properties of the Portland cement.

Property	**Value**	**Standards**
Density [g/cm³]	2.965	ABNT NBR NM 23[34] equivalent to ASTM C188 – 17 [35]
Specific surface area (Blaine) [m²/kg]	460	ABNT NBR 16372 [36] equivalent to ASTM C204 -18e1 - [37]
Water for standard cement paste [%]	31	ABNT NBR NM 43[38] equivalent to ASTM C187 – 16 -[39]
Initial setting time, min.	190	ABNT NBR 16607 [40] equivalent to ASTM C191-19 - [41]
Final setting time, min.	251	ABNT NBR 16607 [40] equivalent to ASTM C191-19- [41]
Compressive strength (3/ 7/ 28 days) [MPa]	(12.3/ 25.2/ 39.2)	ABNT NBR 7215 [42] equivalent to ASTM C109M – 21 [43]

Source: Author (2021).

Table 4.
Properties of the aggregates.

Property	**River sand**	**Granite gravel**	**NORMA**
Specific gravity [g/cm³]	2.594	2.794	ABNT NBR NM 45 [44] equivalent to ASTM C29M – 17a [45]
Water absorption [%]	1.21	0.48	ABNT NBR NM 30 [46] equivalent to ASTM C128 – 15 [47]
Fineness modulus	2.71	6.97	ABNT NBR NM 248 [48] equivalent to ASTM C136M – 19 [49]
Maximum dimension [mm]	4.80	19.0	ABNT NBR NM 248 [48] equivalent to ASTM C136M – 19 [49]

Source: Author (2021).

For each concrete mix and temperature, three 100 mm diameter and 200 mm height cylindrical specimens were prepared to analyze the effect of heat exposure on the concrete's residual mechanical properties. The exception was the shear strength analysis, which required a particular specimen, as shown in Fig. 2.

Fig. 2. Details of the shear strength specimen in a) front view and b) top view.

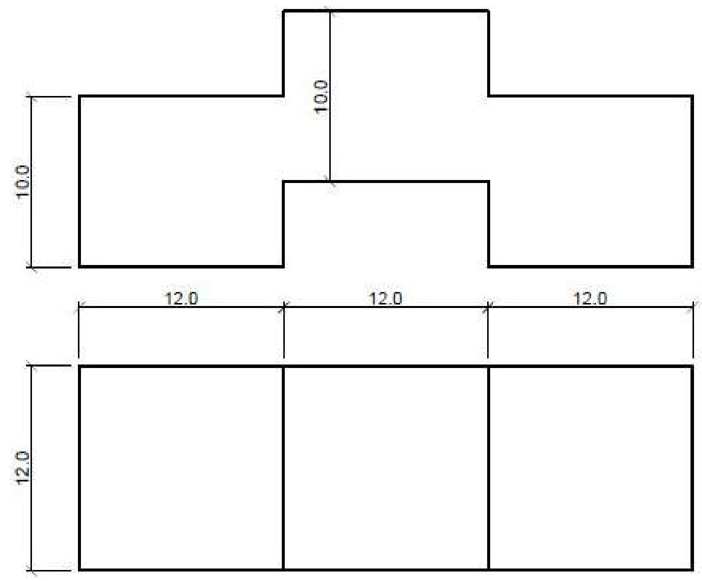

Source: Adapted from [50].

The effect of exposure to elevated temperatures on the reinforcing steel was analyzed for three different bar diameters, 8.0 and 12.5 mm deformed CA50 grade rebars and 5.0 mm plain CA60 grade steel. For each bar diameter, three specimens were tested after being subjected to elevated temperatures. The rebar chosen to be embedded into the concrete block for the pull-out tests was the 12.5 mm deformed bar, which properties are detailed in Table 5.

Table 5.
Reinforcing bar properties at room temperature.

Property	5.0 mm	8.0 mm	12.5 mm
Transversal rib spacing (mm)	-	5.32 *	6.95 *
Transversal rib height (mm)	-	0.52	0.77
Yield strength (MPa)	642.5	589	587
Ultimate strength (MPa)	690.6	699	695
Young's Modulus (GPa)	191	214	211

*__Note:__ the transversal rib spacing is 0.66*d* for 8.0 mm bar and 0.56*d* for 12.5 mm bar.

Source: Author (2021).

3.2.3. *Pull-out specimens*

The pull-out specimens were prismatic with a 150x150 mm cross-section and 200 mm long, as shown in Fig. 3. The test rebars were embedded into the concrete block providing the minimum top and side concrete cover allowed by the Brazilian Standards (ABNT NBR 6118 [51]), which is 25 mm.

The test rebar was installed with a 5d embedment length placed in the mid-length of the specimen, and both the loading-end and the free-end were debonded. The pull-out rebar loading-end was prolonged by 150 mm to be attached to the testing machine and the free-end was prolonged by 50 mm to facilitate the bar slip measurements. The debonded length was provided by paper rolled [52] around the rebar and covered in oil to avoid any bond to the concrete. Due to risks during the heat exposure, it was chosen not to work with PVC bond-break, as usual in other bond testing programs.

Three 5.0 mm diameter stirrups were used to provide confinement to the rebar. The center stirrup was placed at the mid-length of the specimens, which was also the mid-length of the embedment length. The other two stirrups were placed symmetrically inside the specimen, at a 50 mm distance in each direction.

For each target temperature and each compressive strength, three pull-out specimens using the 12.5 mm diameter rebar were tested.

Fig. 3. Details of the pull-out specimen (units are in centimeters)

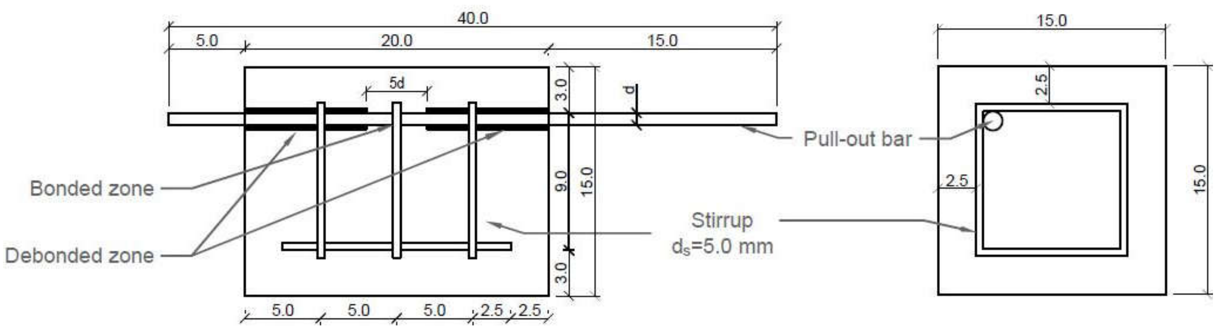

Source: Author (2021).

3.2.4. *Specimen preparation and heating procedure*

The pull-out specimens were cast with the test rebar oriented horizontally near the top of the mold. Both the pull-out and the shear strength specimens were kept in the mold for 72 hours, as shown in Fig. 4, then the specimens were demolded and taken to a water tank where they were cured immersed in water for 28 days. Before the specimens were subjected to the target temperature, they were taken out of the water tank and let dry out at room temperature for a few hours. Then, specimens were kept at 100 ºC for 24 hours to remove the free water and avoid spalling during the heating procedure, and subsequently cooled down to room temperature.

Fig. 4. Specimen preparation: a) shear strength; b) pull-out.

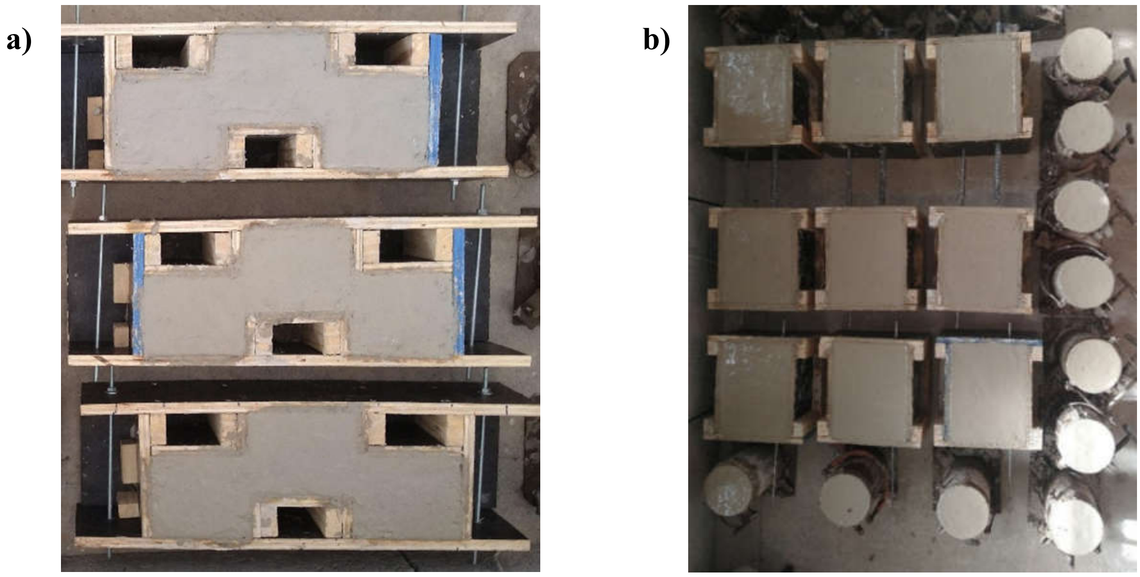

Source: Author (2021).

Finally, the specimens were put in an electric furnace and heated at a rate of approximately 4 ºC/min. A thermocouple (TC1) was used to measure the temperature inside the furnace, and a control specimen was used to determine when the specimen had reached the target temperature. Two thermocouples were cast inside the control specimen, one at the pull-out bar position (TC2) and the other at the center of the specimen's cross-section (TC3), as represented in Fig. 5.

Fig. 5. Position of the: a) thermocouples; b) LVDT.

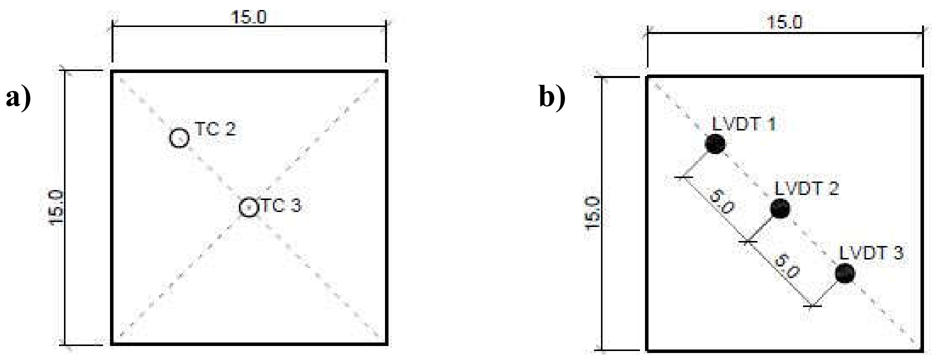

Source: Author (2021).

The furnace was turned off only when TC3 ensured that the whole specimen's cross-section had reached the target temperature, as exemplified by Fig. 6. At that point, the furnace door was opened, and the specimens were allowed to cool down to room temperature overnight. All the time-temperature curves are available in Appendix A.

Fig. 6. Time-temperature curves for C50 specimens and 600 ºC.

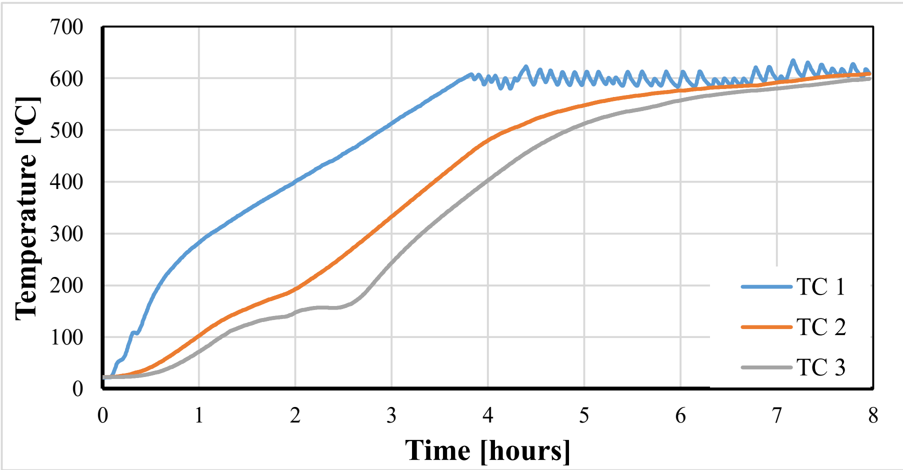

Source: Author (2021).

3.2.5. Pull-out test setup

The pull-out tests were conducted in a universal testing machine, EMIC DL60000, that provides a maximum force of 600 kN. The specimen was placed in a load-transfer apparatus, as shown in Fig. 7. The load-transfer apparatus consisted of two 20 mm thick steel plates, connected by four 16 mm diameter threaded bars, one in each corner of the steel plate. A 150 mm long, 20 mm diameter bar is placed at the center of the top plate to attach the apparatus to the top gripper of the testing machine. The specimen is positioned into the apparatus with the pull-out bar faced down through a hole in the center of the bottom plate and grabbed by the moveable gripper of the testing machine.

The pull-out load was applied by displacement control with a loading speed of 0.6 mm/min until the machine moveable beam reached a maximum of 15 mm. The pull-out force corresponding applied in each step of displacement was measured by four strain gauges, placed one in each threaded bar of the apparatus.

Fig. 7. Pull-out test setup.

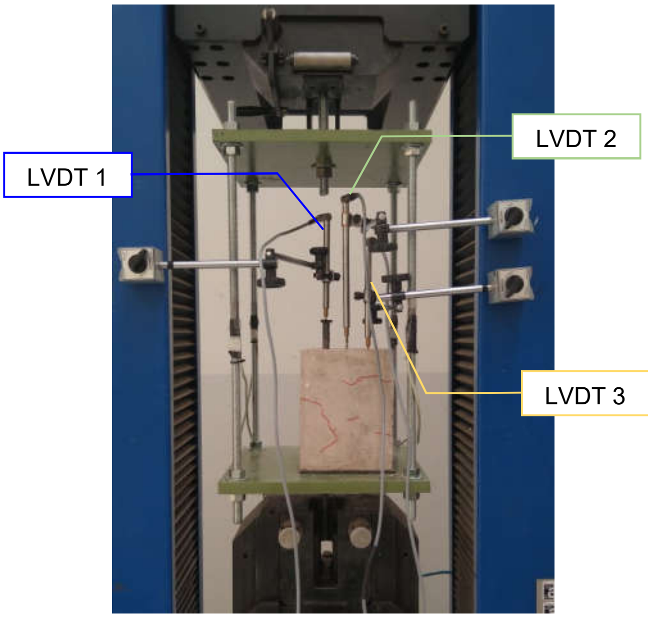

Source: Author (2021).

The bar displacement was measured by LVDT 1, and the concrete displacement was measured by LVDT 2 and LVDT 3, positioned as shown in Fig. 5 and Fig. 7. Based on the values measured by LVDT 2 and LVDT 3, it was estimated the concrete displacement at the bar location, by using a linear equation, Eq. (1). A differential displacement was obtained at that point, here on denominated as the bar slip.

$$\delta = 2\delta_2 - \delta_3 \quad (1)$$

where δ is the calculated concrete displacement at the rebar position; δ_2 and δ_3 are the concrete displacement measured by LVDT 2 and LVDT 3, respectively.

The LVDTs used to measure the displacements were HBM WA20 e HBM WA50. The data acquisition systems (DAS) used were the HBM MX1615 for the strain gauges and the HBM 840A for the displacement transducers.

The bond strength obtained by the pull-out test can be defined as the force being transferred between the materials by unit of surface area along the rebar embedment length. For small embedment length to bar diameter ratios (l_b/d), in which the shear stress can be assumed to be uniformly distributed along the bar, the shear stress of maximum bond can be expressed by Eq. (2):

$$\tau = \frac{P_{max}}{\pi d l_b} \quad (2)$$

where P_{max} is the maximum pull-out load; d is the diameter of the reinforcement and l_b is the embedment length.

3.3. Results and discussion

The results of the present study are reported and discussed in the following sequence. First, the effects of heat exposure on the concrete's physical and mechanical properties are analyzed. Second, the reinforcing bars and the interface of the materials are analyzed for increasing temperatures. Finally, the effects of heat exposure on bond-slip curves and bond failure mechanism are discussed based on the previously analyzed results of the materials' properties.

3.3.1. Effects of elevated temperature exposure on the concrete

3.3.1.1. Effect of elevated temperature exposure on the concrete's residual mechanical properties

The evolution of concrete's residual mechanical properties with increasing the exposure temperature are given in Fig. 8 and Fig. 9. Based on the results obtained in this work, elevated temperature exposure have a positive effect for both concretes compressive and shear strengths after exposure to 200 °C, which results in a 23% compressive strength increase for C30 and 12% for C50. For the shear strength, the increase was 38% and 36% for C30 and C50, respectively. The tensile strength was only slightly affected for both concrete mixes after exposure to 200 ºC.

Fig. 8. C30 residual mechanical properties.

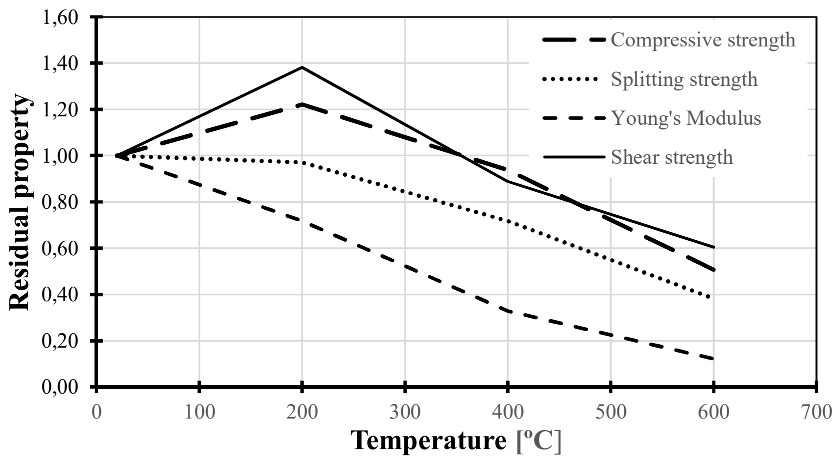

Source: Author (2021).

Fig. 9. C50 residual mechanical properties.

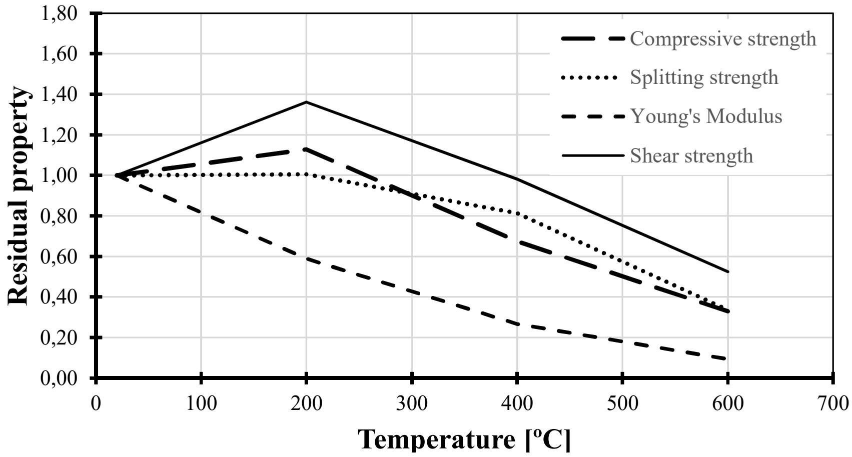

Source: Author (2021).

Although these properties are enhanced after exposure to 200º C, the Young's modulus shows a significant reduction for both concretes, retaining 72% and 59% of its original values for C30 and C50 respectively, which indicates that, despite the apparent strengthening of the concrete, it has been damaged on a microstructural level.

C30 and C50 show evidence of being affected differently by heat exposure at 400 ºC. At this level of temperature, the residual compressive strength of C30 is slightly affected, retaining 94% of its original value, while C50 retains only 68% of its strength at room temperature. On the other hand, the shear and splitting strengths show an opposite trend. C50 retains 81% of its splitting strength and 98% of the shear strength, against 72% and 89% respectively for C30. The Young's modulus seems to be equally affected for both concrete mixes, with relative residual values of 33% and 27%.

When the temperature reaches 600 ºC, concrete is severely damaged and all the analyzed residual mechanical properties decrease drastically irrespective of the mix. C30 concrete retained 51% of its compressive strength, while C50 was even more damaged, and retained only 33% of its strength. Among the analyzed mechanical properties, the Young's modulus was the most damaged by heat exposure at 600 ºC, retaining only 12% of its value at room temperature for C30, and 9% for C50.

The greater damage to the C50 compressive strength observed by the data in Fig. 9 is directly related to the denser microstructure and the heat-induced cracking, as shown in Fig. 10. Due to its low permeability, high-strength concrete experiences the development of higher pore pressures during heating [53]. The pressure increase results in more extensive cracking and could lead to spalling, which was not observed in any specimen in this work.

Fig. 10. Crack pattern at 400 °C and 600 °C for: a) C30; b) C50.

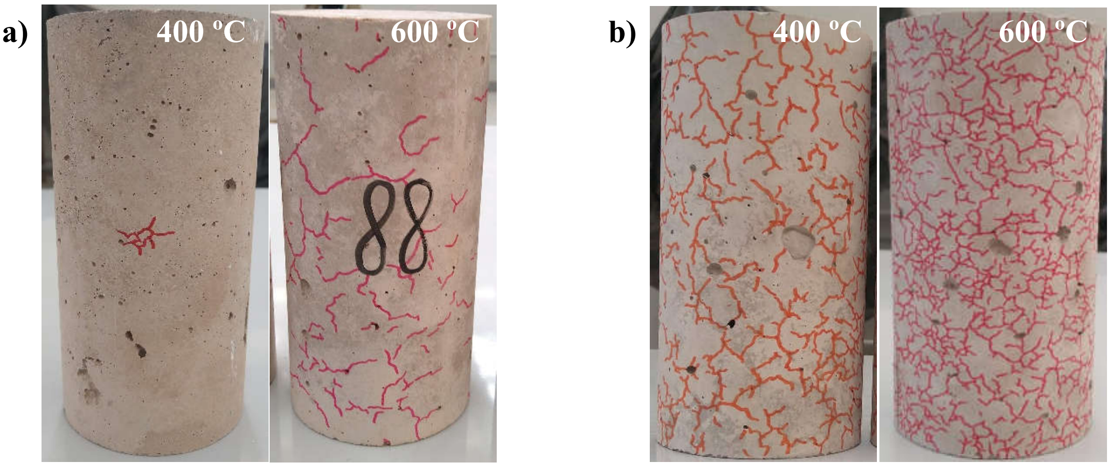

Source: Author (2021).

The results for residual compressive strength of concrete observed in this work agree with the observation of previous researchers, as shown in Fig. 11.

Fig. 11. Evolution of residual compressive strength of concrete with increasing temperatures.

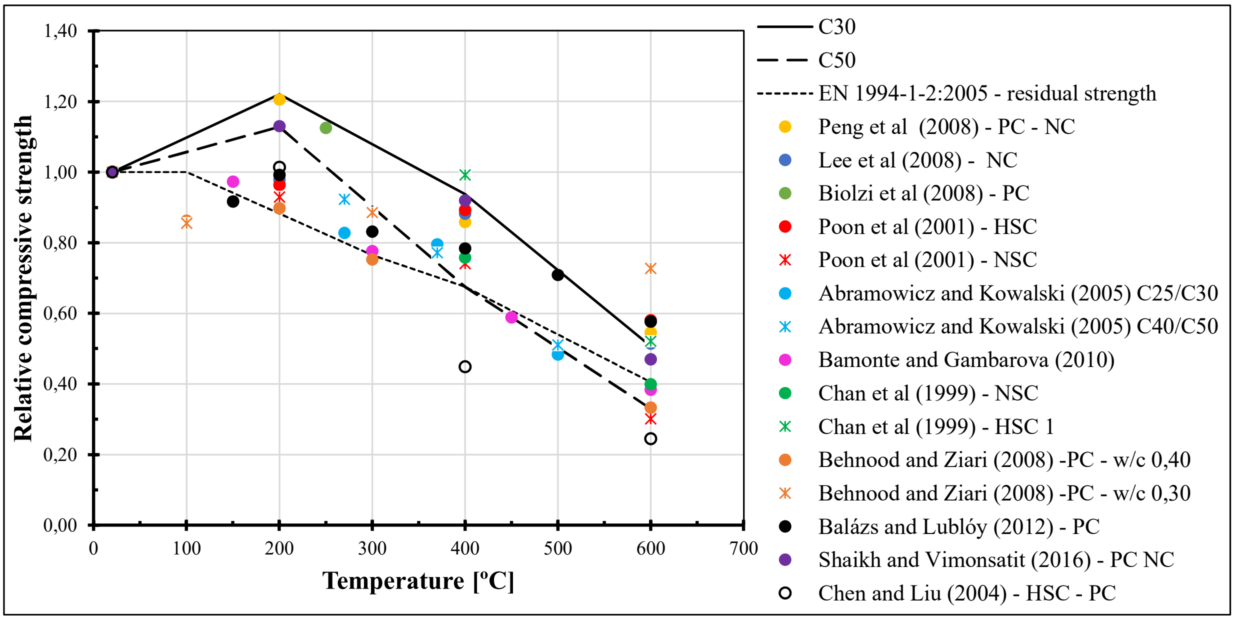

Source: Author (2021). Data extracted from [12,21,23,54–61].

3.3.1.2. Effect of elevated temperature exposure on the concrete's microstructure

The microstructures of both concrete mixes were analyzed by scanning electron microscopic images (SEM). They are shown in Fig. 12 to Fig. 19.

At room temperature, the scanning electron microscopic images (SEM) for C30 concrete show a clear presence of ettringite, the needle shaped structures shown in Fig. 12, on the cement grain surface. When exposed to elevated temperatures, ettringite starts to decompose for temperatures above 70 ºC and is completely decomposed at 90 ºC [62,63]; hence, it was not found in concrete exposed to any other temperature (200 °C, 400 °C and 600 °C).

Fig. 12. Ettringite in C30 concrete at room temperature.

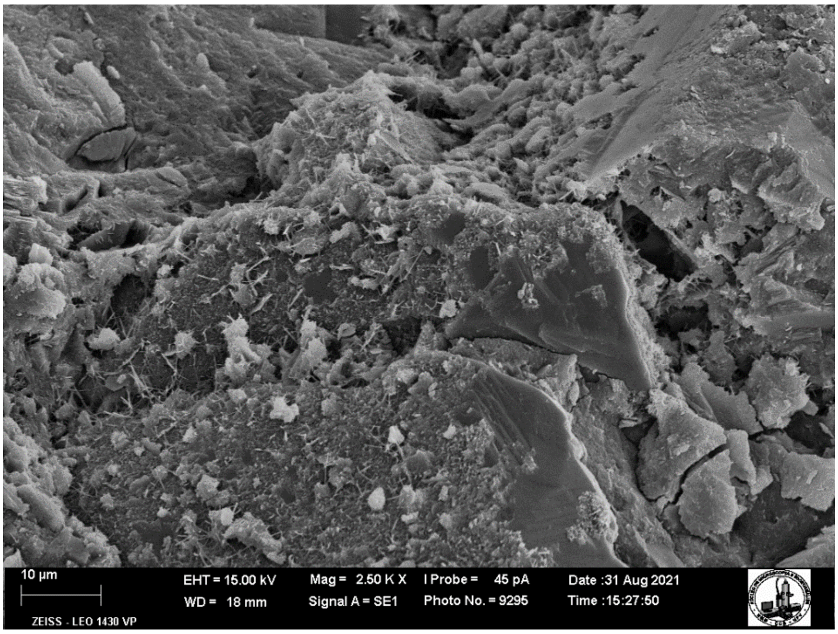

Source: Author (2021).

Fig. 13 shows C50 concrete at room temperature. The orange dashed rectangles indicate what seems to be some unhydrated cement grains, similar to the observation of Lim and Mondal [64]. The area marked in yellow resembles C-S-H observations shown in technical literature [6,63].

Fig. 14 and Fig. 15 show the microstructure of concrete exposed to 200 ºC. The red dashed rectangles observed in these figures mark structures similar to the CH observed by Annerel and Taerwe [63]. Noticeably, CH can be more easily found in C50 concrete and is the one of the reasons why C50 has higher compressive strength.

Fig. 13. Unhydrated cement grains (UCG) in C50 concrete at room temperature.

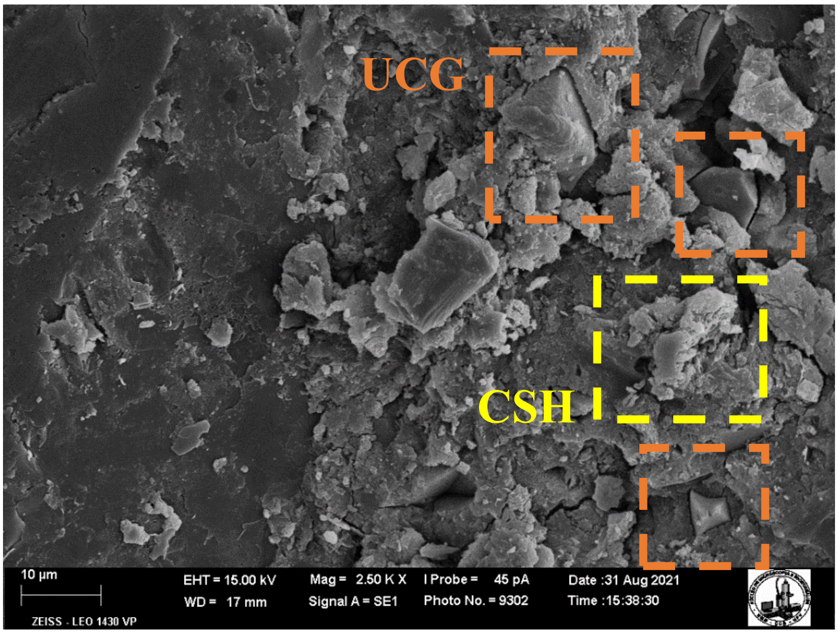

Source: Author (2021).

Fig. 14. C30 concrete after exposure to 200 ºC.

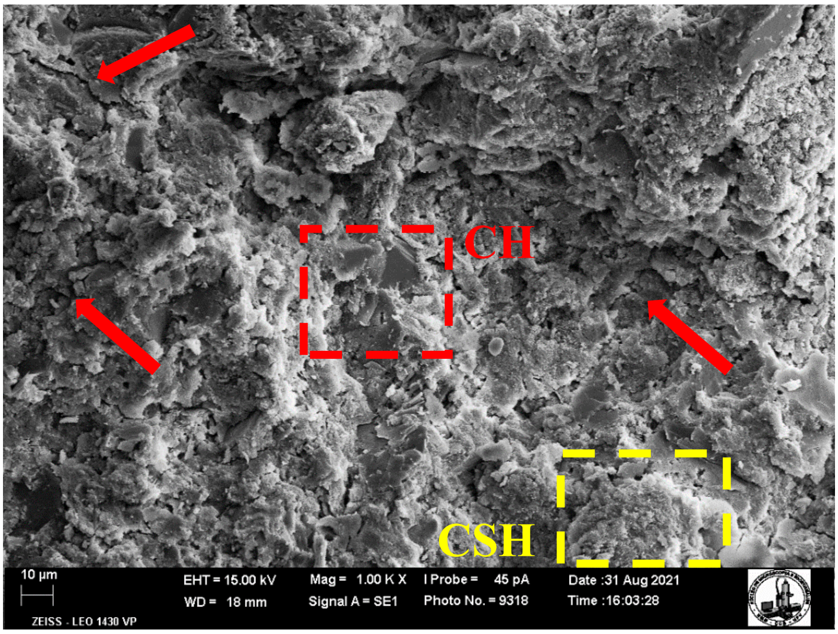

Source: Author (2021).

Additionally, both in Fig. 14 and Fig. 15, the C-S-H structures show early signs of dehydration, which is expected to start when concrete is exposed to 100-200 ºC range [8,10]. Both C30 and C50 samples show the presence of microcracks (indicated by red arrows), which could be the reason for the early deterioration of the concrete residual Young's modulus.

Fig. 15. C50 concrete after exposure to 200 ºC.

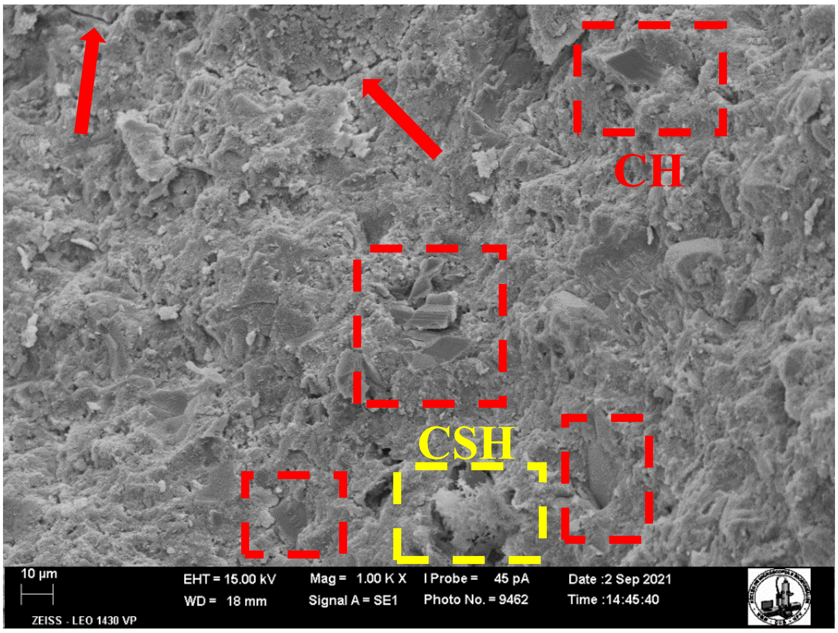

Source: Author (2021).

As temperature increases, it is possible to see the microcracking around the aggregate particle, as indicated by the red arrow in Fig. 16. Additionally, after exposure to 400 ºC, porlandite shows signs of delamination that indicate the beginning of the deterioration process, as marked by the red dashed rectangle in Fig. 16 and can be observed more closely in Fig. 17.

Fig. 16. Cracks in C30 after exposure to 400 ºC.

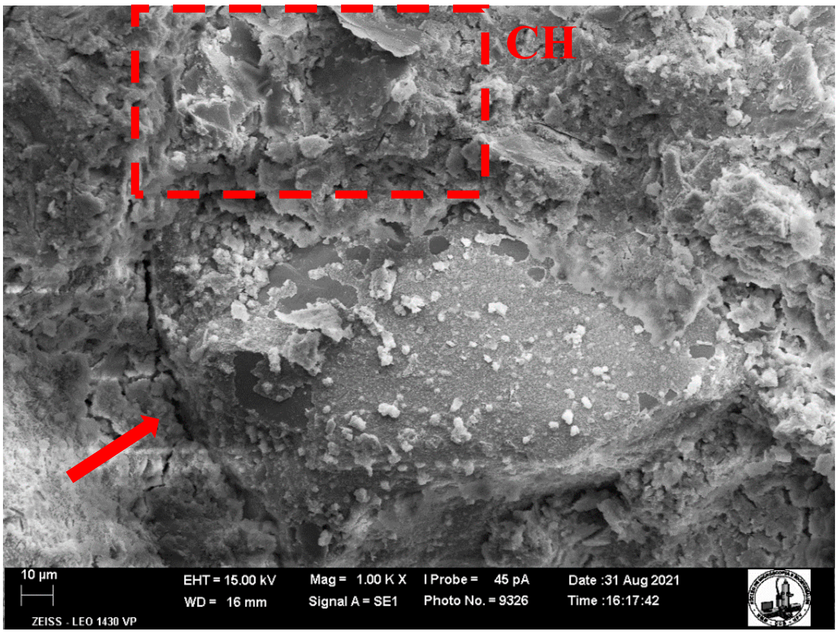

Source: Author (2021).

Fig. 17. Portlandite particle in C50 after exposure to 400 ºC.

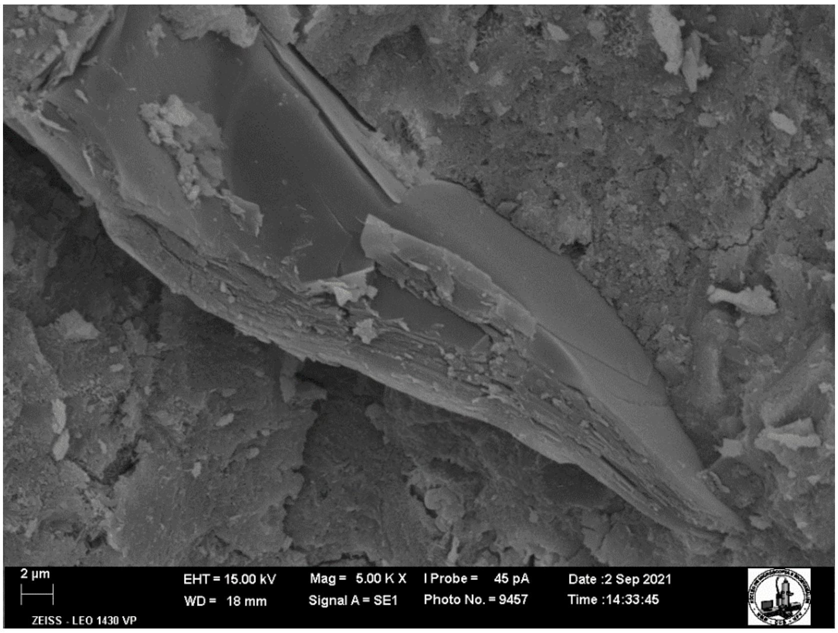

Source: Author (2021).

After exposure to 600 ºC, C30 shows a major crack at the interfacial transition zone between the aggregate and the cement paste, as shown in Fig. 18. Moreover, it was observed a clear dehydration of the CH structure, as shown in Fig. 19, similar to the observed by Kim et al. [6]. Additionally, it is possible to notice the coarsening of the concrete microstructure both for C30 and C50, which is a result from the dehydration process.

Fig. 18. C30 concrete exposed to 600 ºC.

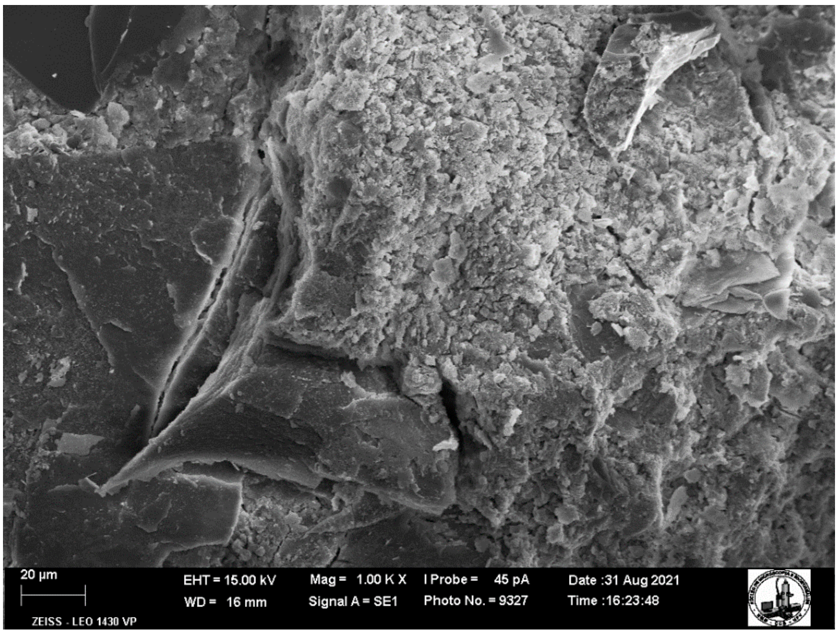

Source: Author (2021).

Fig. 19. Portlandite decomposition in C50 after exposure to 600 ºC.

Source: Author (2021).

3.3.1.3. XRD (X-ray diffraction)

Fig. 20 shows the X-ray diffraction for C30 and C50 concrete after exposure to elevated temperatures. All the XRD curves presented in Fig. 20 were trimmed on the y-axis to reduce to influence of the quartz peaks and better visualize the smaller peaks, which are more important for this analysis.

The main difference between the X-ray diffraction for C30 and C50 concrete, at room temperature, is the higher number of alite (C_3S) and larnite (C_2S) peaks identified for C50 concrete. This could be related to the mix proportions, because C50 concrete requires a higher amount of cement and has a smaller water-cement ratio, which could result in more unhydrated cement grains in the cement paste, as observed in the SEM images (Fig. 13).

As temperature increases, these unhydrated cement grains react with moisture that migrates through the cracked cement matrix after exposure to elevated temperatures. After exposure to 200 °C, the alite and larnite peaks reduces significantly in the XRD.

Fig. 20. X-ray diffraction for: a) C30; b) C50.

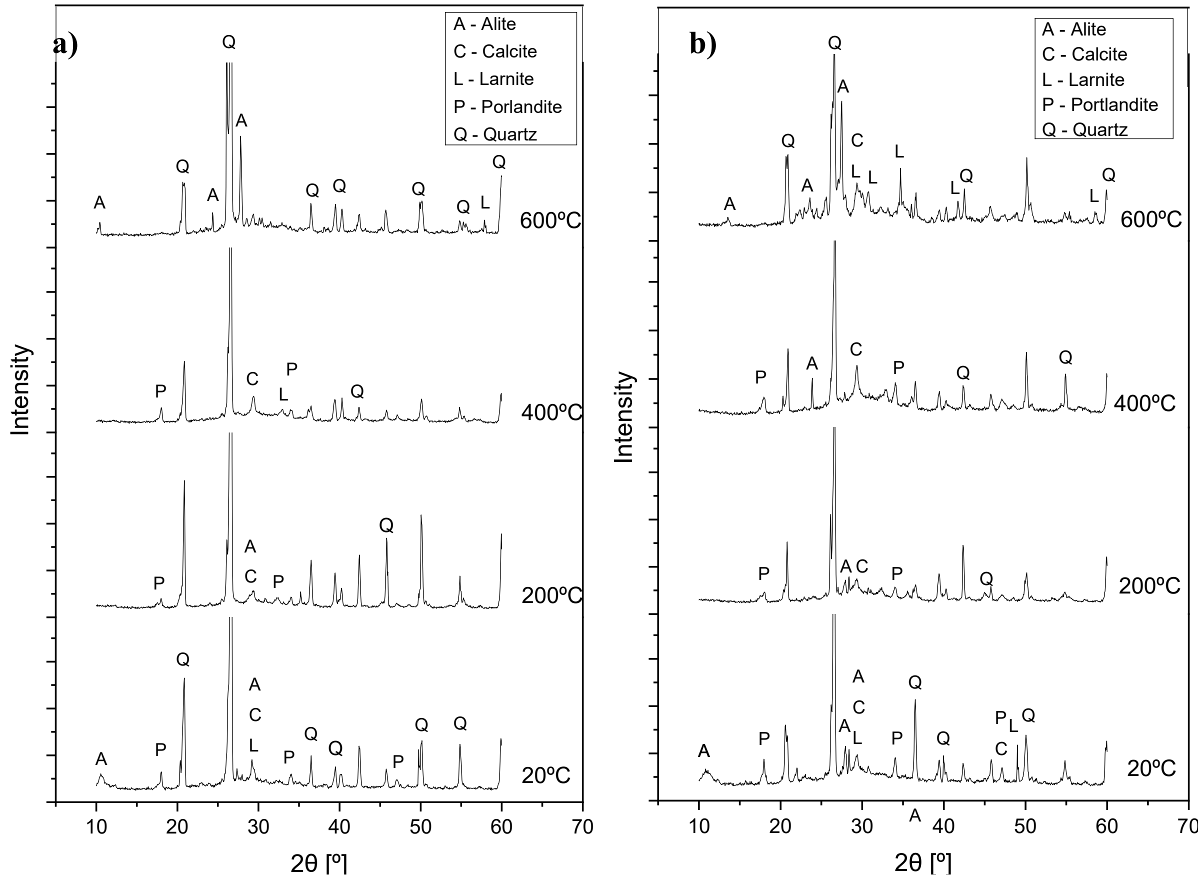

Source: Author (2021).

After exposure to 600 ºC, due to the dehydration of porlandite and partial C-S-H dehydration, alite and larnite peaks are identified in the concrete samples again. Both C30 and C50 showed the presence of marked alite peaks at 23.5º and 27,5º and a larnite peak around 58º. Moreover, C50 shows many other larnite peaks on the analyzed 2θ interval.

Fig. 21 shows the evolution the 18º peak of porlandite in concrete samples obtained by X-ray diffraction. It is possible to notice the clear deterioration of porlandite after exposure to 600 ºC, both for C30 and C50 concrete, similar to what was observed in the SEM images (Fig. 19).

Fig. 21. Decomposition of portlandite after exposure to elevated temperatures for: a) C30; b) C50.

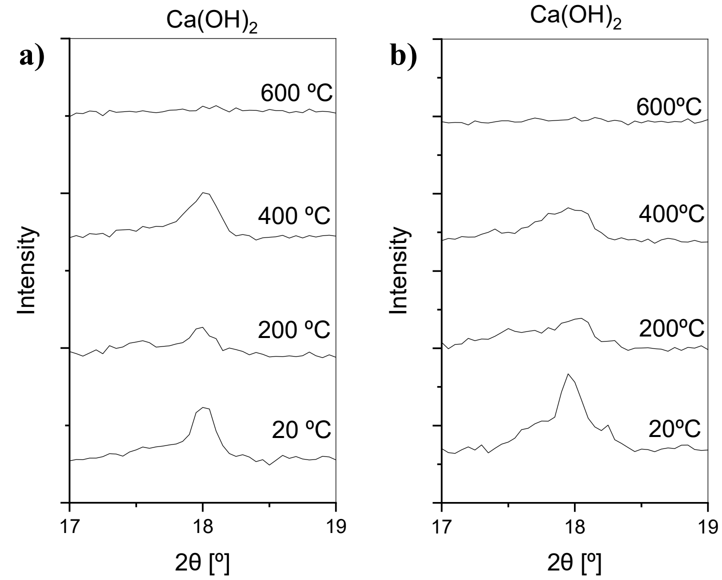

Source: Author (2021).

3.3.2. Effects of elevated temperature exposure on the rebar

The evolution of steel's residual mechanical properties with increasing the exposure temperature are given in Fig. 22 to Fig. 24. The results show that all the analyzed mechanical properties are only slightly affected by temperature exposure up to 400 ºC, which is in agreement with the results previously observed by other researchers [25–32].

Although the damage to the reinforcing steel mechanical properties is limited up to 400 ºC, when the temperature is raised to 600 ºC the 5.0 mm diameter bar shows a drastic reduction of the yield and the ultimate strengths. On the other hand, the Young's Module slightly increases for all the analyzed elevated temperatures, as shown in Fig. 24.

Fig. 22. Rebar relative ultimate strength after exposure to elevated temperature.

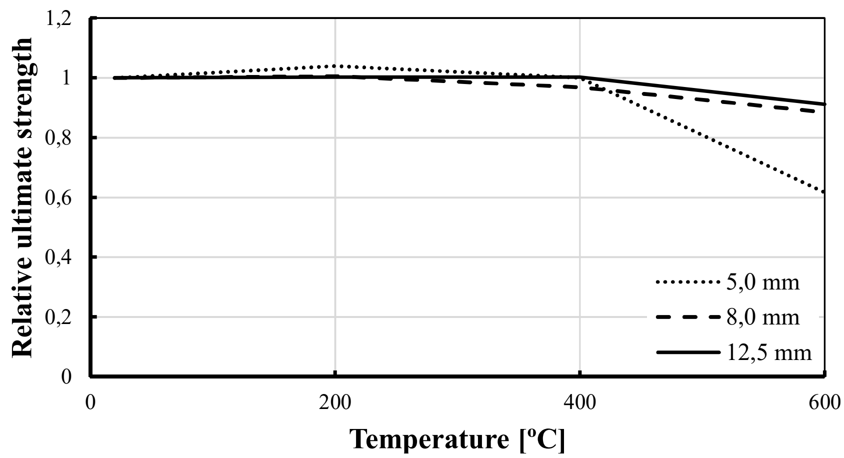

Source: Author (2021).

Fig. 23. Rebar relative yield strength after exposure to elevated temperature.

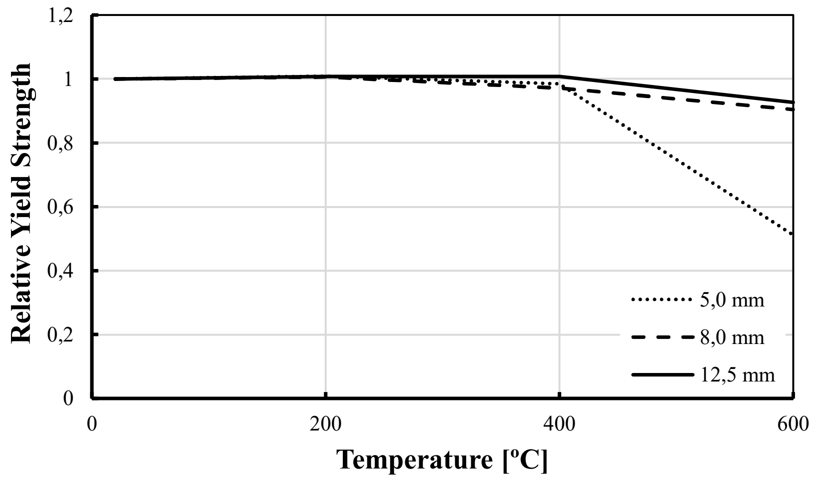

Source: Author (2021).

Fig. 24. Rebar relative Young's Module after exposure to elevated temperature.

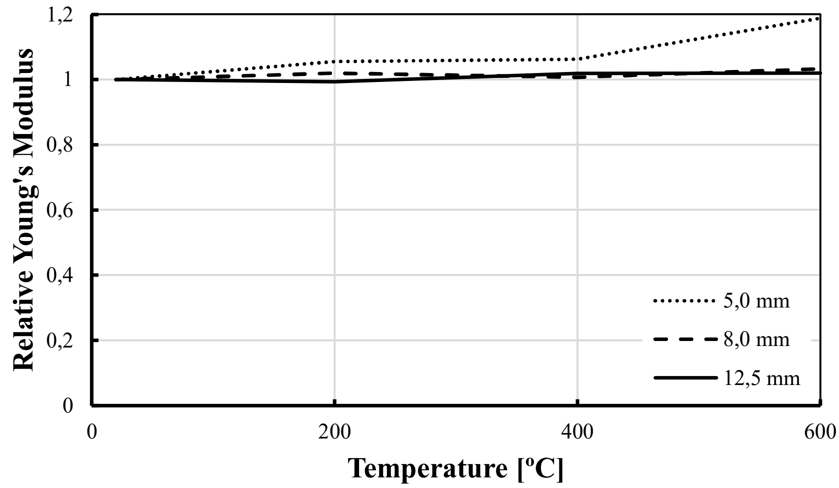

Source: Author (2021).

3.3.3. Effects of elevated temperature exposure at the materials interface

Even though the thermal incompatibility between the cement paste and the aggregates is responsible for the concrete microcracking, which is responsible for a of the concrete strength loss, the differential thermal expansions between the concrete and the reinforcement must also be considered, mainly in the analysis of the bond between the materials.

Fig. 25 and Fig. 26 show the effect of the differential thermal expansion on the materials interface for C30 and C50 concrete, respectively. For specimens subjected to 200 ºC, there are evidence of cement paste dehydration, but the materials interface remains uncracked for both concrete mixes. At 400 ºC, C30 concrete shows a small radial crack and C50 interface is cracked around the rebar, which means that the bond between the materials is already compromised.

Fig. 25. The C30 concrete-reinforcement interface at: a) room temperature; b) 200 ºC; c) 400 ºC; d) 600 ºC

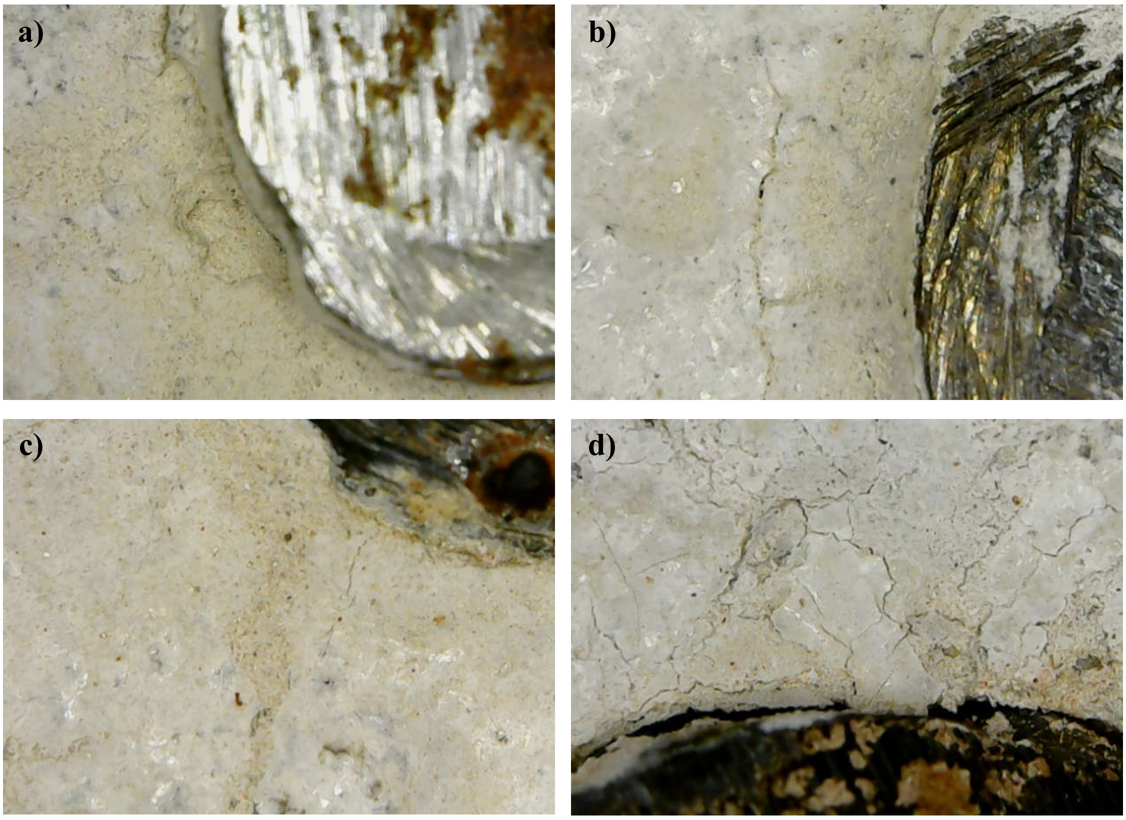

Source: Author (2021)

When the temperature reaches 600 ºC, the interface shows a progressive degradation of the bond at the interface and the advanced cracking of concrete both radially and around the rebar diameter. However, there is an important difference in the cracking pattern at 600 ºC: C50 shows well-defined radial cracks and C30 shows craze cracks. This could mean that interface of C50 cracks primarily due to the differential thermal expansion, while C30 crack pattern suggests that the concrete microcracking was the main deterioration mechanism. Nevertheless, both concretes seem to have lost contact at the interface.

After exposure to 600 ºC, the effect of both concrete microcracking and differential thermal expansion at the interface drastically reduces the confinement of concrete around the rebar. This effect influences not only the maximum bond strength, but also the bond failure mechanism.

Fig. 26. The C50 concrete reinforcement interface at: a) room temperature; b) 200 ºC; c) 400 ºC; d) 600 ºC

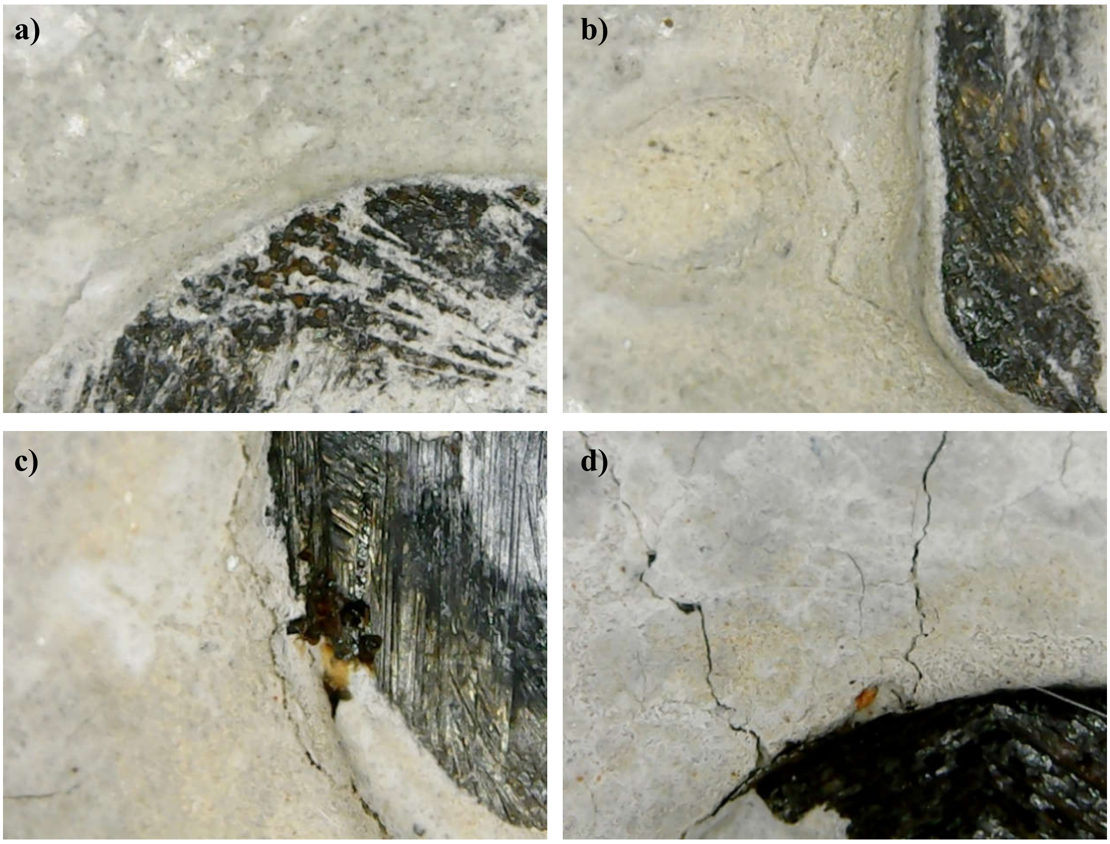

Source: Author (2021).

3.3.4. Effects of elevated temperature exposure on bond strength and failure mechanism

The results obtained from the pull-out tests in this experimental analysis are summarized in Table 6. The bar slip measurements correspond to the slip at the ultimate bond strength. All values presented in Table 6 are the average of three tests performed for each situation.

Table 6.
Bond strength and bar slip for the tested specimens.

Concrete	Temperature [ºC]	Ultimate bond strength [MPa]	Bar slip [mm]
C30	20	7.55	1.45
	200	13.08	0.58
	400	6.17	1.50
	600	4.64	1.03
C50	20	15.47	0.99
	200	14.97	0.76
	400	10.19	0.85
	600	6.36	0.97

Source: Author (2021).

Based on the results observed in this work, elevated temperature exposure seems to have a highly positive effect on the maximum bond strength for C30 at 200 ºC. After being heated to that temperature, the specimens analyzed exhibited an increase in bond strength, with an enhancement up to 73% of its value at room temperature. Moreover, the specimens also showed a reduction of the bar slip, which means that after exposure to 200 ºC the specimens developed higher bond strengths with smaller deformations.

The bond-slip relationships are represented by curves that are plotted in Fig. 27 and Fig. 28. The bond-slip curves are the mean curves of three specimens for each temperature and were obtained by the mean bond strength value for each specific bar slip. Hence, the maximum bond strength represented in the mean curve is not necessarily equal to the ultimate bond strength obtained by statistical analysis, since each individual maximum strength may occur at a different slip value. All the individual bond-slip curves and the corresponding mean curve for each situation are available in Appendix B.

As well as observed for the compressive and shear strengths, there is an improvement of the bond strength when C30 concrete is subjected to 200 ºC. Moreover, after exposure to 200 ºC the curve shows a high initial stiffness that ends on a marked peak and then, it is followed by a drastic degradation in bond strength, which suggests a splitting bond failure. At 400 ºC and 600 ºC, the curves show smaller initial stiffness and a clear plateau at maximum bond strength, which is characteristic of pull-out bond failure. The shape of the bond-slip curves suggests a more ductile bond failure at 400 ºC and 600 ºC, while at 200 ºC the curve indicates a sudden bond failure.

Although the bond-slip curve at 600 ºC show a typical pull-out failure mechanism, the tested specimen present concrete cracking along the rebar axis, as shown in Fig. 29. This could be an indication that even though the radial cracks reached the entire concrete cover, bond failed by the bar pull-out, which means this would be a splitting-induced pull-out bond failure.

Fig. 28 shows the bond-slip curves for specimens with C50 concrete. In contrast to C30 specimens, no significant bond strength enhancement was observed at 200 ºC. All the specimens that were subjected to elevated temperatures show bond-slip curves marked by a peak characteristic of splitting failure. The exposure to elevated temperatures clearly makes C50 specimens more prone to splitting failure, which can be observed both on the bond-slip curves and on the crack pattern of the tested specimens, shown in Fig. 29.

Fig. 27. Bond-slip curves for C30 concrete after exposure to elevated temperatures.

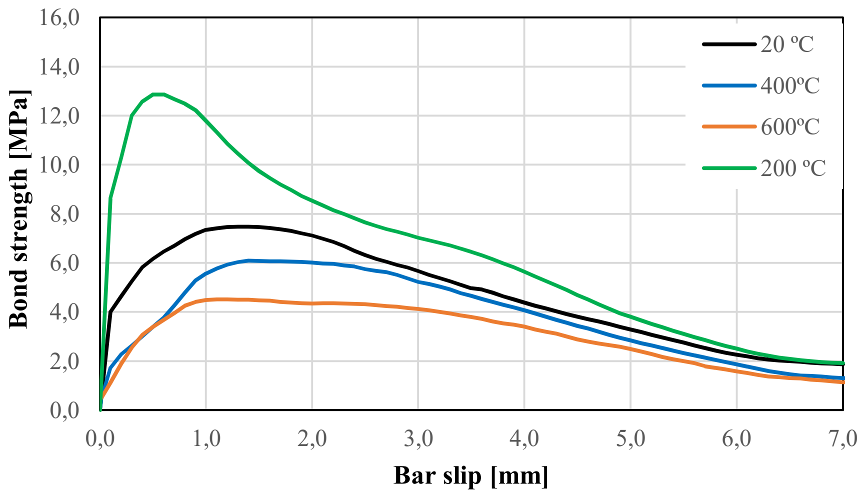

Source: Author (2021).

Fig. 28. Bond-slip curves for C50 concrete after exposure to elevated temperatures.

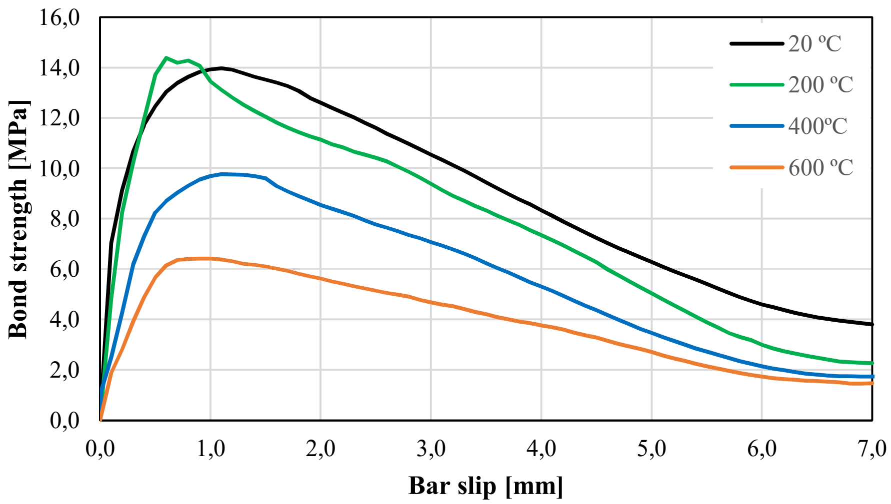

Source: Author (2021).

Fig. 29. Tested pull-out specimens for: a) C30; b) C50.

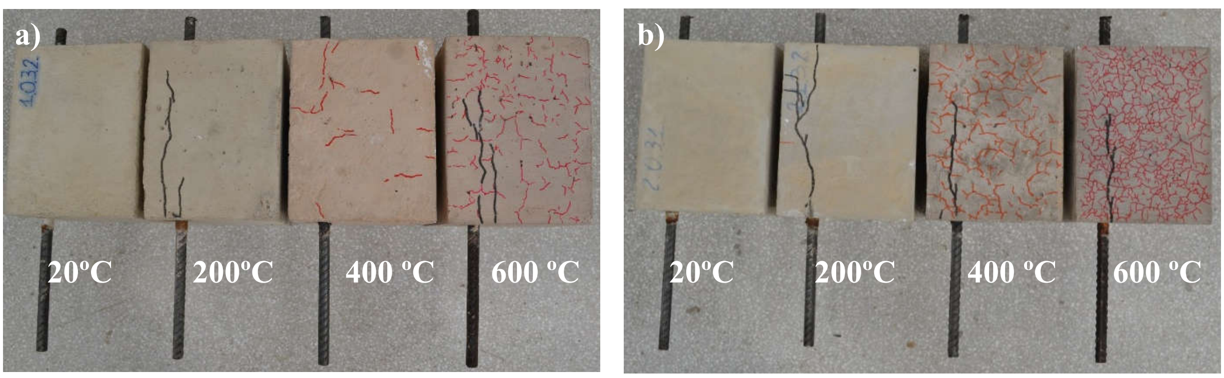

Source: Author (2021).

In addition, the difference in the interfacial cracking between C30 and C50, shown in Fig. 25 and Fig. 26, could contribute to explain the dissimilarity in the bond failure mechanism. The crack pattern observed for C30 could allow higher bar slips, which results in a more ductile bond failure, whereas the pre-existing radial cracks in C50 would be enlarged by the pull-out force, causing a splitting bond failure.

The degradation of the maximum bond strength for C30 and C50 after elevated temperature exposure is exhibited in Fig. 30 and Fig. 31, respectively. In addition, the degradation trends of the concrete's residual mechanical properties are plotted in the same figures for comparison purposes.

Fig. 30. Degradation of bond strength and C30 residual mechanical properties of concrete.

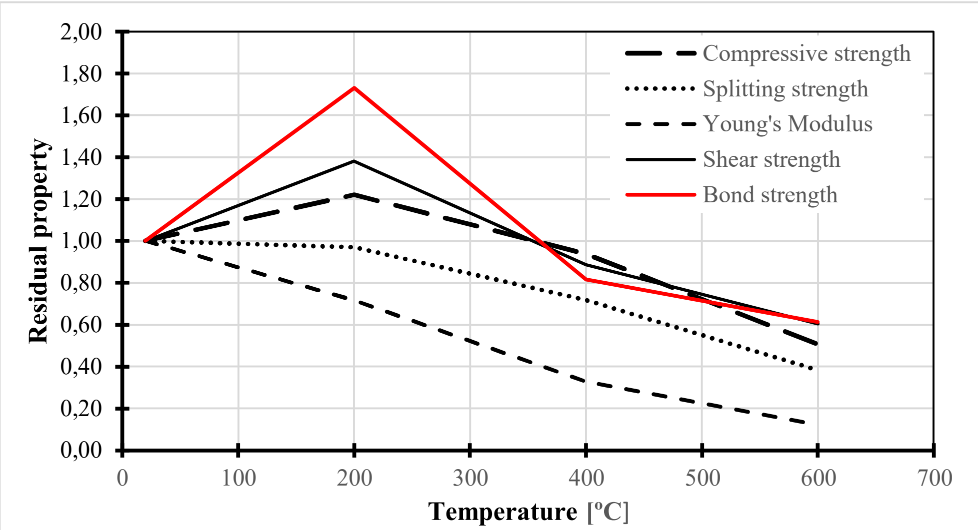

Source: Author (2021).

Fig. 31. Degradation of bond strength and C50 residual mechanical properties of concrete.

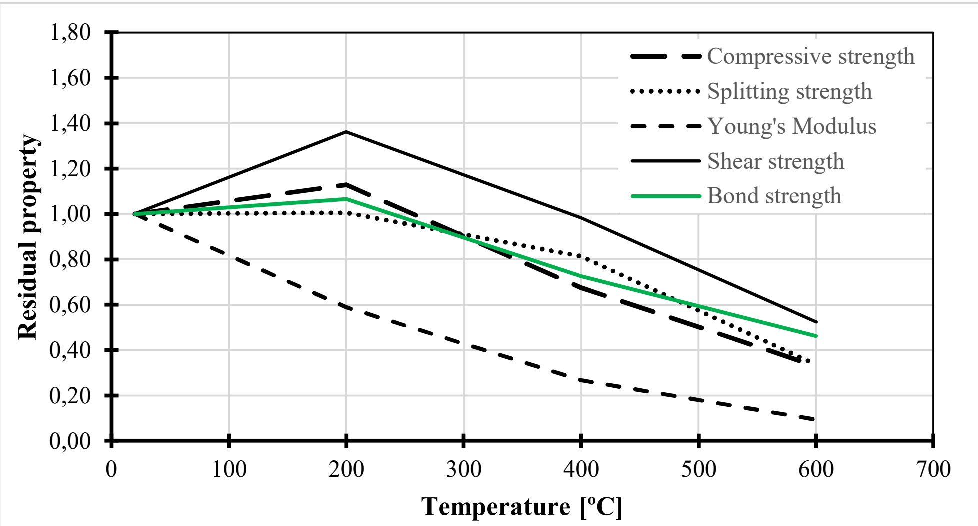

Source: Author (2021).

By analyzing the comparison graph of the proportional degradation of bond strength and residual mechanical properties of concrete after elevated temperature exposure, it is noticeable that, as the exposure temperature reaches 200 ºC, there is an enhancement in both concrete's compressive and shear strengths, whereas the splitting tensile strength suffers negligible variations. It is plausible that the enhancement of the compressive and shear strengths for C30 made it possible for the concrete in front of the bar ribs to bear higher stresses before crushing, hence transferring higher tensile stresses to the surrounding concrete. As the splitting tensile strength did not follow a similar enhancement trend, the concrete cover cracked, which negatively affected the adhesion between the materials at the interface and led to bond failure. Therefore, there was a change of the bond failure mechanism at 200 ºC, as can be seen in the bond-slip curve and by the splitting of the concrete cover of the tested specimen.

3.4. Conclusions

An experimental investigation of the effects of materials properties on bond strength and bond failure mechanism was developed in this work. Based on the results obtained, the following conclusions can be drawn:

- The CA50 reinforcing steel is only slightly affected by temperature exposure and maintained 90% of its yield strength at 600 ºC. On the other hand, the CA60 rebar does not show meaningful strength loss up to 400 ºC, but it is drastically damaged at 600 ºC.
- Elevated temperature exposure have different effects on each residual mechanical property of concrete and at each temperature level. After the exposure to 200 ºC, the compressive and shear strengths are positively affected, while the splitting tensile strength is slightly affected. For higher exposure temperatures, all the analyzed mechanical properties progressively deteriorated.
- Both concrete mixes showed early signs of deterioration of the Young's modulus, which was extremely weakened at 600 ºC, retaining only 12% and 9% of its original value for C30 and C50, respectively.
- C50 concrete showed a denser crack pattern after exposure to 400 ºC and 600 ºC. Furthermore, C50 showed well-defined radial cracks at the interface, while C30 presented craze cracking.

- Portlandite dehydration was verified through SEM and XRD analyses and it is directly related to the concrete residual compressive strength degradation. The pore structure coarsening was also observed after exposure to elevated temperatures.
- The effects of elevated temperature exposure on the concrete's residual mechanical properties showed to be crucial to the bond failure mechanism. The effects combination on the residual mechanical properties determines the bond failure mechanism.
- The increase in compressive and shear strengths is responsible for the bond failure mechanism change observed for C30 concrete after exposure to 200 ºC.
- High-temperature exposure did not affect the bar slip at ultimate bond strength, although C30 showed a higher bond failure ductility.

References

[1] Tepfers R, Achillides Z, Azizinamini A, Balázs G, Bigaj-van-Vliet A, Cabrera J, et al. fib Bulletin 10. Bond of reinforcement in concrete. vol. 7. fib. The International Federation for Structural Concrete; 2000. https://doi.org/10.35789/fib.BULL.0010.

[2] fib. fib Model Code 2010 - Final draft - Volume 1. vol. 7. Weinheim, Germany: Wiley-VCH Verlag GmbH & Co. KGaA; 2013.

[3] Cülfik MS, Özturan T. Mechanical properties of normal and high strength concretes subjected to high temperatures and using image analysis to detect bond deteriorations. Constr Build Mater 2010;24:1486–93. https://doi.org/10.1016/j.conbuildmat.2010.01.020.

[4] Georgali B, Tsakiridis PE. Microstructure of fire-damaged concrete. A case study. Cem Concr Compos 2005;27:255–9. https://doi.org/10.1016/j.cemconcomp.2004.02.022.

[5] Feldman RF, Ramachandran VS. Differentiation of interlayer and adsorbed water in hydrated portland cement by thermal analysis. Cem Concr Res 1971;1:607–20. https://doi.org/10.1016/0008-8846(71)90016-0.

[6] Kim KY, Yun TS, Park KP. Evaluation of pore structures and cracking in cement paste exposed to elevated temperatures by X-ray computed tomography. Cem Concr Res 2013;50:34–40. https://doi.org/10.1016/j.cemconres.2013.03.020.

[7] Arioz O. Effects of elevated temperatures on properties of concrete. Fire Saf J 2007;42:516–22. https://doi.org/10.1016/j.firesaf.2007.01.003.

[8] Khoury GA. Compressive strength of concrete at high temperatures: A reassessment. Mag Concr Res 1992;44:291–309. https://doi.org/10.1680/macr.1992.44.161.291.

[9] Lin W, Lin TD. Microstructures of Fire-Damaged Concrete 1997:199–205.

[10] Hertz KD. Concrete strength for fire safety design. Mag Concr Res 2005;57:445–53. https://doi.org/10.1680/macr.2005.57.8.445.

[11] Piasta J. Heat deformations of cement paste phases and the microstructure of cement paste. Matériaux Constr 1984;17:415–20. https://doi.org/10.1007/BF02473981.

[12] Behnood A, Ziari H. Effects of silica fume addition and water to cement ratio on the properties of high-strength concrete after exposure to high temperatures. Cem Concr Compos 2008;30:106–12. https://doi.org/10.1016/j.cemconcomp.2007.06.003.

[13] Ma Q, Guo R, Zhao Z, Lin Z, He K. Mechanical properties of concrete at high temperature-A review. Constr Build Mater 2015;93:371–83. https://doi.org/10.1016/j.conbuildmat.2015.05.131.

[14] Janotka I, Bágel L. Pore structures, permeabilities, and compressive strengths of concrete at temperatures up to 800°C. ACI Mater J 2002;99:196–200. https://doi.org/10.14359/11713.

[15] Rostásy FS, Weiß R, Wiedemann G. Changes of pore structure of cement mortars due to temperature. Cem Concr Res 1980;10:157–64. https://doi.org/10.1016/0008-8846(80)90072-1.

[16] Mendes A, Sanjayan J, Collins F. Phase transformations and mechanical strength of OPC/Slag pastes submitted to high temperatures. Mater Struct Constr 2008;41:345–50. https://doi.org/10.1617/s11527-007-9247-8.

[17] Chan YN, Luo X, Sun W. Compressive strength and pore structure of high-performance concrete after exposure to high temperature up to 800 °C. Cem Concr Res 2000;30:247–51. https://doi.org/10.1016/S0008-8846(99)00240-9.

[18] Lea FC, Stradling RE. The resistance to fire of concrete and reinforced concrete. J Soc Chem Ind 1922;41:395R-396R.

[19] Peng GF, Huang ZS. Change in microstructure of hardened cement paste subjected to elevated temperatures. Constr Build Mater 2008;22:593–9. https://doi.org/10.1016/j.conbuildmat.2006.11.002.

[20] Mendes A, Sanjayan JG, Collins F. Long-term progressive deterioration following fire exposure of OPC versus slag blended cement pastes. Mater Struct Constr 2009;42:95–101. https://doi.org/10.1617/s11527-008-9369-7.

[21] Lee J, Xi Y, Willam K. Properties of concrete after high-temperature heating and cooling. ACI Mater J 2008;105:334–41. https://doi.org/10.14359/19894.

[22] Peng G-F, Bian S-H, Guo Z-Q, Zhao J, Peng X-L, Jiang Y-C. Effect of thermal shock due to rapid cooling on residual mechanical properties of fiber concrete exposed to high temperatures. Constr Build Mater 2008;22:948–55. https://doi.org/10.1016/j.conbuildmat.2006.12.002.

[23] Biolzi L, Cattaneo S, Rosati G. Evaluating residual properties of thermally damaged concrete. Cem Concr Compos 2008;30:907–16. https://doi.org/10.1016/j.cemconcomp.2008.09.005.

[24] Janotka I, Nürnbergerová T. Effect of temperature on structural quality of the cement paste and high-strength concrete with silica fume. Nucl Eng Des 2005;235:2019–32. https://doi.org/10.1016/j.nucengdes.2005.05.011.
[25] Xiao J, Hou Y, Huang Z. Beam test on bond behavior between high-grade rebar and high-strength concrete after elevated temperatures. Fire Saf J 2014;69:23–35. https://doi.org/10.1016/j.firesaf.2014.07.001.
[26] Topçu IB, Karakurt C. Properties of reinforced concrete steel rebars exposed to high temperatures. Res Lett Mater Sci 2008;2008. https://doi.org/10.1155/2008/814137.
[27] Neves IC, Rodrigues JPC, Loureiro A de P. Mechanical properties of reinforcing and presstressing stells after heating. J Mater Civ Eng 1996;8:189–94.
[28] Elghazouli AY, Cashell KA, Izzuddin BA. Experimental evaluation of the mechanical properties of steel reinforcement at elevated temperature. Fire Saf J 2009;44:909–19. https://doi.org/10.1016/j.firesaf.2009.05.004.
[29] Tao Z, Wang XQ, Uy B. Stress-strain curves of structural and reinforcing steels after exposure to elevated temperatures. J Mater Civ Eng 2013;25:1306–16. https://doi.org/10.1061/(ASCE)MT.1943-5533.0000676.
[30] Ahmad MS. Effect of Sustained Elevated Temperature on Mechanical Behavior of Reinforcing Bar. Procedia Eng 2017;173:905–9. https://doi.org/10.1016/j.proeng.2016.12.139.
[31] Qian H, Yan D, Chen S, Chen G, Tian Y, Chen G. Effect of High Temperature Exposure and Strain Rate on Mechanical Properties of High-Strength Steel Rebars. J Mater Civ Eng 2019;31:04019261. https://doi.org/10.1061/(asce)mt.1943-5533.0002906.
[32] Qiang X, Bijlaard FSK, Kolstein H. Post-fire mechanical properties of high strength structural steels S460 and S690. Eng Struct 2012;35:1–10. https://doi.org/10.1016/j.engstruct.2011.11.005.
[33] ASTM C595-03. Standard Specification for Blended Hydraulic Cements. Annu B Am Soc Test Mater ASTM Stand 2003;14:1–7. https://doi.org/10.1520/C0595.
[34] ABNT - Associação Brasileira de Normas Técnicas. ABNT NBR NM 23:2000 - Cimento Portland e outros materiais em pó - Determinação da massa específica 2019.
[35] ASTM International. ASTM C188, Standard Test Method for Density of Hydraulic Cement 2017:3. https://doi.org/10.1520/C0188-17.
[36] ABNT - Associação Brasileira de Normas Técnicas. ABNT NBR 16372 - Cimento Portland e outros matertiais em pó - Determinação da finura pelo método da permeabilidade de ar (método de Blaine) 2015:11.
[37] International A. ASTM C204-18e1, Standard Test Methods for Fineness of Hydraulic Cement by Air-Permeability Apparatus 2018:11. https://doi.org/10.1520/C0204-18E01.
[38] ABNT. NBR NM 43 - Determinação da pasta de consistência normal. Rio Janeiro Assoc Bras Normas Técnicas 2003:17.
[39] ASTM International. ASTM C187-16, Standard Test Method for Amount of Water Required for Normal Consistency of Hydraulic Cement Paste 2016:3. https://doi.org/10.1520/C0187-16.
[40] ABNT - Associação Brasileira de Normas Técnicas. ABNT NBR 16607 - Cimento Portland — Determinação dos tempos de pega 2018:4.
[41] ASTM International. ASTM C191-19, Standard Test Methods for Time of Setting of Hydraulic Cement by Vicat Needle 2019:8. https://doi.org/10.1520/C0191-19.
[42] ABNT - Associação Brasileira de Normas Técnicas. NBR 7215: Cimento Portland - Determinação da resistência à compressão. Assoc Bras Normas Técnicas 2019:8.
[43] International A. ASTM C109/C109M-21, Standard Test Method for Compressive Strength of Hydraulic Cement Mortars (Using 2-in. or [50 mm] Cube Specimens) n.d. https://doi.org/10.1520/C0109_C0109M-21.
[44] ABNT - Associação Brasileira de Normas Técnicas. NBR NM 45: Agregados – Determinação da massa unitária e do volume de vazios. Abnt Nbr 452006 2006:18.
[45] ASTM International. ASTM C29/C29M - 17a, Standard Test Methos for Bulk Density (“Unit Weight”) and Voids in Aggregate 2017:5. https://doi.org/10.1520/C0029_C0029M-17A.
[46] ABNT - Associação Brasileira de Normas Técnicas. ABNT NBR NM 30 - Agregado miúdo - Determinaçao da absorção de água. Abnt Nbr Mn 30 2001:3p.
[47] ASTM International. ASTM C128-15, Standard Test Method for Relative Density (Specific Gravity) and Absorption of Fine Aggregate 2015:6. https://doi.org/10.1520/C0128-15.
[48] Associação Brasileira De Normas Técnicas (ABNT). ABNT NBR NM 248: Análise Granulométrica. Assoc Bras Normas Técnicas 2003:6.

[49] ASTM International. ASTM C136/ C136M-19, Standard Method for Sieve Analysis of Fine and Coarse Aggregates 2019:5. https://doi.org/10.1520/C0136_C0136M-19.

[50] Gusmão AC. Utilização do concreto de pós reativos como material de reparo - Ênfase na resistência de aderência 2017:143.

[51] Associação Brasileira de Normas Técnicas (ABNT). NBR 6118:2014 Design of concrete structures — Procedure. Assoc Bras Normas Técnicas 2014:238.

[52] Varona FB, Baeza FJ, Bru D, Ivorra S. Evolution of the bond strength between reinforcing steel and fibre reinforced concrete after high temperature exposure. Constr Build Mater 2018;176:359–70. https://doi.org/10.1016/j.conbuildmat.2018.05.065.

[53] Khoury GA. Effect of fire on concrete and concrete structures. Prog Struct Eng Mater 2000;2:429–47. https://doi.org/10.1002/pse.51.

[54] prEN 1992-1. prEN 1992-1 2001;1:53–156.

[55] Peng GF, Bian SH, Guo ZQ, Zhao J, Peng XL, Jiang YC. Effect of thermal shock due to rapid cooling on residual mechanical properties of fiber concrete exposed to high temperatures. Constr Build Mater 2008;22:948–55. https://doi.org/10.1016/j.conbuildmat.2006.12.002.

[56] Poon CS, Azhar S, Anson M, Wong YL. Comparison of the strength and durability performance of normal- and high-strength pozzolanic concretes at elevated temperatures. Cem Concr Res 2001;31:1291–300. https://doi.org/10.1016/S0008-8846(01)00580-4.

[57] Abramowicz M, Kowalski R. The influence of short time water cooling on the mechanical properties of concrete heated up to high temperature. J Civ Eng Manag 2005;11:85–90. https://doi.org/10.1080/13923730.2005.9636336.

[58] Bamonte P, Gambarova PG. Thermal and mechanical properties at high temperature of a very high-strength durable concrete. J Mater Civ Eng 2010;22:545–55. https://doi.org/10.1061/(ASCE)MT.1943-5533.0000058.

[59] Balázs GL, Lublóy É. Post-heating strength of fiber-reinforced concretes. Fire Saf J 2012;49:100–6. https://doi.org/10.1016/j.firesaf.2012.01.002.

[60] Shaikh FUA, Vimonsatit V. Effect of cooling methods on residual compressive strength and cracking behavior of fly ash concretes exposed at elevated temperatures. Fire Mater 2016;40:335–50. https://doi.org/10.1002/fam.2276.

[61] Chen B, Liu J. Residual strength of hybrid-fiber-reinforced high-strength concrete after exposure to high temperatures. Cem Concr Res 2004;34:1065–9. https://doi.org/10.1016/j.cemconres.2003.11.010.

[62] Castellote M, Alonso C, Andrade C, Turrillas X, Campo J. Composition and Microstructural Changes of Cement Pastes Upon Heating , as Studied by Neutron Diffraction Composition and microstructural changes of cement pastes upon heating , as studied by neutron diffraction 2004;8846. https://doi.org/10.1016/S0008-8846(03)00229-1.

[63] Annerel E, Taerwe L. Revealing the temperature history in concrete after fire exposure by microscopic analysis. Cem Concr Res 2009;39:1239–49. https://doi.org/10.1016/j.cemconres.2009.08.017.

[64] Lim S, Mondal P. ScienceDirect Micro- and nano-scale characterization to study the thermal degradation of cement-based materials. Mater Charact 2014;92. https://doi.org/10.1016/j.matchar.2014.02.010.

CHAPTER 4:

Experimental evaluation of the influence of concrete cover to bar diameter ratio on concrete-reinforcement bond failure mechanism after exposure to elevated temperatures

Abstract

This work presents an experimental assessment of the influence of concrete cover to bar diameter ratio on concrete-reinforcement bond failure mechanism. Pull-out tests were used to evaluate the bond behavior. Two concrete mixes were analyzed, with 30 and 50 MPa compressive strength, and three different configurations of concrete cover to bar diameter ratio were subjected to 200 ºC, 400 ºC, and 600 ºC. For these cases, the specimens were first heated in an electric furnace and kept until they reached thermal equilibrium. Thus, they were cooled to room temperature and after then were tested. Exposure to 200 ºC has been shown to positively affect bond strength; however, as the temperature increases above this range, the bond strength progressively deteriorates. Elevated temperature exposure did not seem to influence the bar slip for any of the analyzed configurations. The bar slip was affected only by the bond failure mechanism change between C30 concrete and deformed rebars at 200 ºC. Moreover, the results of this work show that bond failure mechanisms cannot be easily distinguished after exposure to elevated temperatures. Finally, there is no clear relationship between the residual compressive strength of concrete and residual bond strength after exposure to elevated temperatures; however, the fib Model Code account for bond strength in structures design can represent safely both the bond strength at room temperature and the residual bond strength after exposure to elevated temperatures.

Keywords: Reinforced Concrete. Bond strength. Elevated temperatures. Concrete cover to bar diameter ratio. Bond-slip relationship. Bond failure mechanism.

4.1. Introduction

Reinforced concrete is a composite material capable of bearing both compressive and tensile stresses. This unique composite behavior is only possible due to the force-transfer mechanism between the materials; hence, to the bond between them. When a structure is affected by fire, not only the materials are damaged, but also the bond at their interface. In this situation, the force-transfer mechanisms are compromised, as well as the bearing capacity of the structure itself.

Bond strength can be defined as the force being transferred between the materials by unit of surface area along the rebar embedment length. For small embedment length to bar diameter ratios (l_b/d), in which the shear stress can be assumed to be uniformly distributed along the bar, the shear stress of maximum bond can be expressed by Eq. (1):

$$\tau = \frac{P_{max}}{\pi d l_b} \tag{1}$$

where P_{max} is the maximum pull-out load; d is the diameter of the reinforcement and l_b is the embedment length.

At room temperature, short specimens (l_b/d <10) exhibit mainly two bond failure mechanisms, pull-out and splitting. Pull-out failure is due mostly to the shearing-off of the concrete between the rebar transversal ribs, while splitting failure is due mostly to the longitudinal splitting of the concrete surrounding the rebar. Splitting failure is characterized by the concrete cover cracking and bond capacity vanishes once the radial cracks get to the outer surface of the specimen. On the other hand, pull-out failure does not show any visible cracks [1].

According to the fib Model Code (2010) [2], the analytical bond stress-slip relationship for monotonic loading at room temperature can be represented by the curves shown in Fig. 1. In this model, maximum bond strength for pull-out failure is valid for well-confined concrete (concrete cover ≥ $5d$) and can be estimated as a function of the concrete compressive strength itself, as shown in Eq. (2). On the other hand, splitting failure is described as a much more complex mechanism that can be estimated as a function of various geometric parameters, according to Eq. (3).

Fig. 1. Bond-slip relationship and bond failure mechanisms at room temperature

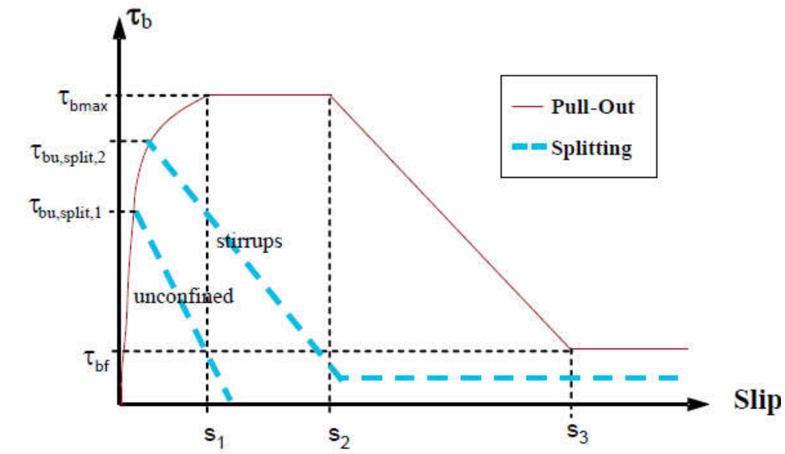

Source: fib Model Code (2010) [2].

$$\tau_{bmax} = 2.5\sqrt{f_{cm}} \quad (2)$$

$$\tau_{bu,split} = 6.5\,\eta_2\left(\frac{f_{cm}}{25}\right)^{0.25}\left(\frac{25}{\Phi}\right)^{0.25}\left[\left(\frac{c_{max}}{\Phi}\right)^{0.33}\left(\frac{c_{max}}{c_{min}}\right)^{0.10} + k_m k_{tr}\right] \leq \tau_{bmax} \quad (3)$$

where:

η_2 is the factor to consider whether the bar is anchored in good or bad conditions;

f_{cm} is the mean concrete compressive strength [MPa];

Φ is the bar diameter [mm];

c_{max}/c_{min} are the maximum and minimum concrete covers;

$k_m k_{tr}$ are factors to consider the existence of confinement by transverse reinforcement;

τ_{bmax} is the ultimate pull-out strength [MPa].

Although short specimens usually fail by pull-out or splitting, long specimens ($l_b/d > 10 - 20$), may present a third bond failure mechanism, which is the combination of the other two, a pull-out failure induced by concrete splitting. This mechanism is identified when there are visible splitting cracks on the concrete cover but the bond fails by the concrete shear between the rebar transversal ribs [1].

The Brazilian Standard [3] and the fib Model Code [2] account for the bond strength in structures design through Eq. (4) and Eq. (5), respectively.

$$f_{bd} = \eta_1\eta_2\eta_3\eta_4(f_{ck}/25)^{0.5} \quad (4)$$

$$f_{bd} = \eta_1\eta_2\eta_3(0.21{f_{ck}}^{2/3}) \tag{5}$$

where:

η_1 is the factor to consider the bar surface condition (plain, deformed);

η_2 is the factor to consider whether the bar is anchored in good or bad conditions;

η_3 is the factor to consider the influence of the bar diameter;

η_4 is the factor to consider the reinforcing bar yield strength;

f_{ck} is the concrete compressive strength [MPa].

During its lifespan, a reinforced concrete structure may be subjected to a fire condition. Generally, when exposed to elevated temperatures, the higher the temperature, the greater the reduction of the residual mechanical properties of concrete (e.g. modulus of elasticity, compressive and tensile strengths) [4,5,14–20,6–13].

Elevated temperature exposure causes the deterioration of concrete due to physical and chemical changes in its microstructure, to the thermal incompatibility between the cement paste and the aggregates, and to the conditions to which the structure is subject in the heating and cooling processes [4,5,21]. Variation in residual mechanical properties of concrete due to exposure to elevated temperature has been studied by many researchers over the years. It has been established that, depending on its constitution, concrete may present insignificant compressive strength loss, or even a slight increase for elevated temperatures up to 300 ºC [9,16,22,23]. However, for temperatures above 400 ºC, concrete is highly damaged and a drastic reduction of the compressive strength is observed [7,15,24–28].

Since heating seems to have a limited effect on the mechanical properties of reinforcing steel for temperatures up to 600 ºC [29–36], changes in the bond-slip relationship and in its characteristics upon fire exposure may be attributed mainly to physical and chemical changes of the concrete. Mostly, bond strength behavior with increasing temperatures is governed by concrete degradation in the heating and cooling phases. Hence, for exposition to elevated temperatures up to 200 ºC, maintenance or a slight increase of bond strength has been observed. At 300 ºC, residual bond strength is around 80% of its value at room temperature. For temperatures above 400 ºC, a distinct fall in maximum mean bond strength occurs [29,37,46–49,38–45].

Over the years, researchers have tried to relate the residual compressive strength of concrete to the residual bond strength; however, no clear relationship was identified. Some researchers have observed that the residual bond strength follows a similar trend than the concrete compressive strength [37,49–52]; in contrast, there are also reports that the bond strength was more affected than the compressive strength [38,40,53]. Similar conflicting results have been reported for the bar slip at maximum bond strength as well. In some experiments, a higher slip was observed [29,44,47–49], whereas others exhibited a reduction of the slip at bond failure [39,40,46].

The present study experimentally investigates the influence of the concrete cover to bar diameter ratio on concrete-reinforcement bond after exposure to elevated temperatures, especially focusing on the elevated temperature exposure effect on the change of bond failure mechanism. In addition, this study aims to evaluate whether the concrete strength could be a major factor affecting bond properties. The analysis of bond properties is made both by the mean values of maximum bond strength and bar slip and by the shape of bond-slip curves.

4.2. Experimental procedure

4.2.1. Design of experiments (DOE)

This experimental program proposed to study the influence of elevated temperature exposure and concrete cover to bar diameter ratio on bond properties, including the ultimate bond strength, the associated bar slip, the development of the bond-slip curve, and the bond failure mechanism.

The concrete cover to bar diameter ratio was analyzed by maintaining the concrete cover depth constant and changing the bar diameter. Three different bar diameters were tested, two deformed bars and one plain bar. In addition, to evaluate the concrete strength influence, two concrete mixes with compressive strength of 30 and 50 MPa were tested.

Hence, this research was designed as a factorial experiment with three factors, the concrete strength, the bar diameter, and the exposure temperature. The residual bond properties were measured after exposure to elevated temperatures and compared to that of room temperature. The target temperatures examined in this work are 200 ºC, 400 ºC and 600 ºC.

4.2.2. Test program and materials

The test program consisted of testing seventy-two pull-out specimens to analyze the effect of elevated temperature exposure on bond properties and bond failure mechanism. Two different concrete mixes were tested, with initial compressive strengths of 30 MPa (named C30) and 50 MPa (named C50), which proportions are detailed in Table 1.

Table 1.
Concrete mixes used for the tests.

Component	Quantity (kg/m³)	
	Mix 1 – C30	Mix 2 – C50
Cement	330	690
River quartz sand	841	432
Gravel	1051	1051
Water	190	228

Source: Author (2021)

The concrete mixes were prepared with Portland cement CP II-E-32, which is a slag-modified Portland cement that complies with the type I (SM) cement of ASTM C595 [54]. The aggregates used in this work were river natural sand and granite gravel, which properties are shown in Table 2.

Table 2.
Properties of the aggregates.

Property	River sand	Granite gravel	Standards
Specific gravity [g/cm³]	2.594	2.794	ABNT NBR NM 45 [55] equivalent to ASTM C29M – 17a [56]
Water absorption [%]	1.21	0.48	ABNT NBR NM 30 [57] equivalent to ASTM C128 – 15 [58]
Fineness modulus	2.71	6.97	ABNT NBR NM 248 [59] equivalent to ASTM C136M – 19 [60]
Maximum dimension [mm]	4.80	19.0	ABNT NBR NM 248 [59] equivalent to ASTM C136M – 19 [60]

Source: Author (2021)

In order to determine the residual properties of concrete after exposure to elevated temperatures, three 100 mm diameter and 200 mm height cylindrical specimens were casted for each combination of: concrete strength class (C30 and C50) and maximum exposure temperature (room temperature, 200 °C, 400 °C and 600 °C). Tests of compressive strength (ABNT NBR 5739[61] /ASTM C39M-14 [62]), tensile strength (ABNT NBR 7222 [63] /ASTM C496M-17 [64]) and modulus of elasticity (ABNT NBR 8522 [65] /ASTM C469M-14[66]) were performed.

Likewise, three specific specimens described in Chapter 3 (3.2.2) were also casted for each concrete strength and maximum exposure temperature to perform the shear test [67].

All specimens were subjected to submerged curing for 28 days. After this period, they were dried in an oven for 24 hours and then cooled for another 24 hours. For the elevated temperature exposure step, the specimens were heated in an electric furnace until reaching the reference temperature. The furnace was opened and the specimens cooled in natural air. In the sequence, the specimens were submitted to the aforementioned mechanical tests. The residual mechanical properties of concrete obtained are detailed in Table 3.

Table 3.
Concrete mechanical properties after exposure to elevated temperatures.

Concrete	Property	20 °C	200 °C	400 °C	600 °C
C30	f_c (MPa)	30.48	37.20	21.41	15.46
	f_{ct} (MPa)	2.65	2.57	1.90	0.72
	f_{cs} (MPa)	11.09	15.33	9.84	6.70
	E_c (GPa)	21.50	15.41	7.06	2.63
C50	f_c (MPa)	53.33	58.58	34.97	17.65
	f_{ct} (MPa)	3.18	3.20	2.59	1.07
	f_{cs} (MPa)	14.12	19.23	13.86	7.41
	E_c (GPa)	29.10	17.14	7.80	2.74

Note: f_c is the compressive strength, f_{ct} is the splitting strength, f_{cs} is the shear strength and E_c is the Young's modulus. The results presented herein are the mean values of three tests for each condition.

Source: Author (2021)

With respect to rebars, three different bar diameters were analyzed, 8.0 and 12.5 mm deformed CA50 grade rebars and 5.0 mm plain CA60 grade steel. Three specimens of each rebar diameter were tested at room temperature (ABNT NBR ISO 6892 [68] / ASTM A370-20 [69]) and the properties are given in Table 4.

Table 4.
Reinforcing bar properties (at room temperature).

Property	5.0 mm	8.0 mm	12.5 mm
Transversal rib spacing (mm)	-	5.32	6.95
Transversal rib height (mm)	-	0.52	0.77
Yield strength (MPa)	642.5	589.0	587.4
Ultimate strength (MPa)	690.6	699.3	694.5
Young's Modulus (GPa)	191.6	214.7	211.1

Source: Author (2021)

In sequence, the reinforcing bars were heated in an electric furnace until reaching the reference temperatures (200 ºC, 400 ºC and 600 ºC). The furnace was opened and the specimens cooled in natural air. The mechanical tests performed after elevated temperature exposure obtained the residual mechanical properties detailed in Table 5.

Table 5.
Reinforcing bar mechanical properties, measured at room temperature, after exposure to elevated temperatures.

Bar diameter	Property	200 °C	400 °C	600 °C
5.0	f_y (MPa)	648.1	632.5	328.5
	f_u (MPa)	717.5	691.0	426.1
	E_s (GPa)	202.2	203.5	227.6
8.0	f_y (MPa)	592.5	572.1	532.7
	f_u (MPa)	702.9	676.9	618.8
	E_s (GPa)	218.9	216.1	221.8
12.5	f_y (MPa)	592.0	591.9	544.2
	f_u (MPa)	696.7	696.7	633.1
	E_s (GPa)	209.8	215.1	215.2

Note: f_y is the yield strength, f_u is the ultimate strength and E_s is the Young's modulus. The results presented herein are the mean values of three tests for each condition.

Source: Author (2021)

4.2.3. Pull-out test specimens

The pull-out specimens used in this work are the same described in Chapter 3 (item 3.2.3) and are shown in Fig. 2. The only difference between the specimens used in this chapter and the last one is the variable diameter of the rebar. None of the geometric parameters of specimens have been changed further.

Fig. 2. Details of the pull-out specimen (units are in centimeters).

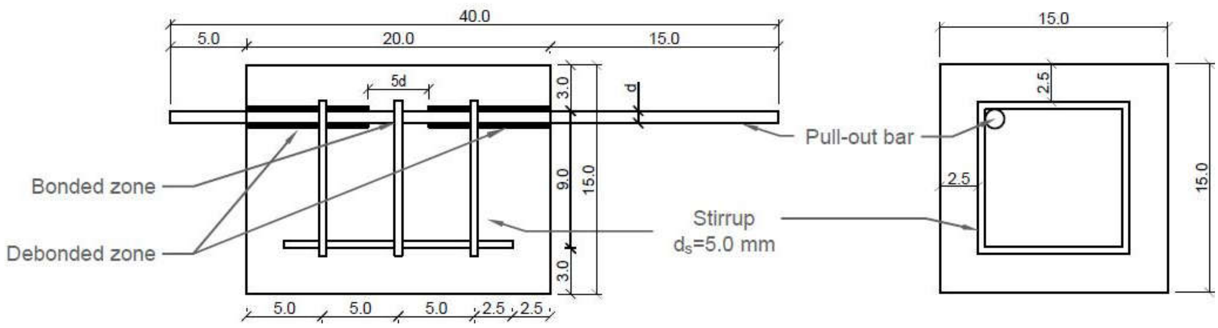

Source: Author (2021)

4.2.4. Specimen preparation and heating procedure

The specimens were cast in batches defined according to the electric furnace capacity. In each batch were cast the specimens that would be exposed to elevated temperatures at the same time, as shown in Fig. 3. Each batch produced nine pull-out specimens (3 repeats for each bar diameter) and three cylindrical specimens, which were used to ensure all batches had the same compressive strength before exposure to elevated temperatures.

As shown in Fig. 3, the pull-out test specimens were cast with the test rebar oriented horizontally near the top of the mold. The specimens were kept in the molds for three days and then demolded and taken to a water tank, where they were cured immersed in water for 28 days. After the curing period, the specimens were taken out of the water tank and let dry out at room temperature for a few hours. After that, the specimens were kept at 100 ºC for 24 hours and subsequently cooled down to room temperature. This 24 h period at 100 ºC was used to remove the free water and avoid spalling during the heating procedure.

Fig. 3. Specimens produced in one batch.

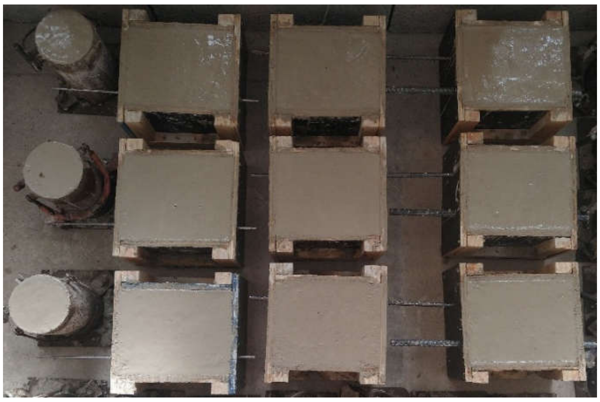

Source: Author (2021)

Finally, the specimens were put in an electric furnace and heated at a rate of approximately 4 ºC/min. The heating of the specimens inside the furnace was measured using thermocouples. One thermocouple (TC1) was used to measure the temperature inside the furnace and two thermocouples were cast inside a control specimen (TC2 and TC3). The control specimen was used to monitor the temperature increase inside the specimen and to determine whether the specimen had reached thermal equilibrium. TC2 was placed at the pull-out bar position and TC3 at the center of the specimen's cross-section (TC3), as represented in Fig. 4.

Fig. 4. Position of the: a) thermocouples; b) LVDT.

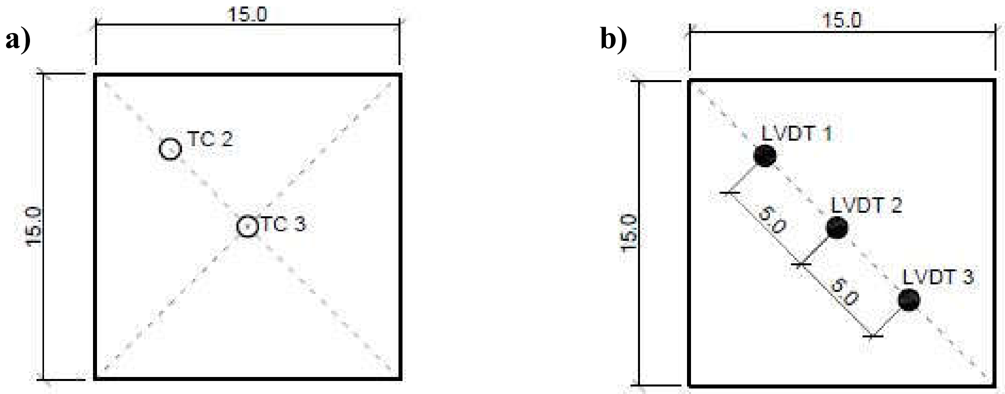

Source: Author (2021)

The furnace was turned off only when TC3 ensured that the whole specimen's cross-section had reached the target temperature, as exemplified by Fig. 5. At that point, the oven door was opened, and the specimens were allowed to cool down to room temperature overnight. All the time-temperature curves are available in Appendix A.

Fig. 5. Time-temperature curve for C50 concrete specimens.

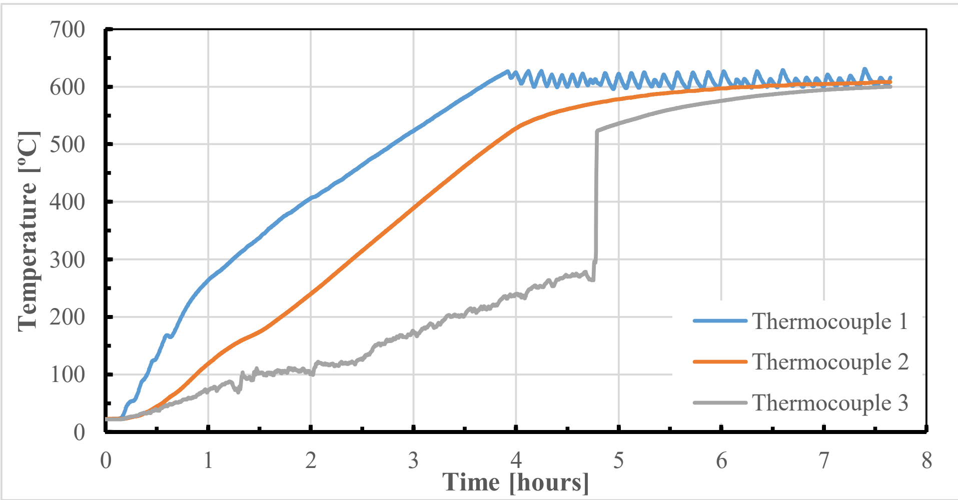

Source: Author (2021)

Due to a thermocouple malfunction, the time-temperature curve for C50 specimens subjected to 600 ºC shows an unusual behavior for Thermocouple 3. Apparently, the malfunction influenced only the initial part of the time-temperature curve, since the final branch of the curve seems compatible with the observed for the other specimens and temperatures.

4.2.5. Pull-out test setup

The pull-out tests were conducted in a universal testing machine (UTM) using a load-transfer apparatus, as shown in Fig. 6. The load-transfer apparatus was made up of two 20 mm thick steel plates, connected by four 16 mm diameter threaded bars, one at each corner of the steel plate. Both steel plates have a centered hole used to connect the apparatus to the UTM. The specimen is positioned into the apparatus with the pull-out bar faced down through the hole in the bottom plate and grabbed by the moveable gripper of the testing machine. Through the hole in top plate, a 150 mm long, 20 mm diameter bar is placed to attach the apparatus to the top gripper of the testing machine.

The pull-out load was applied to the specimen by moving down the bottom gripper of the UTM, at the constant displacement rate of 0.6 mm/min. It was chosen to work with a constant loading speed in order to avoid sudden bond failure and to collect data on the descending branch of the bond-slip relationship. Load was applied until the machine moveable gripper reached a maximum displacement of 15 mm.

Fig. 6. Pull-out test setup.

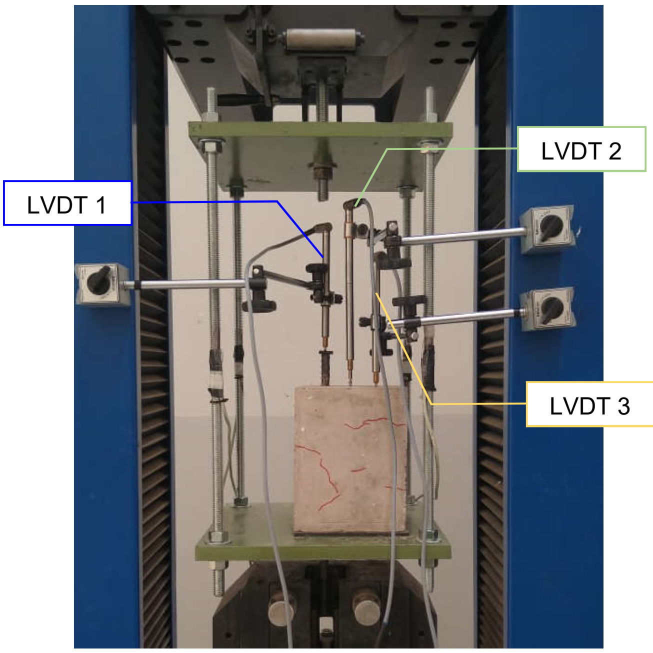

Source: Author (2021).

The corresponding pull-out force applied in each step of displacement was measured by four strain gauges, placed one in each bar of the apparatus. The strain gauges were calibrated to match the force measurements of the UTM load cell. This additional force-measurement system was used to match the data acquisition rate of the LVDT system; hence, to each step of displacement applied there is a corresponding pull-out load.

The bar slip was extrapolated from the displacement measurement obtained by three LVDT, positioned as shown in Fig. 4 and Fig. 6. LVDT 1 measured the displacement of the rebar, while LVDT 2 and LVDT 3 measured the concrete displacement. Based on the values of LVDT 2 and LVDT 3, it was estimated the concrete displacement at the bar location by using the linear equation, Eq. (6). A differential displacement was obtained at that point, here on denominated as the bar slip.

$$\delta = 2\delta_2 - \delta_3 \tag{6}$$

where δ is the calculated concrete displacement at the rebar position; δ_2 and δ_3 are the concrete displacement measured by LVDT 2 and LVDT 3, respectively.

The UTM used in the tests was an EMIC DL60000, that provides a maximum force of 600kN. The LVDTs used to measure the displacements were HBM WA20 and HBM WA50. The data acquisition systems used were the HBM MX1615 for the strain gauges and the HBM 840A for the displacement transducers.

4.3. Results and discussion

4.3.1. Overview of test results

The results obtained from the pull-out specimens in this experimental program are summarized in Table 6, in which the bar slip measurements correspond to the slip at the residual ultimate bond strength. All values presented in Table 6 are the average of three tests performed in each situation.

Table 6.
Residual bond strength and bar slip for the tested specimens.

Concrete	Bar diameter [mm]	Temperature [ºC]	Residual ultimate bond strength [MPa]	Bar slip [mm]
C30	5.0	20	2.98	1.32
C30	5.0	200	3.10	1.29
C30	5.0	400	1.55	1.09
C30	5.0	600	2.21	1.57
C30	8.0	20	6.63	1.17
C30	8.0	200	8.71	0.94
C30	8.0	400	5.71	1.07
C30	8.0	600	4.32	1.31
C30	12.5	20	7.55	1.45
C30	12.5	200	13.08	0.58
C30	12.5	400	6.17	1.50
C30	12.5	600	4.64	1.03
C50	5.0	20	6.94	1.29
C50	5.0	200	8.71	1.41
C50	5.0	400	3.67	2.01
C50	5.0	600	2.05	1.64
C50	8.0	20	14.73	0.74
C50	8.0	200	16.03	0.91
C50	8.0	400	10.45	0.91
C50	8.0	600	7.13	1.03
C50	12.5	20	14.01	0.99
C50	12.5	200	14.97	0.76
C50	12.5	400	10.19	1.04
C50	12.5	600	6.48	0.97

Source: Author (2021).

Based on the results observed in this work, heat exposure seems to have a highly positive effect on the residual maximum bond strength for specimens with deformed rebar and C30 concrete at 200 ºC. At this temperature, all the bar diameters analyzed exhibited an increase in residual bond strength, with an enhancement of 56% and 73% of the values at room temperature for 8.0 mm and 12.5 mm bars, respectively. Moreover, the deformed bars also showed a reduction of the bar slip, which means that after exposure to 200 ºC, the specimens sustained higher residual bond strengths with smaller deformations.

Alternatively, C50 concrete specimens showed slightly different behavior. Although residual bond strength was also enhanced for 5.0 and 8.0 mm rebars, the increase in bond strength was only 11% for the 8.0 mm deformed bars. Bond strength of 5.0 mm plain bars seemed to be more affected than the deformed bars, with a 25% enhancement. On the other hand, 12.5 mm bars did not show improvement of residual bond properties, retaining its room temperature strength without significant differences.

For 400 ºC, the residual bond strength of plain bars is highly damaged, retaining less than 60% of its value at room temperature for both concrete mixes. For the deformed bars, concrete strength seems to be significant at this temperature level, as 8.0 mm bars showed an 86% residual bond strength for C30, against 71% for C50. Bond of 12.5 mm rebars was more damaged for C50 as well, with 82% and 73% residual bond strengths. A similar trend is observed at 600 ºC.

4.3.2. Crack pattern

The 12.5 mm tested pull-out specimens are shown in Fig. 7 and the 8.0 mm in Fig. 8. The red marked lines on the specimens represent the heat-induced cracking and the thicker black lines show the cracking of the specimen during the pull-out test. Plain bar crack patterns are not presented because none of the specimens exhibited pull-out-induced cracking.

Fig. 7. Tested specimens with 12.5 mm for: a) C30; b) C50.

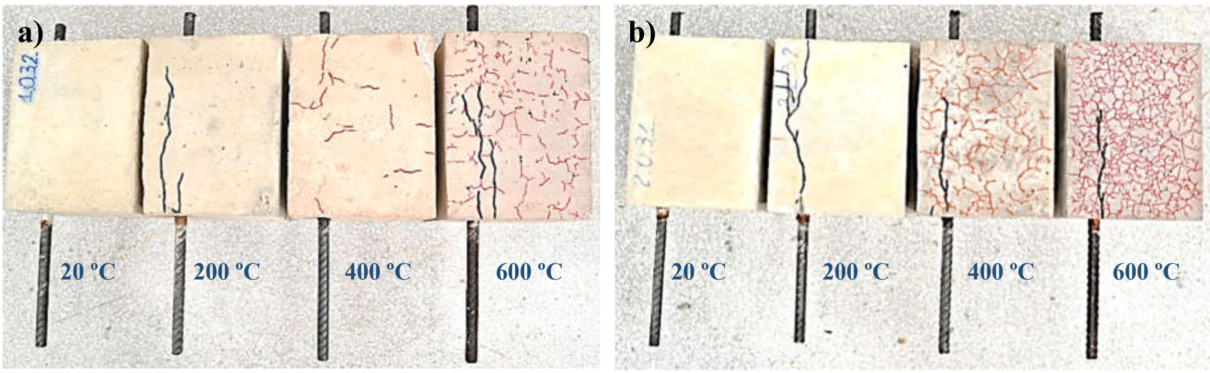

Source: Author (2021).

Fig. 8. Tested specimens with 8.0 mm for: a) C30; b) C50.

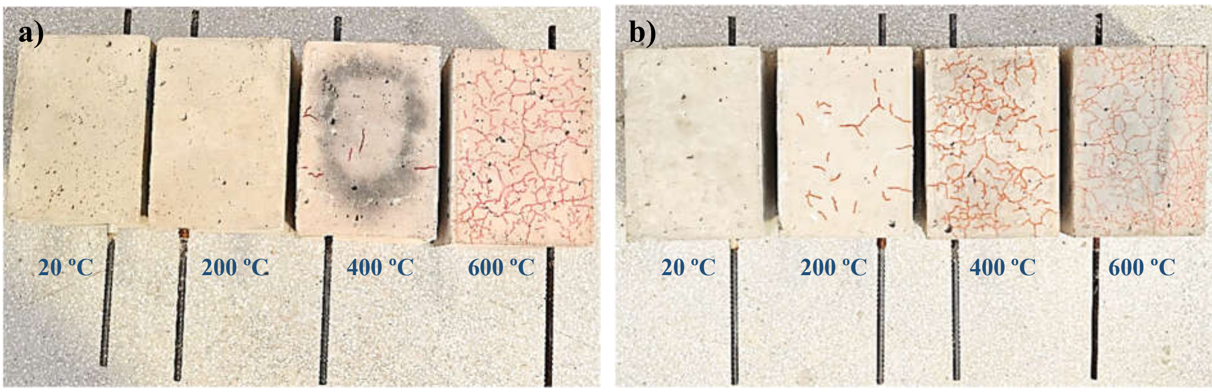

Source: Author (2021).

Specimens with C50 concrete are more damaged by elevated temperature exposure itself, as can be seen by the denser crack pattern, both for 8.0 mm and for 12.5 mm. The C30 concrete remains uncracked up to 200 ºC and exhibits scarce cracks at 400 ºC; only at 600 ºC it is possible to notice the damage in concrete due to exposure to elevated temperatures.

4.3.3. Bond-slip curves

The bond-slip curves resulting from the pull-out tests performed are plotted in Fig. 9 to Fig. 14. The bond-slip curves are the mean curves of three specimens for the same condition of temperature, concrete strength and bar diameter. These curves were obtained by the mean value of residual bond strength for each specific bar slip. Hence, the maximum residual bond strength represented by the mean curve is not necessarily equal to the ultimate residual bond strength showed in Table 6, since each individual maximum strength may occur at a different slip value. All the individual bond-slip curves and the corresponding mean curve for each situation are available in Appendix B.

Due to the elastic deformation of the rubber pad in the pull-out test setup, for very small displacement values, the method used to determine differential slip at the bar location may result in negative values for the bar slip. Once the settling of the rubber pad is over, this phenomenon is surpassed and the differential slip measure does not show any further external factor interference.

Moreover, the bond-slip curves for different bar diameters are plotted in graphs with different maximum slips, which were chosen based on the values corresponding to the rib spacing for each bar diameter (approximately 0.66 d for 8.0 mm and 0.56 d for 12.5 mm). Although the graphs are trimmed at different values, all specimens were tested to a maximum bar slip value of 10 mm (test setup). Based on the results, a tendency was observed, specifically for the 5.0 mm bar: to regain some of the residual bond strength after the slip was higher than the rib spacing value.

4.3.3.1. Specimen with c/d = 2.4 (12.5 mm bars)

The bond-slip curves for C30 concrete and 12.5 mm bars are shown in Fig. 9. At room temperature, the bond-slip curves for C30 show a high initial stiffness, with minor bar slip up to a stress of 4 MPa, followed by an increase in residual bond strength with a reduced stiffness until maximum residual bond strength is reached.

Furthermore, after exposed to 200 ºC the resulting curve shows an even higher initial stiffness with no significant slip up to 8 MPa, which winds up on a marked peak and then is followed by a drastic degradation in residual bond strength, that clearly suggests a splitting bond failure. At 400 ºC and 600 ºC, the curves exhibit the effect of elevated temperature exposure on the degradation of the initial stiffness and present a clear plateau at maximum bond strength, which is characteristic of pull-out bond failure.

Although the bond-slip curve at 600 ºC shows a typical pull-out failure mechanism, the tested specimens exhibit concrete cracking along the rebar axis, as shown in Fig. 7. This could be an indication that even though the radial cracks reached the entire concrete cover, bond failed by the bar pull-out, which means this would be a splitting-induced pull-out bond failure.

The high initial stiffness and the reduced bar slip values at 200 ºC suggest a sudden bond failure, while the reduced bond stiffness associated with higher slips and a plateau at maximum residual bond strength could be an indication of a more ductile bond failure at 400 ºC and 600 ºC. The apparent change in bond failure mechanism seems to be the key factor influencing the bar slip at maximum residual bond strength after exposure to elevated temperatures.

Fig. 10 presents the bond-slip curves for C50 concrete. At room temperature, the bond-slip behavior of C50 seems to be similar to C30, only reaching higher residual bond strengths due to the higher mechanical properties. In contrast to C30, which seems to suffer a change in bond failure mechanism after elevated temperature exposure, C50 exhibits evidence to be afflicted by splitting bond failure in all the analyzed high temperatures. Specimens subjected to 200 ºC, 400 ºC, and 600 ºC show a marked peak in the bond-slip curves, and visible concrete cover cracking along the rebar axis, as shown in Fig. 7.

Fig. 9. Bond-slip curves for C30 concrete and 12.5 mm bar.

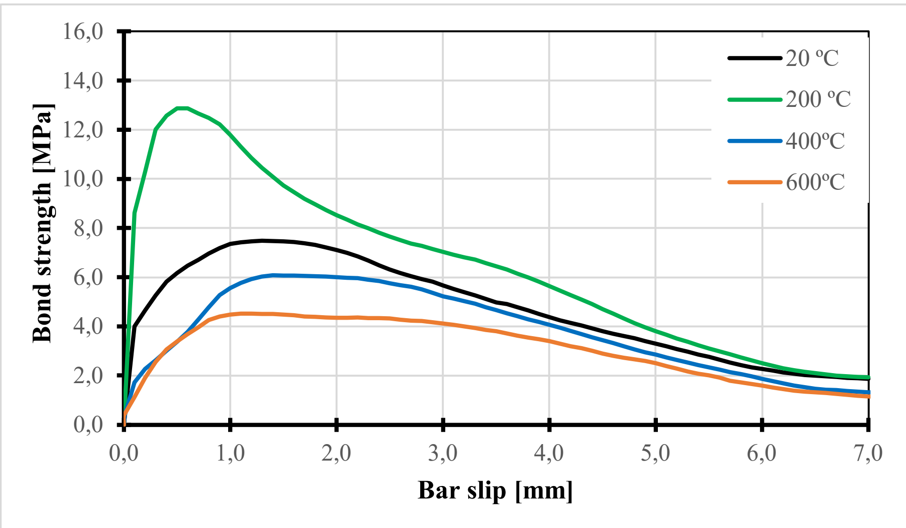

Source: Author (2021).

Fig. 10. Bond-slip curves for C50 concrete and 12.5 mm bar.

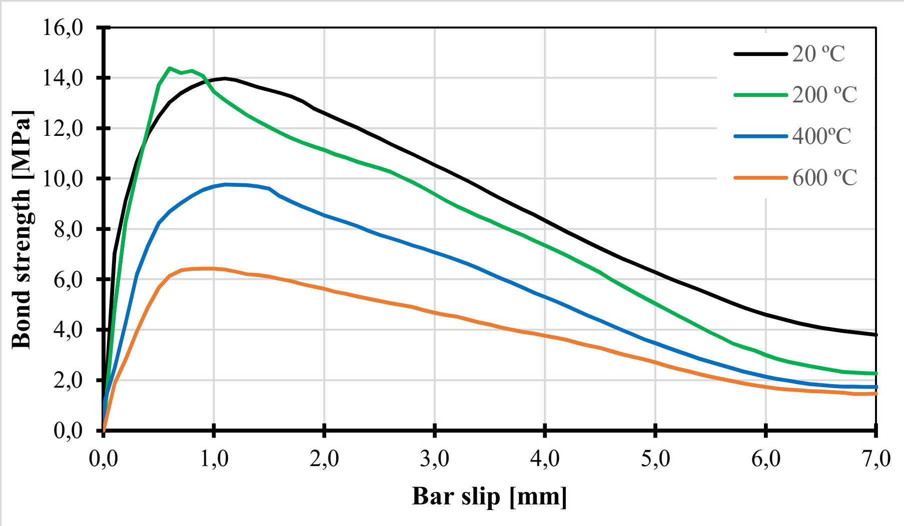

Source: Author (2021).

Furthermore, Fig. 10 shows no evidence that exposure to elevated temperatures influences bar slip at maximum residual bond strength, which could also be related to the sustained splitting bond failure. As well as observed for C30, the change in bond failure mechanism could be the most important point influencing the bar slip. In this case, since there is no change in bond failure mechanism, bar slip would not be affected by elevated temperatures.

4.3.3.2. Specimens with c/d = 3.75 (*8.0 mm bars*)

The results of the pull-out tests performed on the specimens with C30 concrete and 8.0 mm rebar are shown in Fig. 11. For all the examined temperatures, specimens seem to behave very similarly to C30 specimens with 2.4 *c*/*d*. The main difference is the bond-slip curve after exposure to 400 ºC, which seems to have a marked peak characteristic of splitting bond failure; however, no splitting of the concrete cover was observed in the tested specimens, as shown in Fig. 8.

Fig. 12 shows the bond-slip curves for C50 concrete and 8.0 mm rebar. Once again, the bond failure mechanism and bar slip does not seem to be affected by elevated temperature exposure. As shown in Fig. 8, C50 present a more extensive cracking pattern induced by the elevated temperature exposure when compared to C30. This denser crack pattern results in a noticeable tendency of C50 being more affected by splitting and maintaining this bond failure mechanism irrespective of the temperature level; however, no visible cracks were observed in the specimens after the pull-out test, as shown in Fig. 8. This could be an indication that even though there were no visible cracks on the concrete cover, there was an internal cracking process that did not reach the external surface of the specimen due to the greater *c*/*d* ratio. Nevertheless, it seems like the greater *c/d* ratio did not prevent splitting failure.

Fig. 11. Bond-slip curves for C30 concrete and 8.0 mm bar.

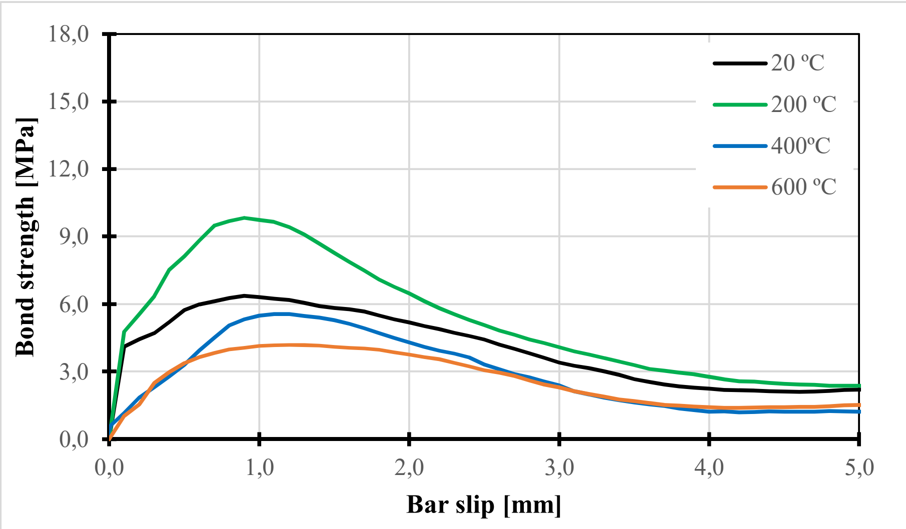

Source: Author (2021).

Fig. 12. Bond-slip curves for C50 concrete and 8.0 mm bar.

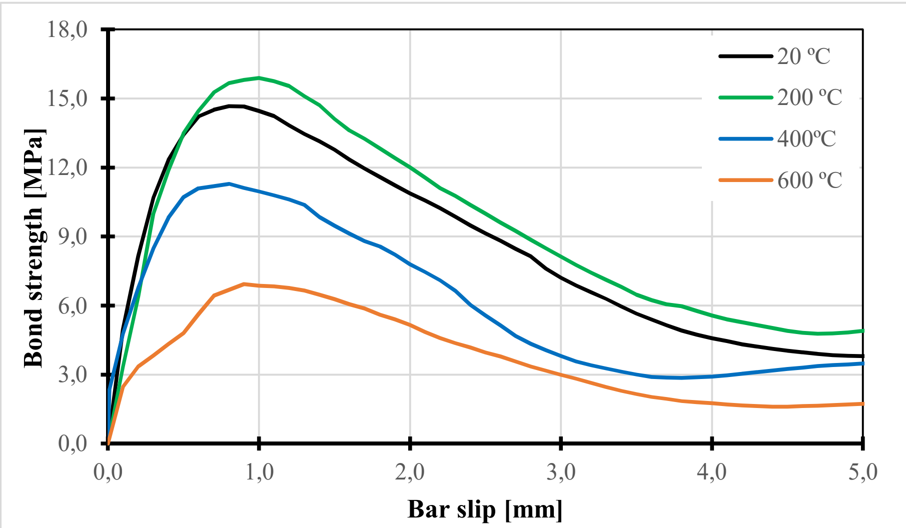

Source: Author (2021).

4.3.3.3. Plain bars (c/d = 6.0)

The bond-slip curves for specimens with 5.0 mm rebar with C30 and C50 concrete are shown in Fig. 13 and Fig. 14, respectively. For this rebar, the bond-slip behavior differs significantly from the previously analyzed bars, mostly because the 5.0 mm rebar is a plain bar, which means the bond develops mainly by adhesion and friction, in spite of the mechanical interlocking for deformed rebars [70–72].

Generally, plain bars fail by pull-out of the rebar, since the splitting of concrete cover is directly related to the tensile stresses transferred to the surrounding concrete due to the crushing of concrete in front of the bar's transversal ribs. The pull-out failure mechanism can be easily observed in both Fig. 13 and Fig. 14 for all the temperature levels.

Fig. 13. Bond-slip curves for C30 concrete and 5.0 mm bar.

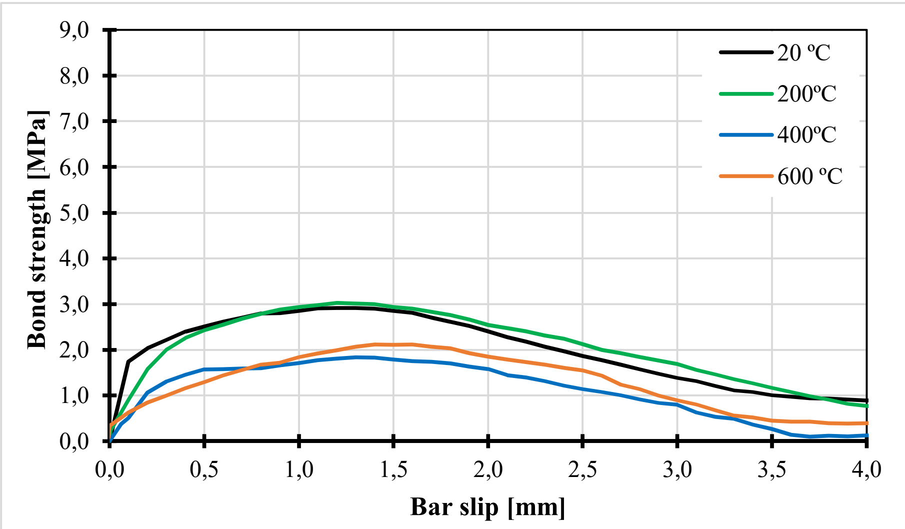

Source: Author (2021).

Fig. 14. Bond-slip curves for C50 concrete and 5.0 mm bar.

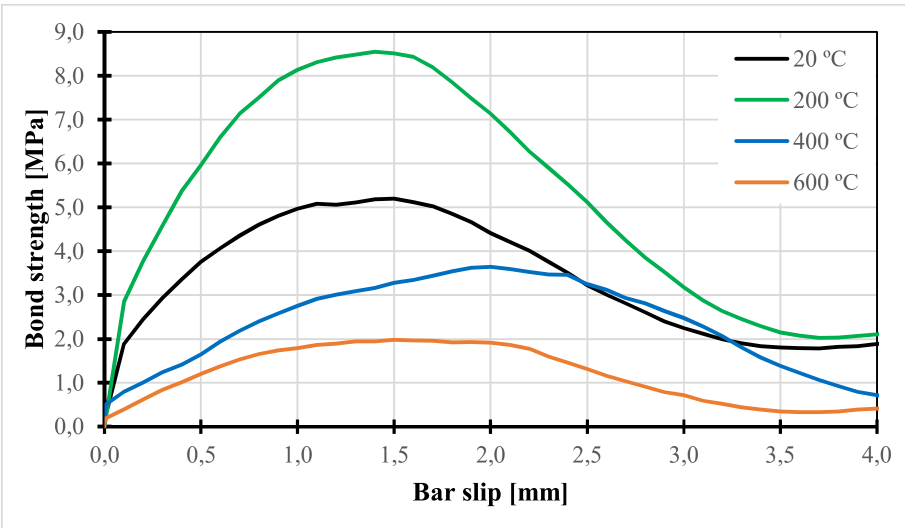

Source: Author (2021).

An unusual behavior was observed for C30 specimens subjected to 400 ºC, in which the residual bond strength decreased substantially compared to that of 200 ºC and was smaller than the values after exposure to 600 ºC, as shown in Fig. 13. Considering that all C30 specimens exposed to 400 ºC were produced in the same batch and taken to the furnace at the same time, it seems plausible to assume that this unusual behavior is not related to problems in these phases of the experimental program. This could indicate that the specimens were affected by some external factor during the other stages of specimen preparation (mishandling) or during the pull-out test (universal testing machine malfunction or excessive pre-load for example).

Moreover, it should be pointed out that specimens with 5.0 mm rebar were the less precise among all results obtained. It means that bond in these specimens could have been easily damaged during all the phases of the experimental program, especially the C30 concrete specimens.

The specimens produced with C50 concrete reproduce the same pattern of bond-slip relationship degradation as 8.0 and 12.5 mm rebar, in which there is an enhancement of residual bond strength at 200 ºC, followed by progressive deterioration as temperature increase above this level. The bond failure mechanism is clearly pull-out failure for all the analyzed temperatures.

4.3.4. The influence of residual mechanical properties of concrete on bond failure mechanism

Fig. 15 and Fig. 16 show the relative residual bond strengths (RBS) for the tests performed in this work. Also, the residual mechanical properties of concrete corresponding to each temperature level are shown in these figures according to the work developed in Chapter 3.

The relative bond strength of C30 specimens showed to be highly affected by temperature exposure of 200 ºC, especially for the deformed rebars. The plain rebar was not significantly affected, retaining its relative bond strength at room temperature. On the other hand, for the deformed rebars, it is conceivable that the enhancement of the compressive and shear strengths made it possible for the concrete in front of the bar transversal ribs to bear higher stresses before crushing, hence transferring higher tensile stresses to the surrounding concrete. As the splitting tensile strength did not follow a similar enhancement trend, the concrete cover cracked, which negatively affected the adhesion between the materials at the interface and led to bond failure.

Therefore, there is a clear distinction in bond failure mechanism for C30 concrete after exposure to 200 ºC and at room temperature. At room temperature, the confinement provided by the concrete cover and the stirrups was enough to avoid splitting of the concrete cover; however, the higher tensile stresses transferred to the concrete were bigger than its splitting strength, which led to the concrete cover cracking, as can be seen in Fig. 7.

Fig. 15. Degradation of residual bond strength (RBS) and concrete mechanical properties for C30.

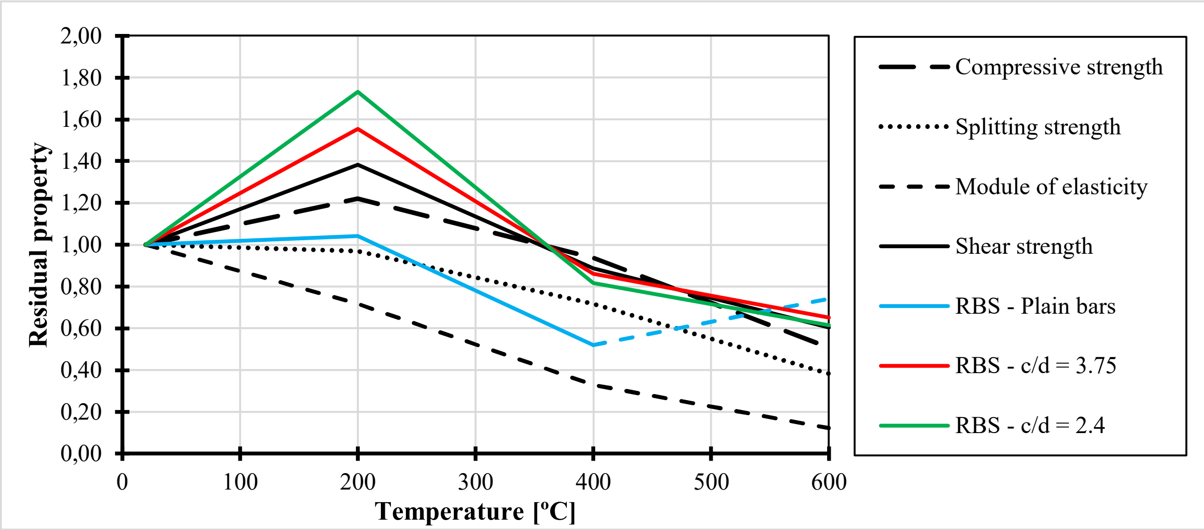

Source: Author (2021).

For the specimens exposed to 400 ºC, as observed in Chapter 3, both concrete's microstructure and the materials interface exhibit signs of cracking, which makes the confinement provided by the concrete cover essential to prevent splitting bond failure. Hence, specimens with smaller concrete cover to bar diameter ratio were more affected by elevated temperature exposure, since both specimens seemed to have failed by splitting-induce pull-out bond failure.

The plain bars curve (blue) is represented by a continuous line only up to 400 ºC and a dotted line between 400 ºC and 600 ºC. This representation was used due to the unexpected behavior of the plain bars at this temperature range. Moreover, it is noticeable that the plain bar behavior up to 400 ºC is well-matched with the deformed bars, while the later branch of the curve seems to be incompatible with both the deformed bars in Fig. 15 and the plain bars in Fig. 16.

Fig. 16 shows the deterioration trends for C50 specimens. C50 behaves a little differently than C30. The denser microstructure, which is responsible for the higher compressive strength, at this point seems to be a weakness. Upon high-temperature exposure, C50 concrete microstructure is more damaged, as can be seen by the deterioration of the modulus of elasticity.

After exposure to 200 ºC, C50 concrete residual Young's modulus retains only 60% of its value at room temperature, against 75% of C30 concrete.

The more extensive microstructural damage can be interpreted as a more denser microcracking pattern, which made C50 more prone to splitting failure. Hence, even though C50 concrete also experienced an enhancement of the mechanical properties of concrete, the cracked concrete surrounding the rebar could not bear higher tensile stresses as C30 did. Instead, the tensile stresses increased the microcracking leading to a thorough concrete cover splitting. Although C50 did not experience a comparable residual bond strength increase as C30, both of them were affected by a change of bond failure mechanism.

The fact that 5.0 mm rebar presented the greatest strength improvement among C50 specimens at 200 ºC suggests that the increase in compressive and shear strength improved the adhesion between the materials. For the deformed rebars, the specimen with 12.5 mm rebar showed to be more affected by the splitting of concrete cover than 8.0 mm. Despite the evidence that both failed by splitting, the smaller *c*/*d* ratio induced a complete splitting of the concrete cover, while the specimens with 8.0 mm apparently were only internally cracked, which could be an explanation for the smaller benefits of concrete's mechanical properties to the 12.5 mm rebar.

Fig. 16. Degradation of residual bond strength (RBS) and concrete mechanical properties for C50.

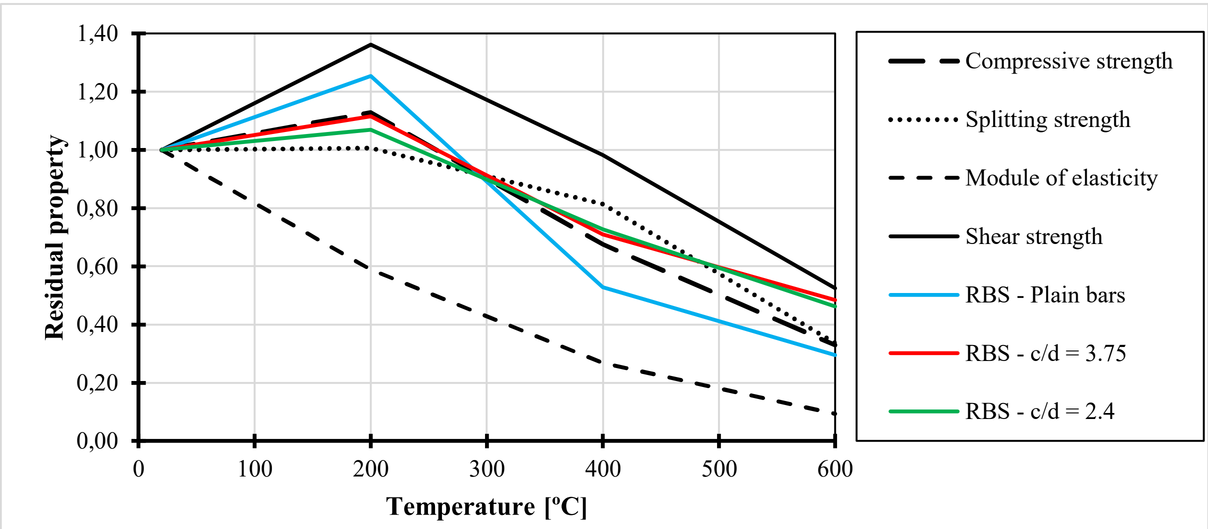

Source: Author (2021).

Up to 400 ºC, C50 specimens with 3.75 *c*/*d* show an extremely close relation with residual compressive strength of concrete at the same temperature. A similar trend can be observed for 2.4 *c*/*d* specimens, although apparently less affected by the elevated temperature effects on concrete, which can be observed by a smaller bond strength increase at 200 ºC and a comparable reduction at 400 ºC.

Between 400 ºC and 600 ºC, the behavior of all specimens seems to be extremely similar, which suggests that the damage to the concrete is so extensive that the *c*/*d* ratio does not significantly affect the bond strength. With exception of the C30 5.0mm bar, which behaved unusually, this seems to be true for both C30 and C50, implying that the level of confinement enforced by concrete is not significant at this level of temperature.

4.3.5. Comparison between fib Model Code analytical model and experimental results

Fig. 17 shows the experimental results obtained by many authors regarding the relationship between the residual concrete compressive strength and the residual bond strength. The data plotted on the graph represent the mean values of concrete compressive strength after exposure to elevated temperature and the corresponding residual bond strength.

The black curve in Fig. 17 represents the relationship between the maximum bond strength and the concrete compressive strength at room temperature for pull-out failure with good bonding conditions, as described by Eq. (2). In another words, this curve represents what could be described as the overall upper limit for bond strength, since it considers the upper limit for bond failure mechanism (pull-out failure) and does not take into account the additional damage to the concrete caused by elevated temperatures.

Fig. 17 also presents the curves for the Brazilian Standard [3] and the fib Model Code [2] for the bond strength in structures design, given by Eq. (4) and Eq. (5), respectively. Both standards are represented by two curves, one for plain and one for deformed rebars.

Fig. 17. Relationship between residual compressive strength and residual bond strength.

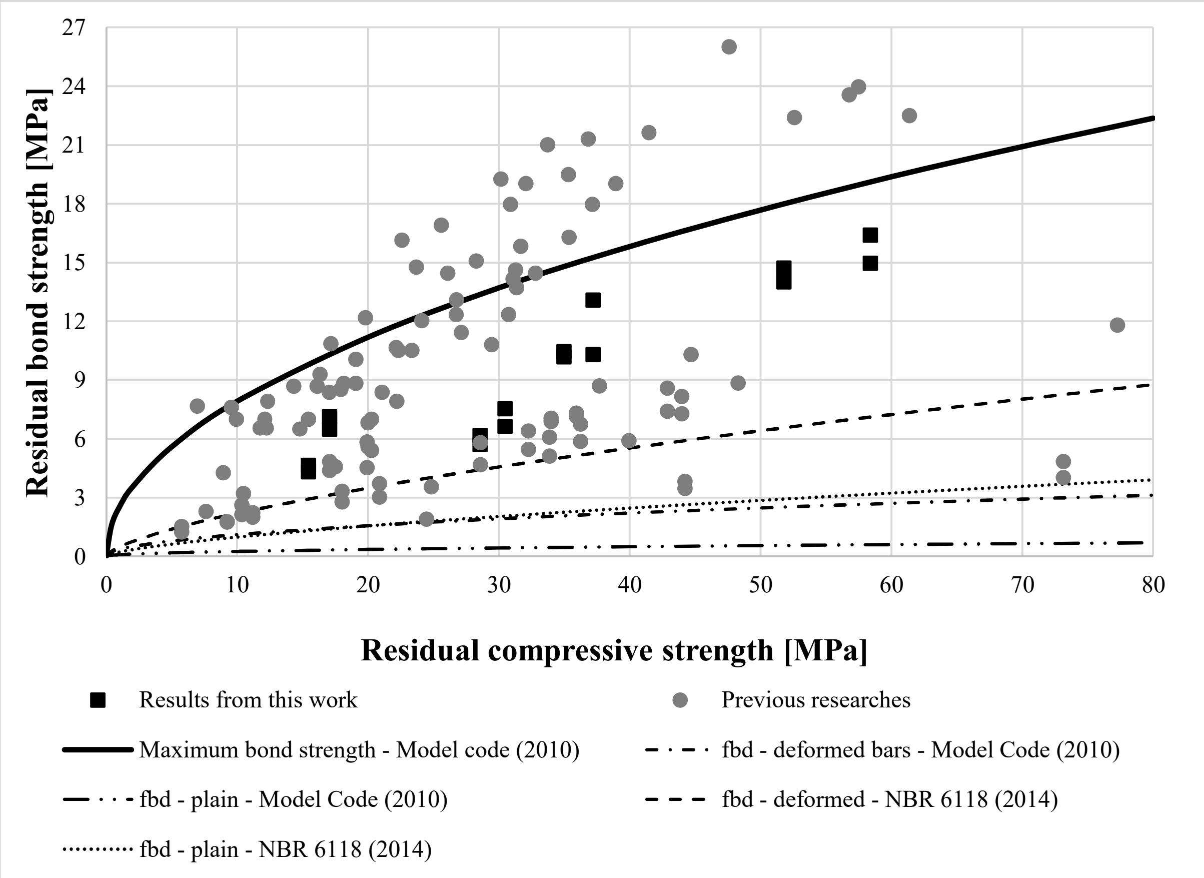

Source: Author (2021). Data extracted from [2,38,41,42,47,48,74].

First, it should be pointed out that the observed data is extremely scattered and no clear relationship can be observed between concrete compressive strength and bond strength after exposure to elevated temperature. As suggested by Bošnjak et al. [73], exposure to elevated temperatures could change the bond failure mechanism. Moreover, Royles and Morley [49] and Sharma et al. [50] observed that the bond strength follows a similar trend as the compressive strength when the specimen fails by pull-out of the rebar. On the other hand, if a splitting failure takes place, the bond strength seems to follow a degradation trend closer to the concrete splitting tensile strength.

This change in bond failure mechanism with increasing temperatures, coupled with the different behavior associated with each bond failure mechanism could be an explanation for the divergence in the plotted data. Additionally, it could also be associated to the heterogeneity of concrete. As shown throughout this work, the behavior of concrete when exposed to elevated temperatures is highly dependent on its constitution, which means that even concretes with the same compressive strength could behave differently based on their composition.

Even though the results available are extremely scattered, all the data observed by previous researches are above the fib Model Code curves, both for plain and deformed bars. Therefore, the fib Model Code account for bond strength in structures design can represent safely both the bond strength at room temperature and the residual bond strength after exposure to elevated temperatures.

On the other hand, the Brazilian Standard curve for deformed bars, which is less conservative than the Model Code curve, does not cover all the data analyzed. Nevertheless, approximately 90% of data on post-fire bond strength can be safely represented.

Moreover, Fig. 17 shows results for concrete exposed to elevated temperatures that are above the upper limit defined by fib Model Code [2]. Due to the abundance of data above the curve, it seems plausible to assume that the damage to the concrete, induced by elevated temperatures, deeply affects bond behavior. Additionally, the prescribed relationship for room temperature is not fit to describe the post-fire relationship simply using the residual compressive strength of concrete in place of the compressive strength at room temperature in Eq. (2).

The experimental results observed in this work are entirely under the maximum bond strength curve, which suggests that all the specimens were influenced by concrete cracking at some level and could not be fully described by the pull-out failure model prescribed by the fib Model Code [2], even at room temperature.

Nevertheless, the excessive divergence in the results plotted in Fig. 17 are an impediment for the proposition of a new empirical model that could describe the relationship between these properties in post-fire situation. Thus, this topic still present a great knowledge gap and should be further studied to delimitate the influence of elevated temperatures on bond development and, more importantly, on bond failure mechanism.

4.4. Conclusions

An experimental investigation of the effects of the concrete cover to bar diameter ratio on bond strength and bond failure mechanism was developed in this work. Based on the results, the following conclusions can be drawn:

- The effect of elevated temperature exposure on the residual bond strength seems to be directly related to the concrete's mechanical properties. Generally, for concretes exposed to 200 ºC, the residual bond strength is positively affected by the exposure; however, as temperature increases above this level, bond progressively deteriorates.

- Elevated temperature exposure did not seem to influence the bar slip at maximum residual bond strength for any of the analyzed configurations. The bar slip was affected only by the bond failure mechanism change between C30 concrete and deformed rebars after exposure to 200 ºC.
- The concrete cover to bar diameter ratio seems to affect especially C50 concrete; however, for 600 ºC, concrete seems to be excessively damaged and cannot provide adequate confinement to the rebar, hence the *c*/*d* ratio does not seem to influence maximum residual bond strength.
- Bond failure mechanisms cannot be easily distinguished after exposure to elevated temperatures. In most cases, the analysis of bond failure mechanism was only possible by the coupled evaluation of the bond-slip diagrams and the crack pattern exhibited by each specimen.
- Even though elevated temperature exposed specimens may show splitting of the concrete cover, it does not mean that the bond failed by splitting, especially at 600 ºC, when concrete is severely damaged and elevated temperature exposure alone causes extensive concrete cracking.
- The analytical model of the fib Model Code [2] for maximum bond strength calculation at room temperature is not fit to describe the post-fire ultimate bond strength.
- There is no clear relationship between the residual compressive strength of concrete and residual bond strength. The data observed in this work and previous researches indicate the need for further studies on this subject.
- The fib Model Code [2] account for bond strength in structures design can represent safely both the bond strength at room temperature and the residual bond strength after exposure to elevated temperatures.

References

[1] Tepfers R, Achillides Z, Azizinamini A, Balázs G, Bigaj-van-Vliet A, Cabrera J, et al. fib Bulletin 10. Bond of reinforcement in concrete. vol. 7. fib. The International Federation for Structural Concrete; 2000. https://doi.org/10.35789/fib.BULL.0010.

[2] fib. fib Model Code 2010 - Final draft - Volume 1. vol. 7. Weinheim, Germany: Wiley-VCH Verlag GmbH & Co. KGaA; 2013.

[3] Associação Brasileira de Normas Técnicas (ABNT). NBR 6118:2014 Design of concrete structures — Procedure. Assoc Bras Normas Técnicas 2014:238.

[4] Chan YN, Peng GF, Anson M. Residual strength and pore structure of high-strength concrete and normal strength concrete after exposure to high temperatures. Cem Concr Compos 1999;21:23–7. https://doi.org/10.1016/S0958-9465(98)00034-1.

[5] Khoury GA. Effect of fire on concrete and concrete structures. Prog Struct Eng Mater 2000;2:429–47. https://doi.org/10.1002/pse.51.

[6] Chan SYN, Luo X, Sun W. Effect of high temperature and cooling regimes on the compressive strength and pore properties of high performance concrete. Constr Build Mater 2000;14:261–6. https://doi.org/10.1016/S0950-0618(00)00031-3.

[7] Arioz O. Effects of elevated temperatures on properties of concrete. Fire Saf J 2007;42:516–22. https://doi.org/10.1016/j.firesaf.2007.01.003.

[8] Behnood A, Ziari H. Effects of silica fume addition and water to cement ratio on the properties of high-strength concrete after exposure to high temperatures. Cem Concr Compos 2008;30:106–12. https://doi.org/10.1016/j.cemconcomp.2007.06.003.

[9] Biolzi L, Cattaneo S, Rosati G. Evaluating residual properties of thermally damaged concrete. Cem Concr Compos 2008;30:907–16. https://doi.org/10.1016/j.cemconcomp.2008.09.005.

[10] Li M, Qian CX, Sun W. Mechanical properties of high-strength concrete after fire. Cem Concr Res 2004;34:1001–5. https://doi.org/10.1016/j.cemconres.2003.11.007.

[11] Cülfik MS, Özturan T. Mechanical properties of normal and high strength concretes subjected to high temperatures and using image analysis to detect bond deteriorations. Constr Build Mater 2010;24:1486–93. https://doi.org/10.1016/j.conbuildmat.2010.01.020.

[12] Arioz O. Retained properties of concrete exposed to high temperatures: Size effect. Fire Mater 2009:211–22. https://doi.org/10.1002/fam.996.

[13] Xiao J, König G. Study on concrete at high temperature in China - An overview. Fire Saf J 2004;39:89–103. https://doi.org/10.1016/S0379-7112(03)00093-6.

[14] Ergün A, Kürklü G, Serhat Başpnar M, Mansour MY. The effect of cement dosage on mechanical properties of concrete exposed to high temperatures. Fire Saf J 2013;55:160–7. https://doi.org/10.1016/j.firesaf.2012.10.016.

[15] Janotka I, Bágel L. Pore structures, permeabilities, and compressive strengths of concrete at temperatures up to 800°C. ACI Mater J 2002;99:196–200. https://doi.org/10.14359/11713.

[16] Peng G-F, Bian S-H, Guo Z-Q, Zhao J, Peng X-L, Jiang Y-C. Effect of thermal shock due to rapid cooling on residual mechanical properties of fiber concrete exposed to high temperatures. Constr Build Mater 2008;22:948–55. https://doi.org/10.1016/j.conbuildmat.2006.12.002.

[17] Poon CS, Azhar S, Anson M, Wong YL. Comparison of the strength and durability performance of normal- and high-strength pozzolanic concretes at elevated temperatures. Cem Concr Res 2001;31:1291–300. https://doi.org/10.1016/S0008-8846(01)00580-4.

[18] Abramowicz M, Kowalski R. The influence of short time water cooling on the mechanical properties of concrete heated up to high temperature. J Civ Eng Manag 2005;11:85–90. https://doi.org/10.1080/13923730.2005.9636336.

[19] Bamonte P, Gambarova PG. Thermal and mechanical properties at high temperature of a very high-strength durable concrete. J Mater Civ Eng 2010;22:545–55. https://doi.org/10.1061/(ASCE)MT.1943-5533.0000058.

[20] Lee J, Xi Y, Willam K. Properties of concrete after high-temperature heating and cooling. ACI Mater J 2008;105:334–41. https://doi.org/10.14359/19894.

[21] Piasta J. Heat deformations of cement paste phases and the microstructure of cement paste. Matériaux Constr 1984;17:415–20. https://doi.org/10.1007/BF02473981.

[22] Janotka I, Nürnbergerová T. Effect of temperature on structural quality of the cement paste and high-strength concrete with silica fume. Nucl Eng Des 2005;235:2019–32. https://doi.org/10.1016/j.nucengdes.2005.05.011.

[23] Ma Q, Guo R, Zhao Z, Lin Z, He K. Mechanical properties of concrete at high temperature-A review. Constr Build Mater 2015;93:371–83. https://doi.org/10.1016/j.conbuildmat.2015.05.131.

[24] Lin W, Lin TD. Microstructures of Fire-Damaged Concrete 1997:199–205.

[25] Mendes A, Sanjayan J, Collins F. Phase transformations and mechanical strength of OPC/Slag pastes submitted to high temperatures. Mater Struct Constr 2008;41:345–50. https://doi.org/10.1617/s11527-007-9247-8.

[26] Lea FC, Stradling RE. The resistance to fire of concrete and reinforced concrete. J Soc Chem Ind 1922;41:395R-396R.

[27] Kim KY, Yun TS, Park KP. Evaluation of pore structures and cracking in cement paste exposed to elevated temperatures by X-ray computed tomography. Cem Concr Res 2013;50:34–40. https://doi.org/10.1016/j.cemconres.2013.03.020.

[28] Hertz KD. Concrete strength for fire safety design. Mag Concr Res 2005;57:445–53. https://doi.org/10.1680/macr.2005.57.8.445.

[29] Xiao J, Hou Y, Huang Z. Beam test on bond behavior between high-grade rebar and high-strength concrete after elevated temperatures. Fire Saf J 2014;69:23–35. https://doi.org/10.1016/j.firesaf.2014.07.001.

[30] Topçu IB, Karakurt C. Properties of reinforced concrete steel rebars exposed to high temperatures. Res Lett Mater Sci 2008;2008. https://doi.org/10.1155/2008/814137.

[31] Neves IC, Rodrigues JPC, Loureiro A de P. Mechanical properties of reinforcing and presstressing stells after heating. J Mater Civ Eng 1996;8:189–94.

[32] Elghazouli AY, Cashell KA, Izzuddin BA. Experimental evaluation of the mechanical properties of steel reinforcement at elevated temperature. Fire Saf J 2009;44:909–19. https://doi.org/10.1016/j.firesaf.2009.05.004.

[33] Tao Z, Wang XQ, Uy B. Stress-strain curves of structural and reinforcing steels after exposure to elevated temperatures. J Mater Civ Eng 2013;25:1306–16. https://doi.org/10.1061/(ASCE)MT.1943-5533.0000676.

[34] Ahmad MS. Effect of Sustained Elevated Temperature on Mechanical Behavior of Reinforcing Bar. Procedia Eng 2017;173:905–9. https://doi.org/10.1016/j.proeng.2016.12.139.

[35] Qian H, Yan D, Chen S, Chen G, Tian Y, Chen G. Effect of High Temperature Exposure and Strain Rate on Mechanical Properties of High-Strength Steel Rebars. J Mater Civ Eng 2019;31:04019261. https://doi.org/10.1061/(asce)mt.1943-5533.0002906.

[36] Qiang X, Bijlaard FSK, Kolstein H. Post-fire mechanical properties of high strength structural steels S460 and S690. Eng Struct 2012;35:1–10. https://doi.org/10.1016/j.engstruct.2011.11.005.

[37] Diederichs U, Schneider U. Bond strength at high temperatures. Mag Concr Res 1981;33:75–84. https://doi.org/10.1680/macr.1981.33.115.75.

[38] Hlavička ÉLV. Bond after fire. Constr Build Mater 2017;132:210–8. https://doi.org/10.1016/j.conbuildmat.2016.11.131.

[39] Ghazaly N, Rashad A, Kohail M, Nawawy O. Evaluation of bond strength between steel rebars and concrete for heat-damaged and repaired beam-end specimens. Eng Struct 2018;175:661–8. https://doi.org/10.1016/j.engstruct.2018.08.056.

[40] Rashid MH, Molla MM, Taki IM. Effect of Elevated Temperature on Bond Strength of Concrete. Mater Sci Forum 2019;972:26–33. https://doi.org/10.4028/www.scientific.net/msf.972.26.

[41] Ergün A, Kürklü G, Başpinar MS. The effects of material properties on bond strength between reinforcing bar and concrete exposed to high temperature. Constr Build Mater 2016;112:691–8. https://doi.org/10.1016/j.conbuildmat.2016.02.213.

[42] Bingöl AF, Gül R. Residual bond strength between steel bars and concrete after elevated temperatures. Fire Saf J 2009;44:854–9. https://doi.org/10.1016/j.firesaf.2009.04.001.

[43] Arel HŞ, Yazici Ş. Effect of different parameters on concrete-Bar bond under high temperature. ACI Mater J 2014;111:633–40. https://doi.org/10.14359/51686992.

[44] Shamseldein A, Elshafie H, Rashad A, Kohail M. Assessment and restoration of bond strength of heat-damaged reinforced concrete elements. Constr Build Mater 2018;169:425–35. https://doi.org/10.1016/j.conbuildmat.2018.03.008.

[45] Li X, Bao Y, Xue N, Chen G. Bond strength of steel bars embedded in high-performance fiber-reinforced cementitious composite before and after exposure to elevated temperatures. Fire Saf J 2017;92:98–106. https://doi.org/10.1016/j.firesaf.2017.06.006.

[46] Yin K, Han Y, Liu Y. Experimental research on bond strength between rebar and concrete after high temperature. Appl Mech Mater 2011;71–78:1057–61. https://doi.org/10.4028/www.scientific.net/AMM.71-78.1057.

[47] Haddad RH, Al-Saleh RJ, Al-Akhras NM. Effect of elevated temperature on bond between steel reinforcement and fiber reinforced concrete. Fire Saf J 2008;43:334–43. https://doi.org/10.1016/j.firesaf.2007.11.002.

[48] Haddad RH, Shannis LG. Post-fire behavior of bond between high strength pozzolanic concrete and reinforcing steel. Constr Build Mater 2004;18:425–35. https://doi.org/10.1016/j.conbuildmat.2004.03.006.

[49] Royles R, Morley PD. Response of the bond in reinforced concrete to high temperatures. Mag Concr Res 1983;35:157–63. https://doi.org/10.1680/macr.1983.35.124.157.
[50] Sharma A, Bošnjak J, Bessert S. Experimental investigations on residual bond performance in concrete subjected to elevated temperature. Eng Struct 2019;187:384–95. https://doi.org/10.1016/j.engstruct.2019.02.061.
[51] Fakoor M, Nematzadeh M. A new post-peak behavior assessment approach for effect of steel fibers on bond stress-slip relationship of concrete and steel bar after exposure to high temperatures. Constr Build Mater 2021;278:122340. https://doi.org/10.1016/j.conbuildmat.2021.122340.
[52] Raouffard MM, Nishiyama M. Idealization of bond stress-slip relationship at elevated temperatures based on pullout tests. ACI Struct J 2018;115:391–400. https://doi.org/10.14359/51701120.
[53] Lublóy É, György BL. Temperature Effects on Bond Between Concrete and Reinforcing Steel. Zb Rad Građevinskog Fak 2014;30:27–35. https://doi.org/10.14415/zbornikgfs26.03.
[54] ASTM C595-03. Standard Specification for Blended Hydraulic Cements. Annu B Am Soc Test Mater ASTM Stand 2003;14:1–7. https://doi.org/10.1520/C0595.
[55] ABNT - Associação Brasileira de Normas Técnicas. NBR NM 45: Agregados – Determinação da massa unitária e do volume de vazios. Abnt Nbr 452006 2006:18.
[56] ASTM International. ASTM C29/C29M - 17a, Standard Test Methos for Bulk Density ("Unit Weight") and Voids in Aggregate 2017:5. https://doi.org/10.1520/C0029_C0029M-17A.
[57] ABNT - Associação Brasileira de Normas Técnicas. ABNT NBR NM 30 - Agregado miúdo - Determinaçao da absorção de água. Abnt Nbr Mn 30 2001:3p.
[58] ASTM International. ASTM C128-15, Standard Test Method for Relative Density (Specific Gravity) and Absorption of Fine Aggregate 2015:6. https://doi.org/10.1520/C0128-15.
[59] Associação Brasileira De Normas Técnicas (ABNT). ABNT NBR NM 248: Análise Granulométrica. Assoc Bras Normas Técnicas 2003:6.
[60] ASTM International. ASTM C136/ C136M-19, Standard Method for Sieve Analysis of Fine and Coarse Aggregates 2019:5. https://doi.org/10.1520/C0136_C0136M-19.
[61] ABNT - Associação Brasileira de Normas Técnicas. NBR 5739 Concreto - Ensaios de compressão de corpos-de-prova cilíndricos. Assoc Bras Normas Técnicas 2018:9.
[62] ASTM International. ASTM C39/ C39M-14, Standard Test Method for Compressive Strength of Cylindrical Concrete Specimens 2014:7.
[63] ABNT - Associação Brasileira de Normas Técnicas. ABNT NBR 7222 - Concreto e argamassa - Determinação da resistência à tração por compressão diametral de corpos de prova cilíndricos 2011:5.
[64] ASTM International. ASTM C496/C496M - 17 - Standard Test Method for Splitting Tensile Strength of Cylindrical Concrete Specimens 2017:5.
[65] ABNT - Associação Brasileira de Normas Técnicas. ABNT NBR 8522-1 - Concreto - Determinação do módulo estático de elasticidade à compressão. Assoc Bras Normas Técnicas 2021:24.
[66] ASTM International. ASTM C469/ C469M-14 - Standard Test for Static Modulus of Elasticity and Poisson's Ratio of oncrete in Compression 2014:5.
[67] Gusmão AC. Utilização do concreto de pós reativos como material de reparo - Ênfase na resistência de aderência 2017:143.
[68] ABNT - Associação Brasileira de Normas Técnicas. ABNT NBR ISO 6892-1:2013 Versão Corrigida 2:2018 - Materiais metálicos - Ensaio de Tração. Parte 1: Método de ensaio à temperatura ambiente 2018:70.
[69] ASTM International. ASTM A370- 20 Standard Test Methods and Definitions for Mechanical Testing of Steel Products 2020:50.
[70] Sulaiman MF, Ma CK, Apandi NM, Chin S, Awang AZ, Mansur SA, et al. A Review on Bond and Anchorage of Confined High-strength Concrete. Structures 2017;11:97–109. https://doi.org/10.1016/j.istruc.2017.04.004.
[71] Lutz BLA, Gergely P. Mechanics of Bond and Slip of Deformed Bars in Concrete. ACI J Proc 1967;64:711–21. https://doi.org/10.14359/7600.
[72] ACI Committee 408. ACI 408R-03 Bond and Development of Straight Reinforcing Bars in Tension. Am Concr Inst 2003:1–49.
[73] Bošnjak J, Sharma A, Öttl C. Modified beam-end test setup to study the bond behavior of reinforcement in concrete after fire. Mater Struct Constr 2018;51. https://doi.org/10.1617/s11527-018-1138-7.
[74] Yang O, Zhang B, Yan G, Chen J. Bond Performance between Slightly Corroded Steel Bar and Concrete after Exposure to High Temperature. J Struct Eng (United States) 2018;144:1–10. https://doi.org/10.1061/(ASCE)ST.1943-541X.0002217.

CHAPTER 5:

General conclusions

Abstract

Chapter 5 presents a general conclusion of this work, which includes the concluding remarks involving the entire dissertation and some proposals for future work that were identified during the research.

5.1. Concluding remarks

The analysis of the bearing capacity of a structure that has survived a fire situation requires knowledge of the behavior of materials after exposure to elevated temperatures. Specifically in the case of reinforced concrete structures, the bond between the reinforcement and the concrete plays an important role. Degradation of bond strength due to high temperatures has been shown not to directly follow the behavior of each material individually.

In this way, this study comprised a comprehensive literature review and an experimental assessment of the effects of elevated temperature exposure on residual concrete-reinforcement bond properties. The experimental program was divided into two parts: the first part focused on evaluating the effect of elevated temperature exposure on the physical and mechanical properties of materials and how this influenced the bond strength between them. The second part focused on assessing the influence of the concrete cover to bar diameter ratio (*c*/*d*) on bond development and bond failure mechanism after exposure to elevated temperatures.

It was observed that, although elevated temperature exposure positively affects the concrete residual compressive strength for temperatures up to 200 ºC, there is still some damage to its microstructure, which are perceptible by the SEM analysis and resulted in the reduction of the Young Modulus. Moreover, for higher temperatures, the damage to the microstructure of concrete and the decomposition of the hydrated products showed to be detrimental to the mechanical properties of concrete.

Bond development and bond failure mechanism were highly affected by the mechanical properties of concrete. The combination of effects of elevated temperature exposure on the residual mechanical properties of concrete also influenced the change in bond failure mechanism from pull-out to splitting.

Bond failure mechanisms could not be easily distinguished after exposure to elevated temperatures. In most cases, the analysis of bond failure mechanism was only possible by the coupled evaluation of the bond-slip diagrams and the crack pattern exhibited by each specimen.

The influence of the *c*/*d* ratio is directly related to the confinement provided to the rebar. For exposure to elevated temperatures up to 400 ºC, *c*/*d* showed to be a parameter of importance for bond properties. Conversely, for 600 ºC, the damage to the concrete is too extensive and the concrete cover cannot provide enough confinement to the rebar; hence, the *c*/*d* ratio does not seem to influence maximum bond strength.

As the level of confinement provided to the embedded rebar depends not only on the properties of materials (concrete strength) but also on the specimen characteristics (*c*/*d* ratio and the presence of stirrups), it seems problematic to create a general residual-bond-degradation law. However, the change in residual bond failure mechanism needs further clarification and supplementary research should be carried out on this topic.

Even though there is no clear relationship between the residual compressive strength and residual bond strength, the account for bond strength in structures design both from the Brazilian Standard [3] and the fib Model Code [2] showed to represent safely both the bond strength at room temperature and the residual bond strength after exposure to elevated temperatures.

The data observed in this work and previous researches indicate the need for further studies on this subject.

5.2. Proposals for future work

Based on the data collected in this research and the observed bond-slip behavior, a few questions were could not be answered. Some proposals for future work are:

- further explore the relationship between concrete residual compressive strength and the residual bond strength;
- further explore the influence of *c*/*d* ratio on bond failure mechanisms by changing the parameters adopted in this work;
- experimentally assess the residual bond strength degradation using a beam specimen and the minimum steel reinforcement allowed by Standards, in order to confirm the results obtained by pull-out tests;
- experimentally assess the residual bond strength using beam specimens and minimum spacing between reinforcing bars (which is usually smaller than minimum concrete cover), in order to observe how the bond loss due to the internal concrete cracking may influence the global bond deterioration of the element; and
- analyze the effect of the use of crack-control mechanisms, such as fibers, in enhancing bond ductility for specimens that suffered splitting bond failure.

APPENDIX A:

Time-temperature curves

Appendix A contains the time-temperature curves for all the specimens subjected to elevated temperatures. The temperature increase was monitored inside the furnace (thermocouple 1), at the pull-out bar location (thermocouple 2) and at the center of the specimen's cross-section (thermocouple 3).

When the specimens were subjected to 200 ºC, the temperature inside the furnace showed a high initial heating rate and surpassed the target temperature, then it slowed reduced until reaching thermal stability at 200 ºC. Although the furnace reached higher temperatures, the inside of specimens was not affected, as shown in Fig. 1 and Fig. 2. This phenomenon was not observed for the target temperatures of 400 ºC and 600 ºC.

For specimens heated to 200 ºC and 400 ºC, the C50 specimens took a larger amount of time to reach the target temperature on its core than the C30 specimens did. When the specimens were subjected to 600 ºC, both concretes required a similar amount of time to reach the target temperature.

Due to a thermocouple malfunction, the time-temperature curve for C50 specimens subjected to 600 ºC shows an unusual behavior for TC3 (the thermocouple located at the center of the specimen's cross-section). Apparently, the malfunction influenced only the initial part of the time-temperature curve, since the final branch of the curve seems compatible with the observed for the other specimens and temperatures.

Fig. 1. Time-temperature curves - C30 - 200 ºC.

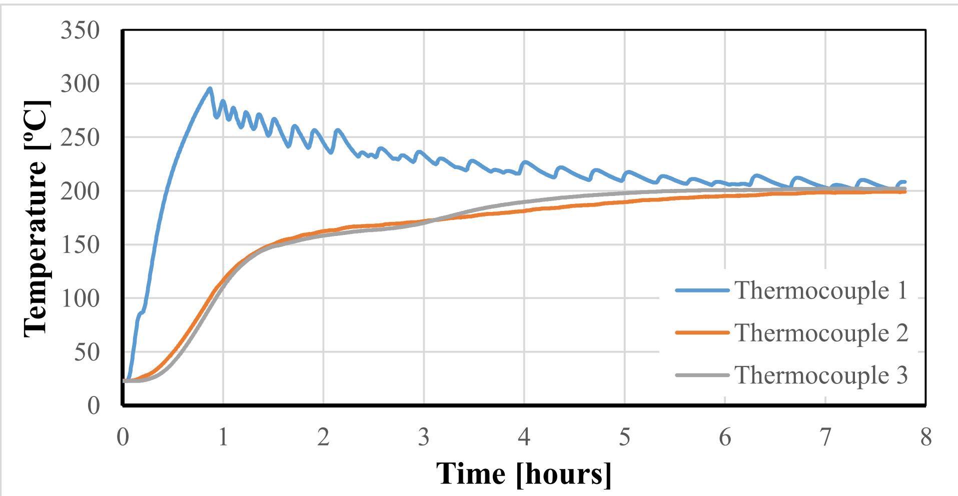

Source: Author (2021).

Fig. 2. Time-temperature curves – C50 - 200 ºC.

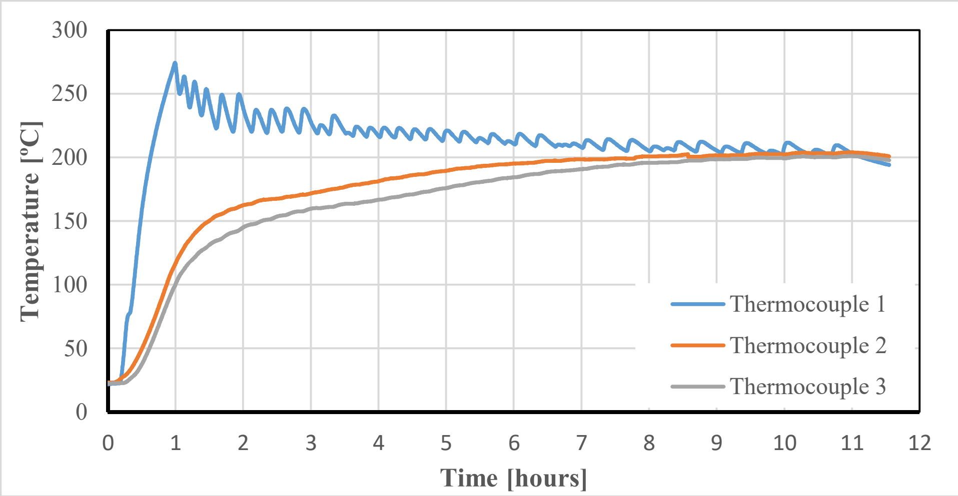

Source: Author (2021).

Fig. 3. Time-temperature curves - C30 - 400 ºC.

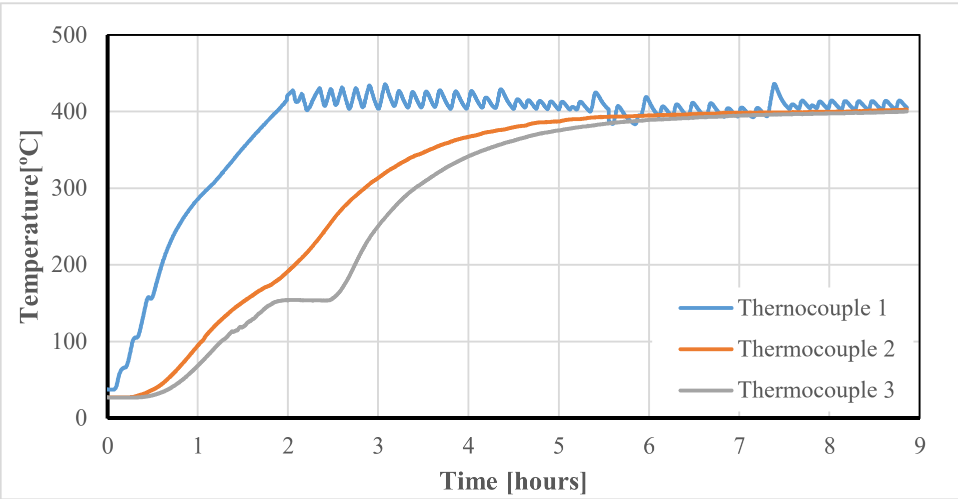

Source: Author (2021).

Fig. 4. Time-temperature curves – C50 - 400 ºC.

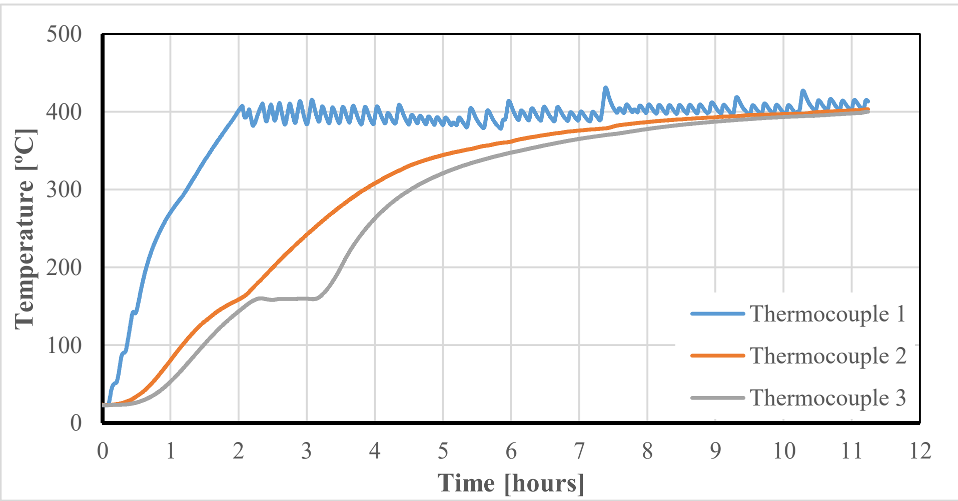

Source: Author (2021).

Fig. 5. Time-temperature curves - C30 - 600 ºC.

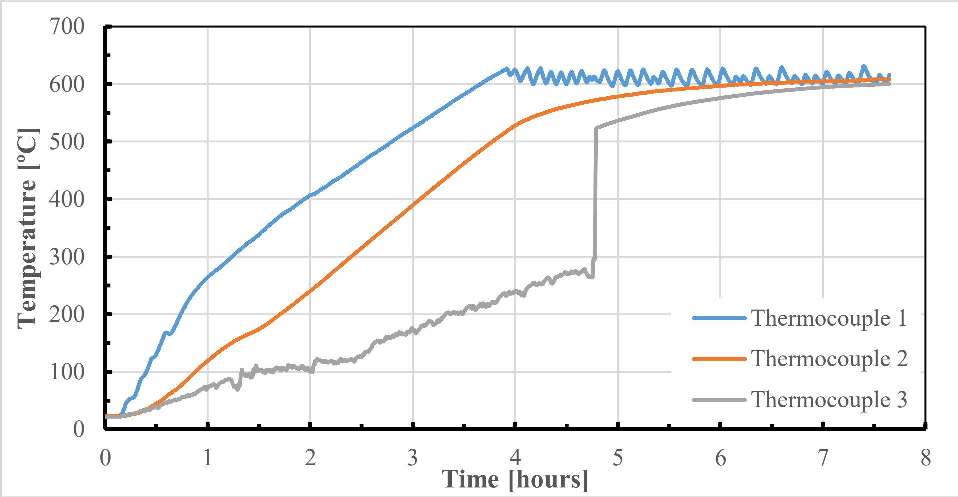

Source: Author (2021).

Fig. 6. Time-temperature curves – C50 - 600 ºC.

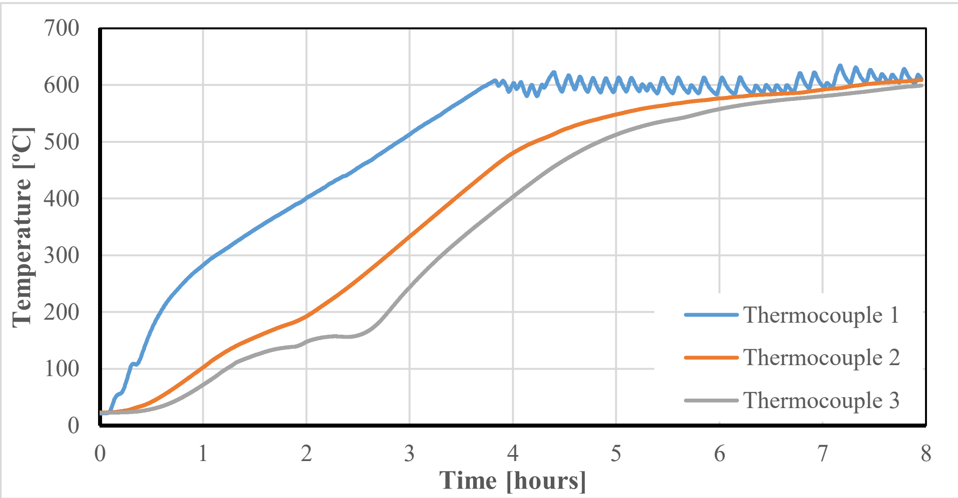

Source: Author (2021).

APPENDIX B:

Bond-slip curves

Appendix B contains the bond-slip curves for all the specimens after exposure to elevated temperatures. Three specimens were tested for each concrete mix, *c/d* ratio, and maximum temperature combination; hence, a total of 72 specimens. Based on the three specimens tested for each situation, a mean bond-slip curve was obtained, as described in items 3.3.4 and 4.3.3.

The pull-out specimens were identified by a four-number code. The first number stands for the concrete strength (1 for C30 and 2 for C50); the second number represents the target temperature (0 for room temperature, 1 for 200 ºC, 2 for 400 ºC and 3 for 600 ºC); the third number denotes the bar diameter (1 for 5.0 mm, 2 for 8.0 mm and 3 for 12.5 mm); the last number indicates repetition for specimens with the same properties (three repeats for each condition).

Table 1 summarizes the specimen identification codes and the corresponding properties.

Table 1. Specimen identification

Specimen code	Concrete strength [MPa]	Temperature [ºC]	Bar diameter [mm]
1.0.1.1 – 1.0.1.3	30	20	5.0
1.0.2.1 – 1.0.2.3	30	20	8.0
1.0.3.1 – 1.0.3.3	30	20	12.5
1.1.1.1 – 1.1.1.3	30	200	5.0
1.1.2.1 – 1.1.2.3	30	200	8.0
1.1.3.1 – 1.1.3.3	30	200	12.5
1.2.1.1 – 1.2.1.3	30	400	5.0
1.2.2.1 – 1.2.2.3	30	400	8.0
1.2.3.1 – 1.2.3.3	30	400	12.5
1.3.1.1 – 1.3.1.3	30	600	5.0
1.3.2.1 – 1.3.2.3	30	600	8.0
1.3.3.1 – 1.3.3.3	30	600	12.5
2.0.1.1 – 2.0.1.3	50	20	5.0
2.0.2.1 – 2.0.2.3	50	20	8.0
2.0.3.1 – 2.0.3.3	50	20	12.5
2.1.1.1 – 2.1.1.3	50	200	5.0
2.1.2.1 – 2.1.2.3	50	200	8.0
2.1.3.1 – 2.1.3.3	50	200	12.5
2.2.1.1 – 2.2.1.3	50	400	5.0
2.2.2.1 – 2.2.2.3	50	400	8.0
2.2.3.1 – 2.2.3.3	50	400	12.5
2.3.1.1 – 2.3.1.3	50	600	5.0
2.3.2.1 – 2.3.2.3	50	600	8.0
2.3.3.1 – 2.3.3.3	50	600	12.5

Source: Author (2021)

Among all tests, the results from three specimens could not be used for specific reasons. For C30 concrete exposed to 400 ºC, specimen 1.2.1.2 bond was broken before the beginning of the pull-out test by a specimen mishandling. For C30 concrete exposed to 600 ºC, the results for 1.3.3.3 were lost by a software malfunction that erased the data collected during the pull-out test. For C50 concrete at room temperature, a testing machine malfunction interrupted the pull-out test and the recorded data could not be used.

Generally, the three specimens tested in each situation presented very similar results; however, a few results showed a distinct behavior. One of these differences occurred when two specimens showed very similar results and the third presented a smaller ultimate residual bond strength, as shown in Fig. 2, Fig. 5, Fig. 10 and Fig. 20. The opposite situation was also observed, when one specimen showed higher ultimate residual bond strength, as shown in Fig. 4 and Fig. 22.

Due to the reduced number of specimens tested in each situation (only three for reasons of cost and infrastructure available), it was chosen not to exclude any result that could be considered as an outlier for the purpose of obtaining the mean bond-slip curves.

Fig. 1. Bond-slip curves for C30 concrete and 5.0 mm bars at room temperature.

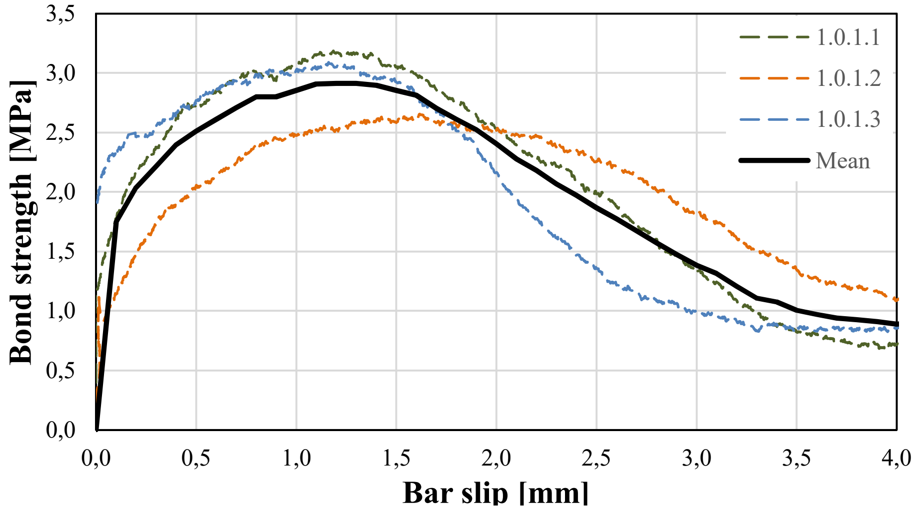

Source: Author (2021).

Fig. 2. Bond-slip curves for C30 concrete and 8.0 mm bars at room temperature.

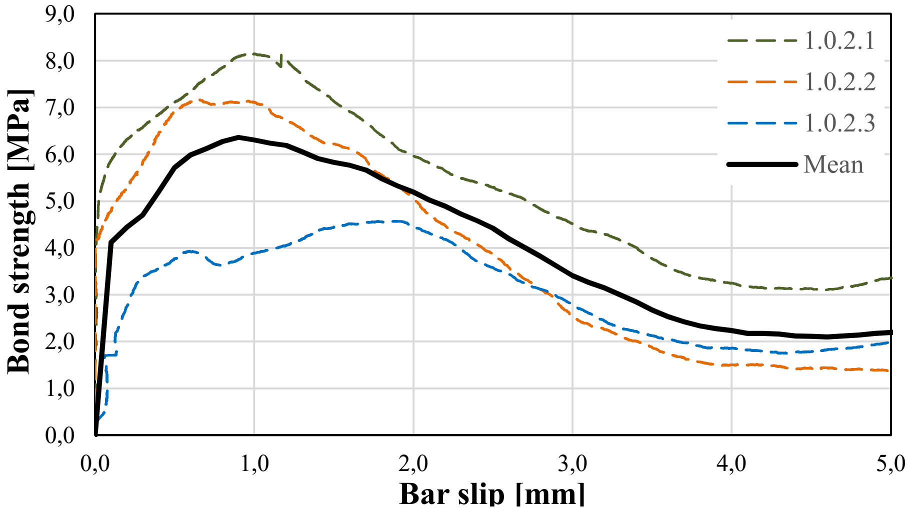

Source: Author (2021).

Fig. 3. Bond-slip curves for C30 concrete and 12.5 mm bars at room temperature.

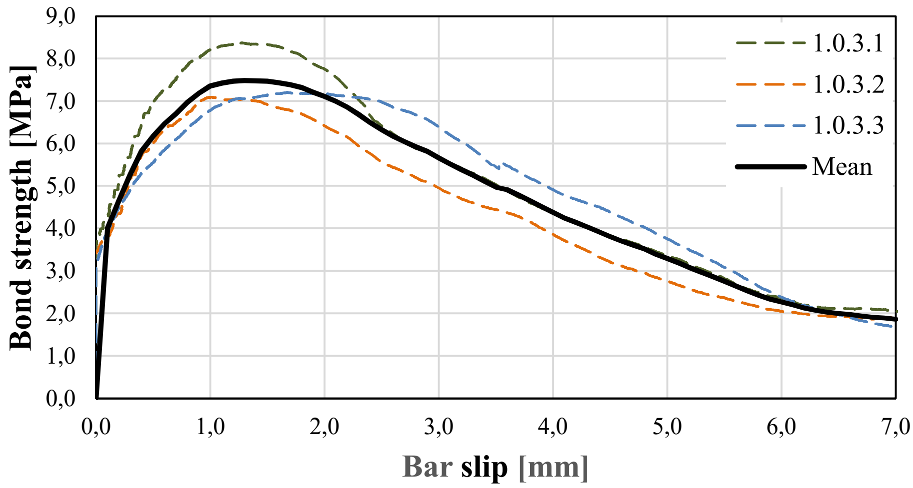

Source: Author (2021).

Fig. 4. Bond-slip curves for C30 concrete and 5.0 mm bars at 200ºC.

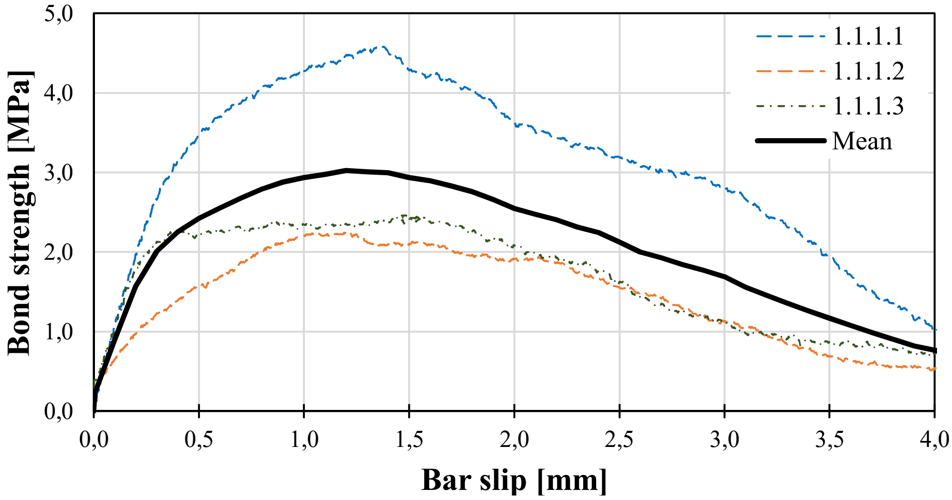

Source: Author (2021).

Fig. 5. Bond-slip curves for C30 concrete and 8.0 mm bars at 200ºC.

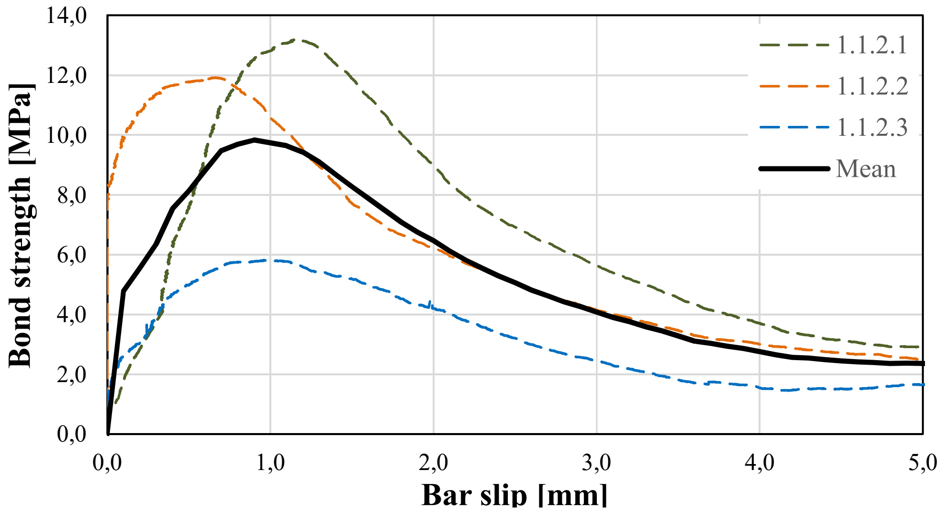

Source: Author (2021).

Fig. 6. Bond-slip curves for C30 concrete and 12.5 mm bars at 200ºC.

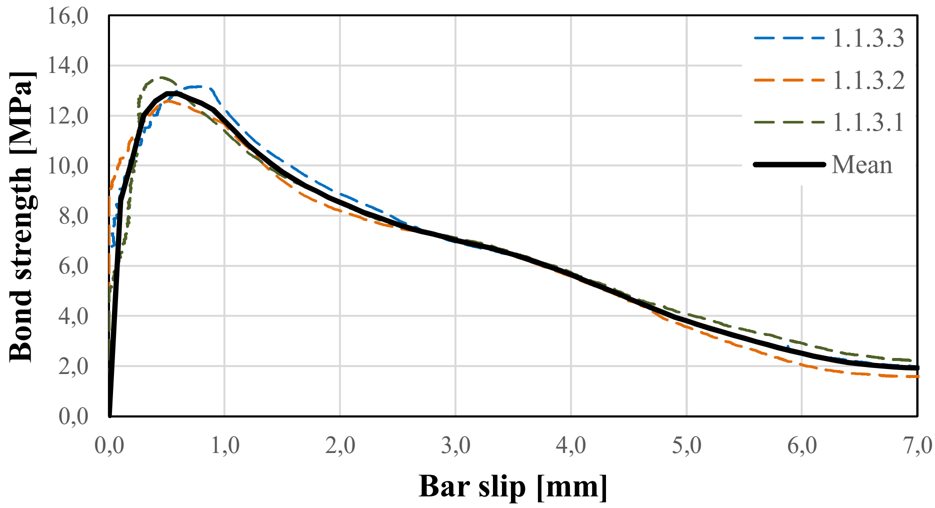

Source: Author (2021).

Fig. 7. Bond-slip curves for C30 concrete and 5.0 mm bars at 400ºC.

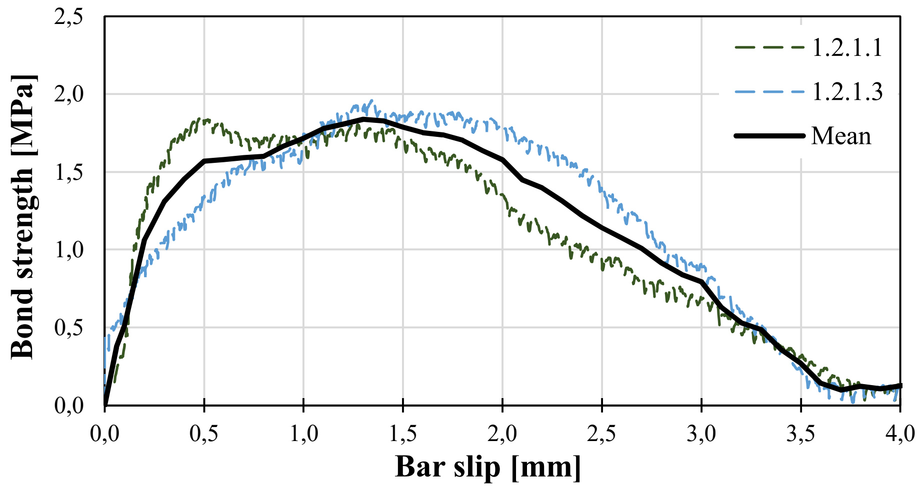

Source: Author (2021).

Fig. 8. Bond-slip curves for C30 concrete and 8.0 mm bars at 400ºC.

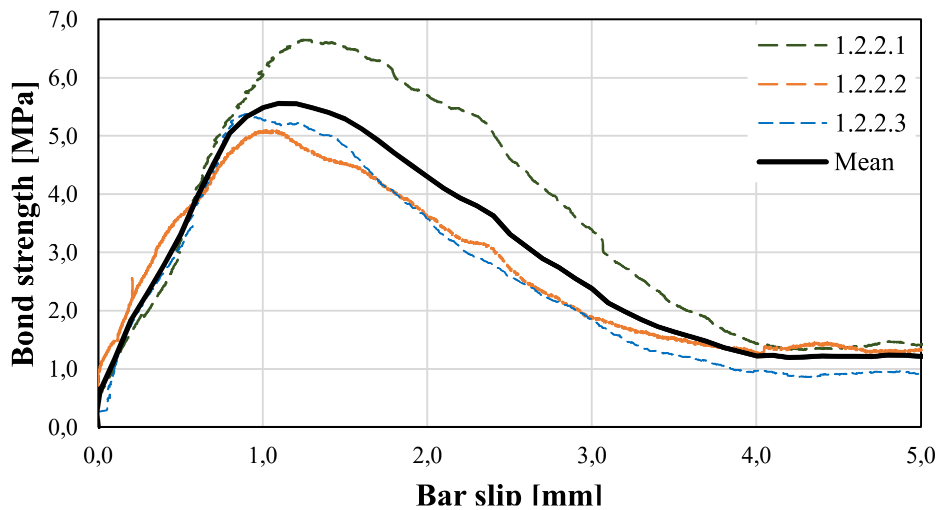

Source: Author (2021).

Fig. 9. Bond-slip curves for C30 concrete and 12.5 mm bars at 400ºC.

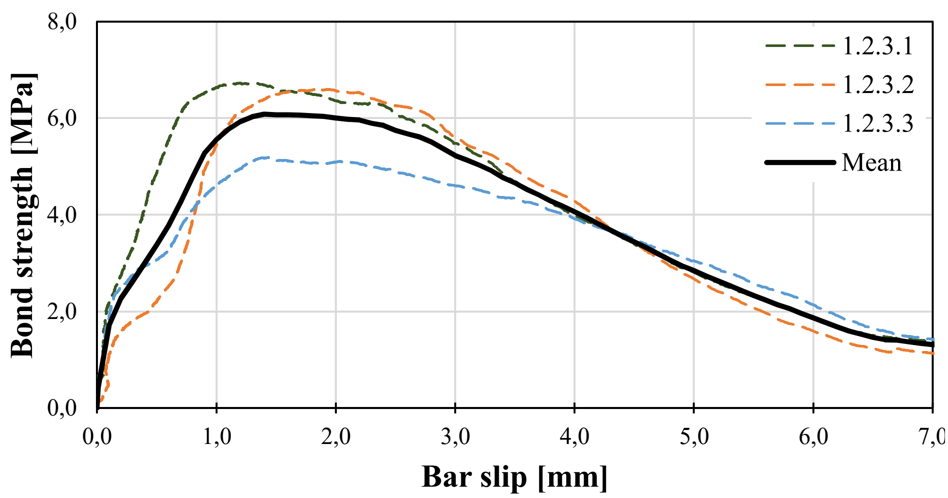

Source: Author (2021).

Fig. 10. Bond-slip curves for C30 concrete and 5.0 mm bars at 600ºC.

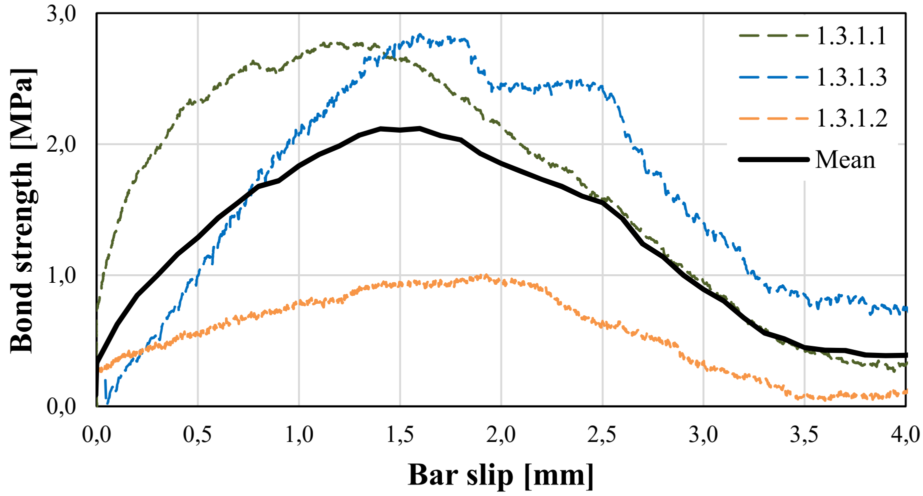

Source: Author (2021).

Fig. 11. Bond-slip curves for C30 concrete and 8.0 mm bars at 600ºC.

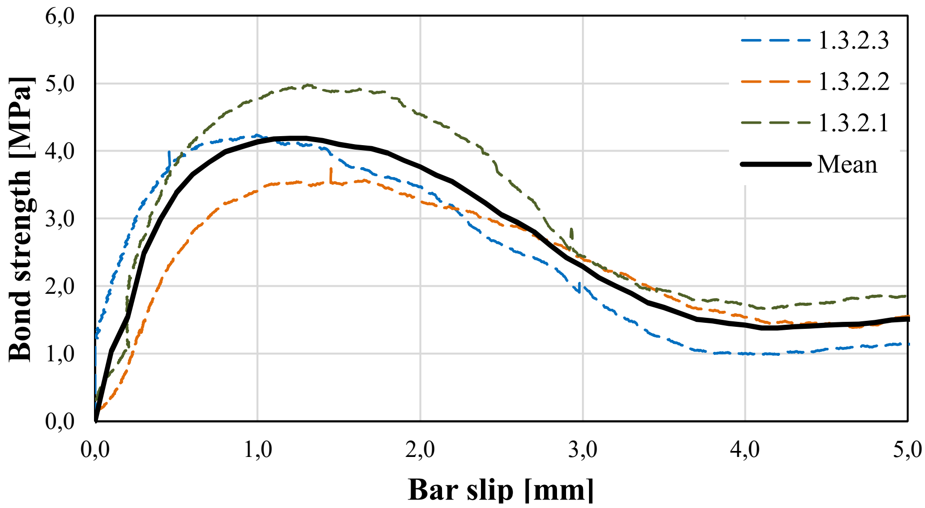

Source: Author (2021).

Fig. 12. Bond-slip curves for C30 concrete and 12.5 mm bars at 600ºC.

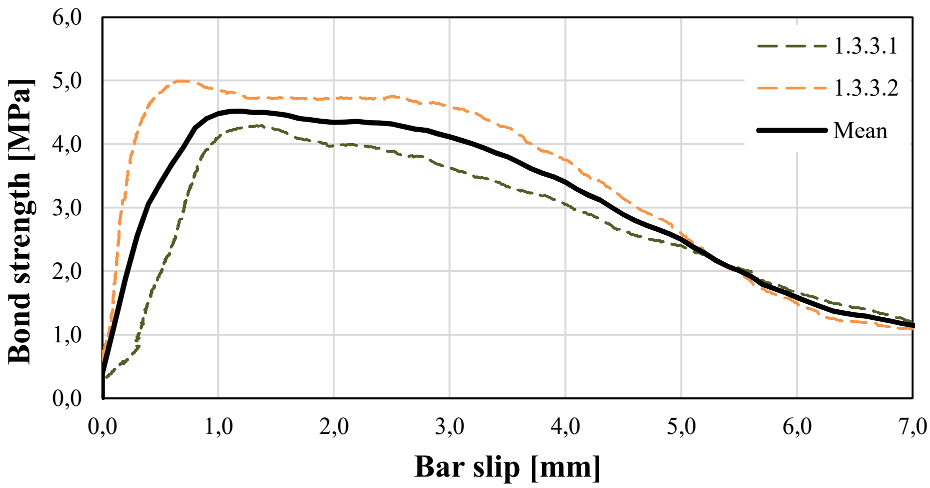

Source: Author (2021).

Fig. 13. Bond-slip curves for C50 concrete and 5.0 mm bars at room temperature.

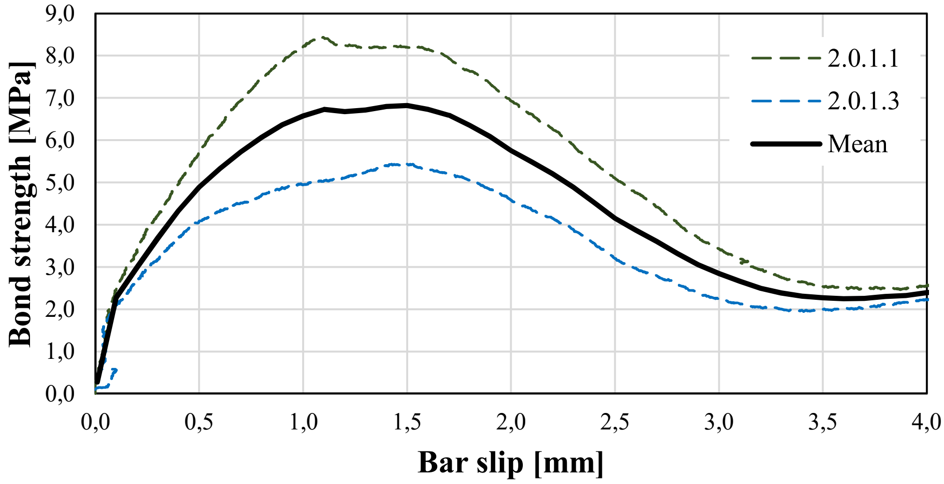

Source: Author (2021).

Fig. 14. Bond-slip curves for C50 concrete and 8.0 mm bars at room temperature.

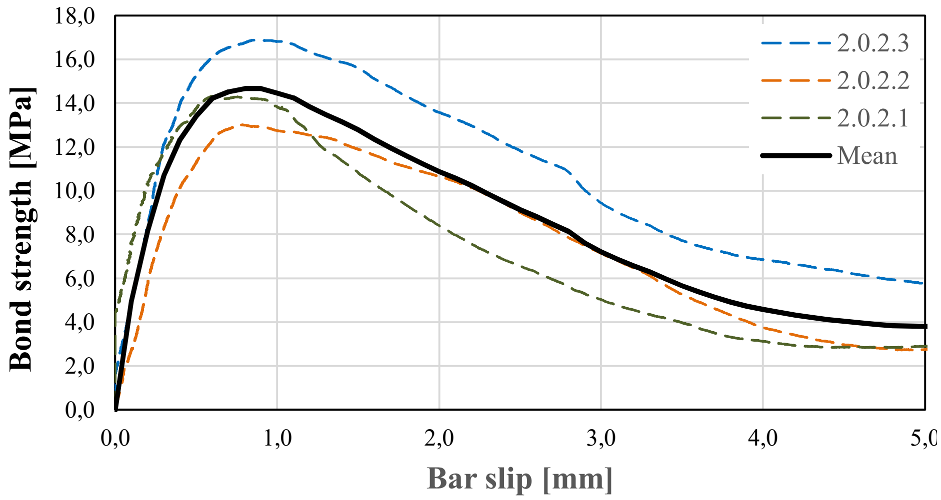

Source: Author (2021).

Fig. 15. Bond-slip curves for C50 concrete and 12.5 mm bars at room temperature.

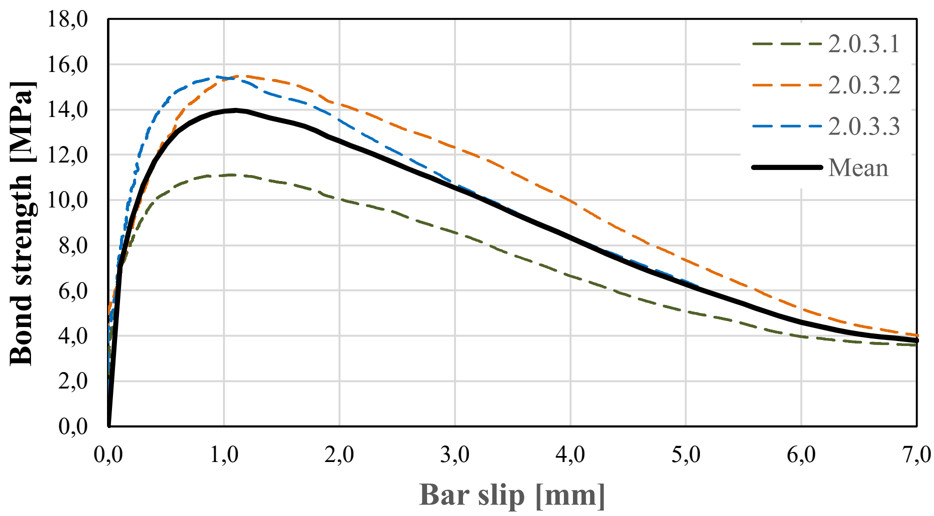

Source: Author (2021).

Fig. 16. Bond-slip curves for C50 concrete and 5.0 mm bars at 200ºC.

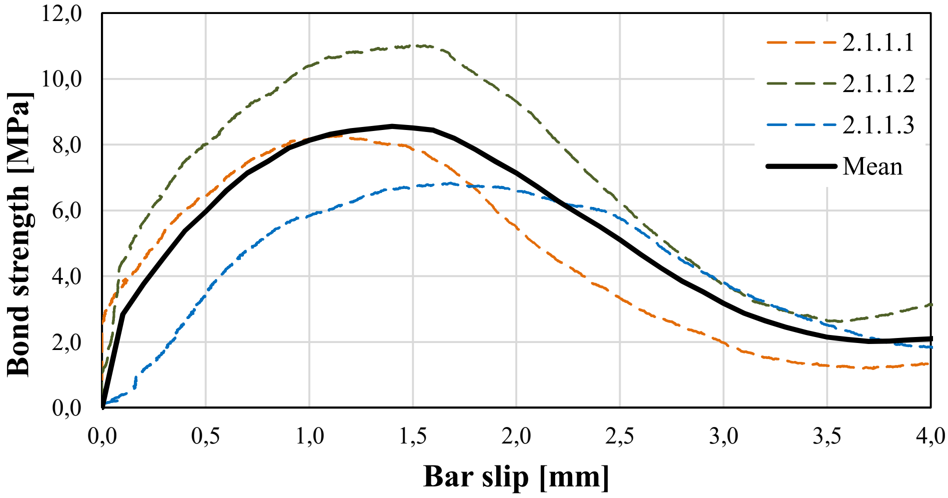

Source: Author (2021).

Fig. 17. Bond-slip curves for C50 concrete and 8.0 mm bars at 200ºC.

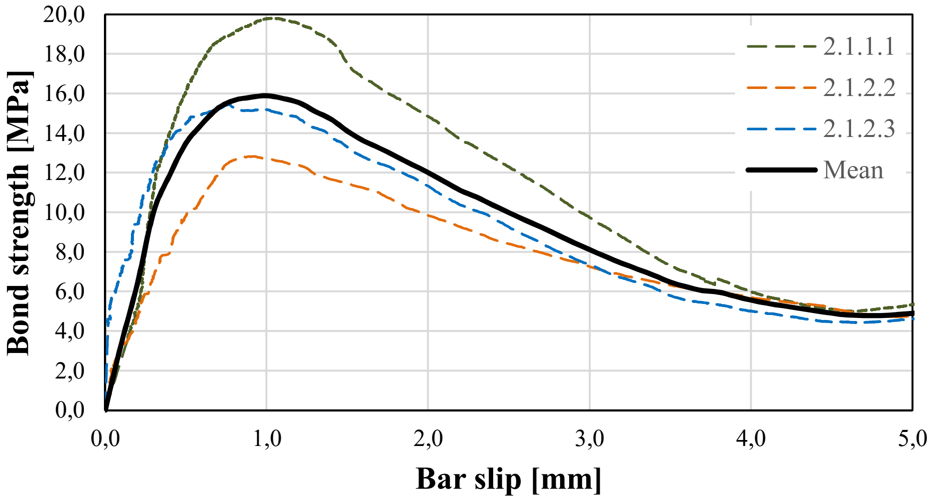

Source: Author (2021).

Fig. 18. Bond-slip curves for C50 concrete and 12.5 mm bars at 200ºC.

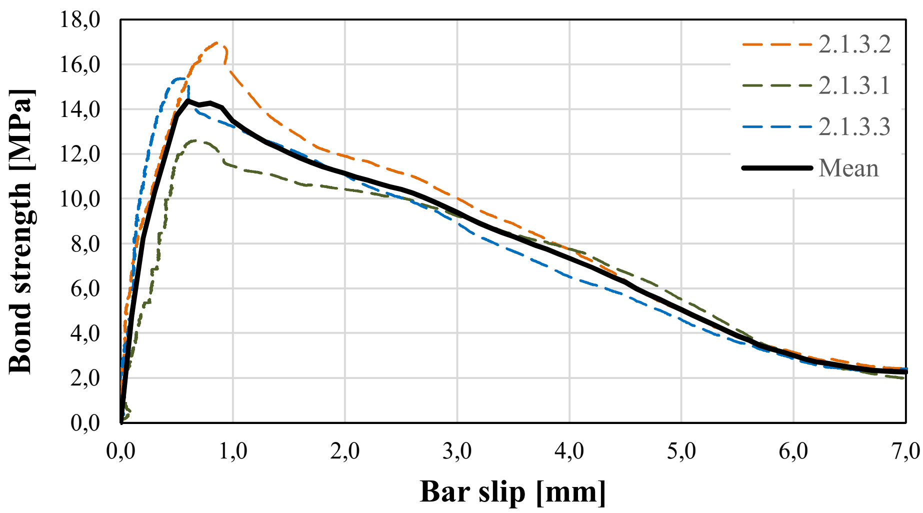

Source: Author (2021).

Fig. 19. Bond-slip curves for C50 concrete and 5.0 mm bars at 400ºC.

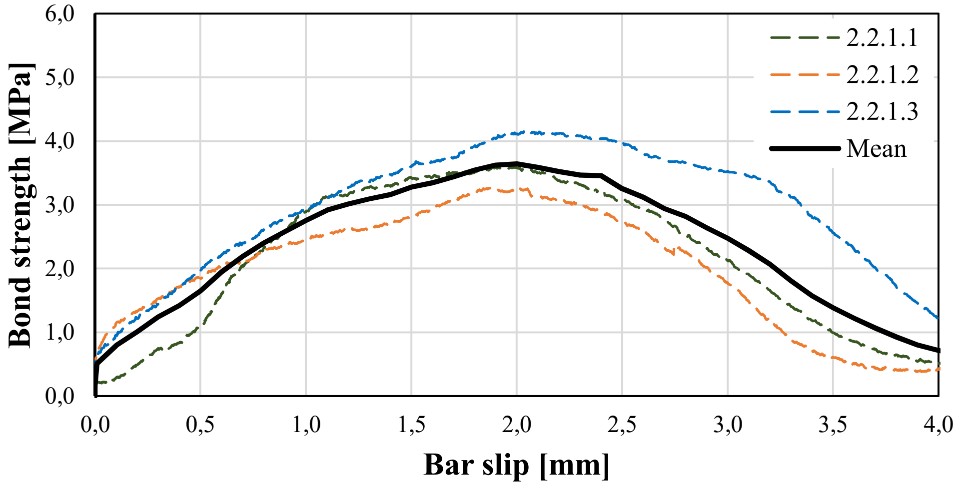

Source: Author (2021).

Fig. 20. Bond-slip curves for C50 concrete and 8.0 mm bars at 400ºC.

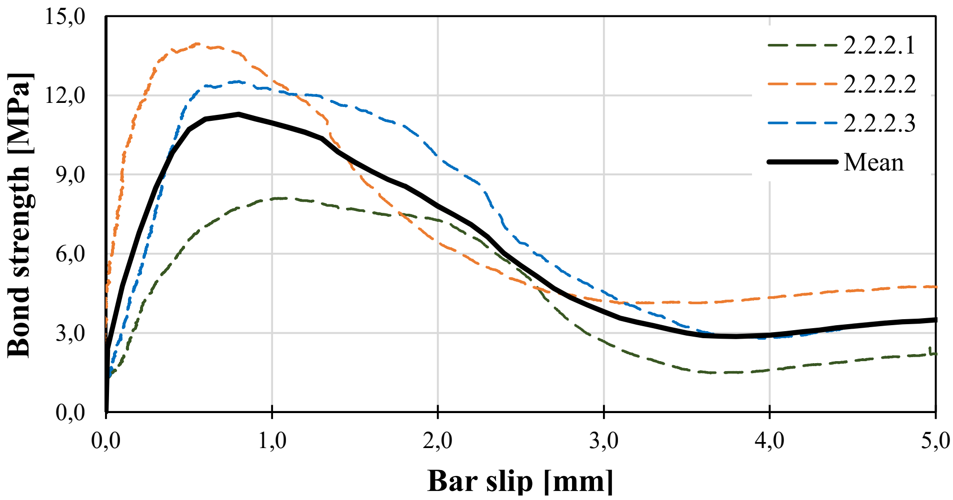

Source: Author (2021).

Fig. 21. Bond-slip curves for C50 concrete and 12.5 mm bars at 400ºC.

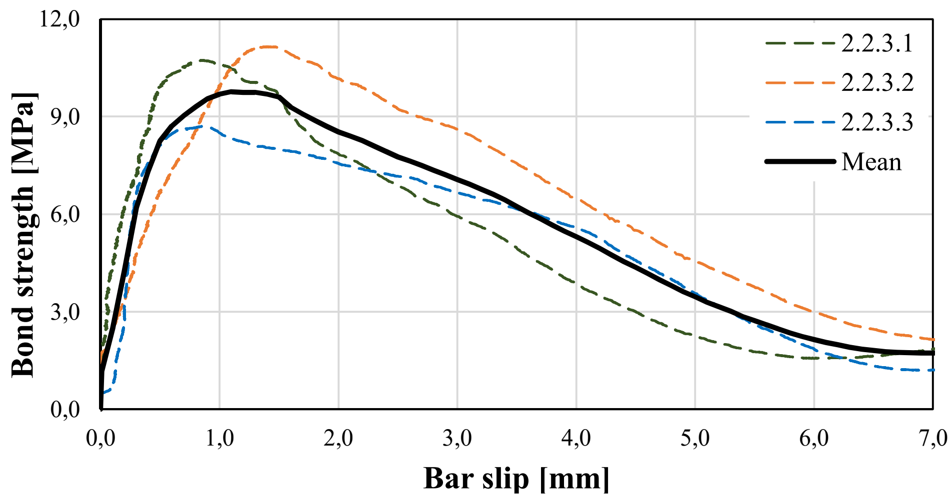

Source: Author (2021).

Fig. 22. Bond-slip curves for C50 concrete and 5.0 mm bars at 600ºC.

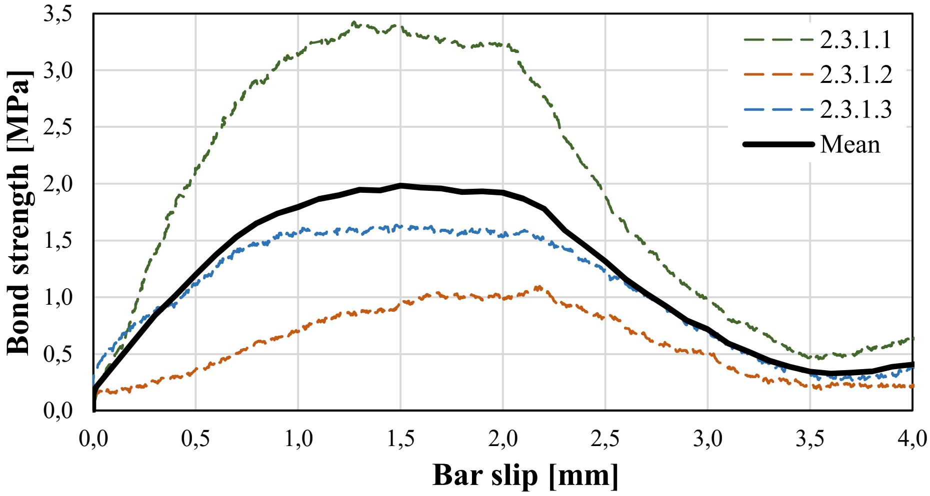

Source: Author (2021).

Fig. 23. Bond-slip curves for C50 concrete and 8.0 mm bars at 600ºC.

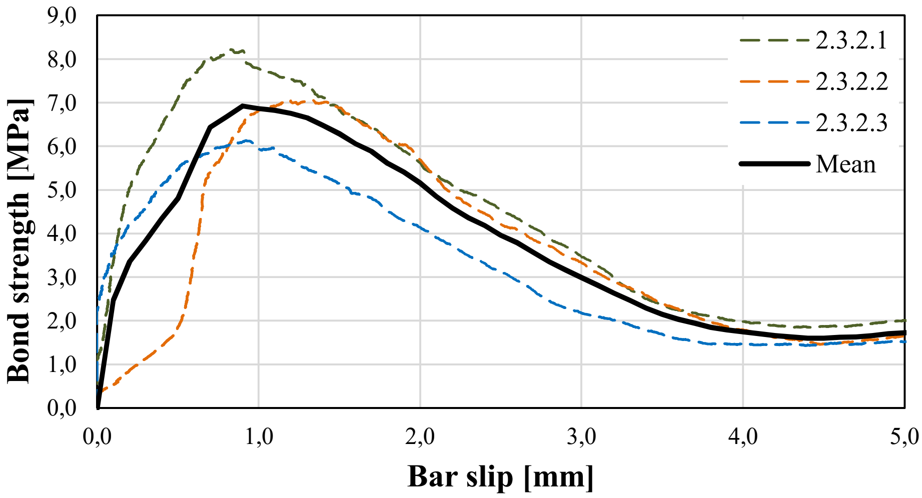

Source: Author (2021).

Fig. 24. Bond-slip curves for C50 concrete and 12.5 mm bars at 600ºC.

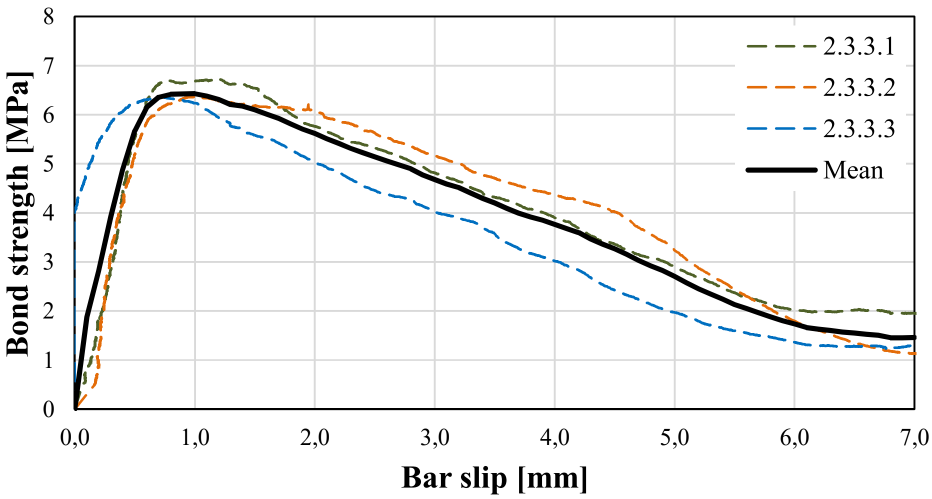

Source: Author (2021).